CONSTRUCTION MATERIALS CONSULTANTS, INC.

Laboratory Investigation Of Coating Failure From Stucco Façades Of An 18th Century Courthouse In Charleston, South Carolina

Charleston County Courthouse Exterior Façade
Charleston, South Carolina

September 29, 2020
CMC 0820145

TABLE OF CONTENTS

EXECUTIVE SUMMARY

Reported herein are the results of detailed laboratory studies of three drilled cores of stucco façade from the Charleston County Courthouse in Charleston, South Carolina. Originally constructed in the 1750's in downtown Charleston, SC and served as the state courthouse until a fire destroyed much of the building, the courthouse was rebuilt circa 1788 and has had numerous repairs due to renovations, hurricanes, earthquakes, and war. The westernmost portion of the North elevation was rebuilt using cast-in-place concrete walls with brick acting as substrate to the stucco façade. Widespread coating distress is visible on all elevations of the building. Areas are peeling and give off white residue when swiped with a finger. Stucco façade largely remains intact on the building except for the columns on the South elevation and some stucco areas closest to the ground have become powder behind the coating and have begun to wear away once the coating has peeled off. There are numerous areas where stucco is delaminated when sounded. This is especially apparent where Portland cement repairs have been completed. All stucco cores taken had good adhesion to the brick substrate. The delamination, when sounded, appeared to come from behind the coating(s) or somewhere within the stucco depth.

Three (3) full-depth stucco with coating cores from different elevations, all 3-inch nominal diameter, 1-inch long were provided. Two cores (S7 and S8) were selected at distressed areas. The distressed areas contained deteriorated coating and delaminated stucco when sounded. One core (S4) was located in a small delaminated area with the stucco coating intact. The surrounding area contained well adhered stucco and coating when sounded. An additional sample from the west elevation was provided to check the composition of the paint coat.

All three stucco samples from north, south, and east elevations were examined by a comprehensive testing protocol including: (1) optical microscopy for overall compositions and microstructures of stuccos, (2) SEM-EDS analysis for the compositions of paint coat and binder phases of stucco, (3) X-ray fluorescence for overall bulk chemical compositions of stuccos, (4) X-ray diffraction for overall mineralogical compositions of sand and binder components of stuccos, (5) gravimetric (acid insoluble residue contents) analysis for sand contents of stuccos, (6) thermal analysis for determining sand and calcite contents and possible presence of a hydraulic phase in the binder, which is confirmed from SEM-EDS analysis, and (7) FTIR techniques for analysis of paint compositions, especially the binder phases of paints besides pigment and filler phases beyond determinations from SEM-EDS analysis.

All three stucco samples from north, south, and east elevations of courthouse are found to be compositionally similar three-coat stuccos consisting of: (1) a crushed silica sand and dolomitic hydraulic lime based scratch coat without any fiber mesh or any metal lath reinforcement, (2) a compositionally similar crushed silica sand (though a bit finer in grain size) and dolomitic hydraulic lime based brown coat, and (3) an alkyd resin-based paint coat containing titanium oxide pigment and talc filler in alkyd resin binder. Total nominal thickness of stuccos are 18 mm in S4 from north elevation, 16 mm in S7 from south elevation, and 22 mm in S8 from east elevation. Paint coats are all less than 0.25 mm in thickness, which shows a clear separate bonding agent coat in S8 but no distinct bonding agent in the other two samples except perhaps a diffused interface of a bonding agent, if applied into the stucco. Brown coats are 8 mm in S4, 7 mm in S7, and 8 mm in S8. Scratch coats are 10 mm in S4, 7 mm in S7, and 14 mm in S8. Bonds between paint and brown coat as well as between brown and scratch coats are good. Scratch and brown coats are differentiated on the basis of overall finer grain size of crushed sand particles in the brown coat in almost all three stuccos, and a variation in overall densities and color tones of coats where brown coats are overall denser than the scratch coats.

Major elemental oxide compositions of all three stuccos from X-ray fluorescence spectroscopy shows overall compositional similarities in having 60 to 70% silica, 0.8 to 1.2% alumina, 0.7 to 1.5% iron, 9.8 to 11.5% lime, 2.5 to 3.1% magnesia, and other oxides at lesser abundances all consistent with a silica sand and dolomitic hydraulic lime composition determined from optical and scanning electron microscopy and X-ray microanalysis. Acid insoluble residue contents are around 70 percent, which correspond to silica sand contents, and closely correspond to silica contents from XRF. Higher magnesia contents in paste from SEM-EDS studies as well as in bulk stucco samples from XRF studies compared to a non-hydraulic lime binder indicates use of a dolomitic lime. Additionally, higher silica contents in paste than a non-hydraulic lime binder and a higher loss of mass from

decomposition of hydrate water in thermal analysis than a paste from a non-hydraulic lime binder indicates use of a hydraulic lime binder. No Portland cement or other cementitious or hydraulic phases are found in the porous, fine-grained severely carbonated lime paste showing characteristic fine discontinuous shrinkage microcracks as seen in many historic lime mortars.

The paint coat is found to be compositionally similar in all samples from all three elevations, including an additional one provided from the west elevation, all of which showed the presence of an alkyd resin-based paint as opposed to more common and alkali-resistant acrylic or latex or siloxane based paint. The talc filler and titanium oxide pigment in the paint are determined best from SEM-EDS studies from characteristic titanium, silica, and alumina enrichments in X-ray elemental maps of those elements in the paste, as well as from FTIR studies from characteristic absorption bands of talc in the FTIR spectra. Absorption bands near 1007 cm^{-1} and 3676 cm^{-1} correspond to talc filler in paint; bands at 876 cm^{-1} and 1452 cm^{-1} correspond to calcite partly from calcite filler in the bonding agent of paint and partly from contaminant carbonated lime binder of stucco. There is no evidence of any other filler found in the optical microscopy, or SEM-EDS, or FTIR scans, which were reportedly suspected in the paint. For example, there is no nepheline syenite, diatom, dolomite, or silicon dioxide fillers found either in optical or electron microscopy, or in FTIR studies. Amorphous silica in diatom gives a large FTIR band near 1100 cm^{-1} with bands at 800 cm^{-1} and 500 cm^{-1}, which are not present. Crystalline silica has a characteristic doublet near 800/780 cm^{-1}, which is not present. Dolomite has large doublet at 1480/1410 cm^{-1} which are not present. Bands found at 1267 cm^{-1} and 1732 cm^{-1} correspond to an alkyd resin or oil-based binder, which is not resistant to the alkaline medium of stucco especially at the newly installed stage before the stucco surface that was painted has had a pH around 9 or lower from atmospheric carbonation to prevent alkali-induced deterioration of alkyd-based paint. For the reported peeling of paint, there is a possibility that the band near 1628 cm^{-1} is indicating saponification of the resin to cause the paint failure from alkaline degradation of alkyd-based paint. An acrylic paint would have produced a band near 1170 cm^{-1} sometimes with a smaller band near 1240 cm^{-1}, which are not found. Siloxane would usually have a broader band between 1100 and 1000 cm^{-1}, which is not found.

The soft, dusty nature of stucco is found to be due to use of a dolomitic hydraulic lime-based binder in all three samples which has softened the overall conditions. The fragmented nature of S4 is judged to be at least partly due to its lime-based composition even though the other two samples have maintained their integrity during sample extraction and shipment to the laboratory.

Petrographic evidence showed overall good bond between paint brown coat and scratch coats of stucco with no evidence of paint peeling or debonding even though the samples reportedly came from locations that have shown paint peeling. Petrographic examinations indicated loss of moisture from stucco coats from many fine hair-line shrinkage microcracks which are also common in many lime pastes where shrinkage occurs not only from loss of mix water of stucco but also from loss of moisture from carbonation of lime binder.

Based on detailed laboratory examinations, failure of paint coat at various locations and elevations of courthouse are judged to be due to a combination of the following factors:

(a) Use of an alkyd resin-based paint as opposed to more common acrylic or latex-based paint, or, the reported alkyl alkoxy siloxane-based paint of TiO_2 pigment, and diatom-quartz-dolomite-syenite fillers. Alkyd resin is vulnerable to degradation in an alkaline environment of stucco, especially at an early age when significant atmospheric carbonation of lime paste of stucco to reduce the pH to 9 or less has not occurred. FTIR studies found evidence of possible saponification of resin to cause peeling from the substrate. Due to pH dependance of paints, application of a paint on a newly placed stucco is usually not done until a pH (e.g., phenolphthalein) test on the stucco surface to be painted shows a pH of 9 or less from atmospheric carbonation;
(b) Absence of a suitable bonding agent or primer prior to the application of the paint coat except a distinct agent found in S8, where lack of adequate bonding agent prevented development of a good mechanical bond to the stucco substrate; and,
(c) The soft porous, lime-based composition of the stucco substrate, which is more porous, dusty, and hence less receptive to a paint than a cement-lime or masonry cement-based stucco substrate.

INTRODUCTION

Reported herein are the results of detailed laboratory studies of three drilled cores of stucco façade from the Charleston County Courthouse in Charleston, South Carolina.

BACKGROUND

The Courthouse was originally constructed in the 1750's in downtown Charleston, SC and served as the state courthouse until a fire destroyed much of the building. It was rebuilt circa 1788 and has had numerous repairs due to renovations, hurricanes, earthquakes, and war. It is known that the westernmost portion of the North elevation was rebuilt using cast-in-place concrete walls with brick acting as substrate to the stucco façade. It is believed the remaining building consists of mass masonry walls (approx. 5 wythes thick). It is visually evident the newer CIP concrete wall areas are performing better, in regards, to the coating than the mass masonry.

Widespread coating distress is visible on all elevations of the building. Areas are peeling and give off white residue when swiped with a finger. In 2012, Prosoco BMC II was applied to the building, which is, reportedly, an alkyl alkoxy siloxane-based paint of TiO_2 pigment, and diatom-quartz-dolomite-nepheline syenite fillers. It is unknown if previous coatings were removed or partially removed.

Stucco façade largely remains intact on the building except for the columns on the South elevation and some stucco areas closest to the ground have become powder behind the coating and have begun to wear away once the coating has peeled off.

There are numerous areas where stucco is delaminated when sounded. This is especially apparent where Portland cement repairs have been completed. All stucco cores taken had good adhesion to the brick substrate. The delamination when sounded appeared to come from behind the coating(s) or somewhere within the stucco depth.

Three (3) full-depth stucco with coating cores from different elevations, all 3-inch nominal diameter, 1-inch long are provided. Two cores (S7 and S8) were selected at distressed areas from the south and east elevations. The distressed areas contained deteriorated coating and delaminated stucco when sounded. One core (S4) was located in a small delaminated area with the stucco coating intact. The surrounding area contained well adhered stucco and coating when sounded. An additional sample from the west elevation was provided to check the composition of the paint coat.

ID	General Description of Condition of Area Associated with Core	Date Extracted	Approx. Diam. And Length	Notes
S4	Stucco coating intact, North elev. Near West corner	7/13/2020	3″ nom diam. Approx. 1″ long	Small stucco delamination in the core area when sounded. No Stucco coating distress in core. Coating and stucco not delaminated in surrounding core area. New brick, likely 20th Century, new brick on CIP concrete walls substrate. Good adhesion to substrate.
S7	Stucco coating delaminated, South elev. Near West corner, severe stucco delamination	7/13/2020	3″ nom diam. Approx. 1″ long	Severe stucco and stucco coating delamination in the core area when sounded. New brick, likely 20th Century, mass masonry substrate. Good adhesion to substrate.
S8	Stucco coating delaminating, East elev. Near South corner, severe stucco delamination	7/13/2020	3″ nom diam. Approx. 1″ long	Severe stucco and stucco coating delamination in the core area when sounded. Historic brick, possibly 18th/19th Century, (5 wythes) substrate. Good adhesion to substrate.

FIELD PHOTOGRAPHS

Figures 1 through 10 show numerous field photos from north, south, east, and west elevations of courthouse, locations of Samples S4, S7, and S8 from north, south, and east elevations, respectively, peeling of paint from the stucco façade at various locations as well as from the columns, and locations of cores examined in relation to the areas of notable coating failures.

PURPOSE

Based on the above background information, the three stucco samples received were examined to determine:

- The overall thickness of the stucco samples, along with thickness of individual coats;
- The overall condition and composition of individual stucco coats applied;
- Soundness and durability of the stucco materials from the sand used in the stucco to the binder phase(s); and,
- Evaluation of materials-related versus construction-related versus environment-related factors to investigate reasons for reported failure of stucco coating.

Figure 1: Field photos of north, south, east, and west elevations of Charleston County courthouse in Charleston, South Carolina. Samples for the present study were collected from the north, south, and east elevations. An additional sample from the west elevation was provided to study the paint coat. The next two photos show the sample locations as well as areas that show peeling of paint from stucco façade.

Figure 2: North (top) and south (bottom) elevations of courthouse showing areas of notable coating failures (boxes) and locations of Samples S4 at north elevation and S7 at south elevation.

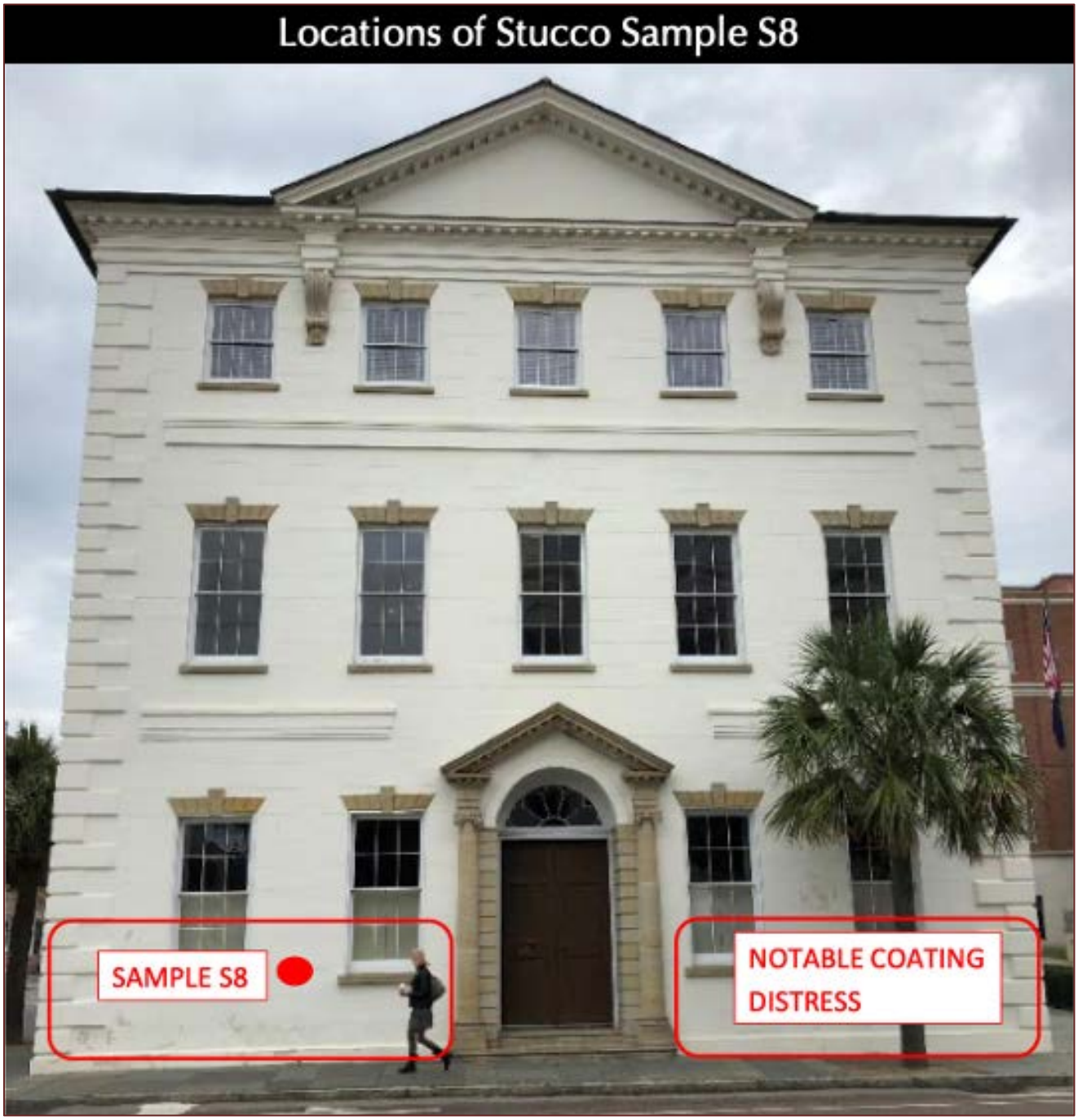

Figure 3: East elevation of courthouse showing area of notable coating failures (box) and location of Sample S8.

Figure 4: Close-up of location of Sample S4 at north elevation. Notice a thin paint coat on stucco where the paint is reportedly adhered well to the stucco base.

Figure 5: Close-up of location of Sample S7 at south elevation. Notice no apparent peeling or delamination of paint at the drilled core location. Two coats of stucco are seen at the drilled wall.

Figure 6: Close-up of location of Sample S8 at east elevation. Notice no apparent peeling or delamination of paint at the drilled core location.

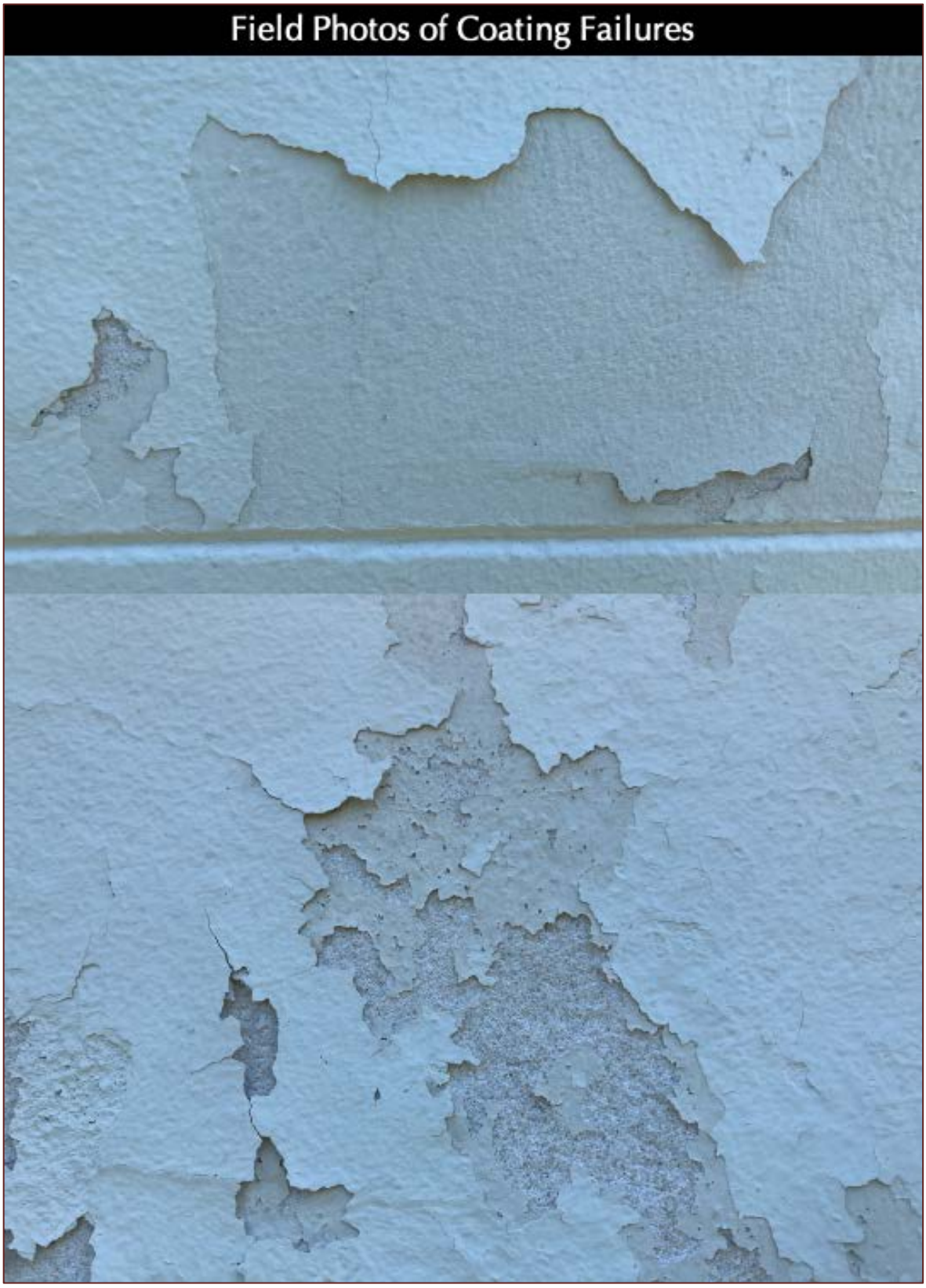

Figure 7: Coating failures as peeling of paint at various locations of stucco façade. Both photos show peeling of at least two applications of paint – peeling of a lighter color top paint coat from the underlying darker toned paint, which, in turn is de-bonded from the underlying soft stucco base.

Figure 8: Coating failures as peeling of paint at various locations of stucco façade.

Figure 9: Coating failures as peeling of paint at columns. Notice relatively thicker paint coat that has been delaminated from the stucco base at this column location compared to the thin paint peeling seen in Figure 7 and 8.

Figure 10: Reddish-brown stain and coating failures as peeling of paint at columns. Figure 9 showed a close-up of this column where paint has been delaminated.

METHODOLOGIES

PETROGRAPHIC EXAMINATIONS

The stucco samples were examined using the methods and procedures of ASTM C 856 "Standard Practice for Petrographic Examination of Hardened Concrete." Details of concrete petrography, and sample preparation techniques for petrographic examinations of stucco are provided in Jana (2006).

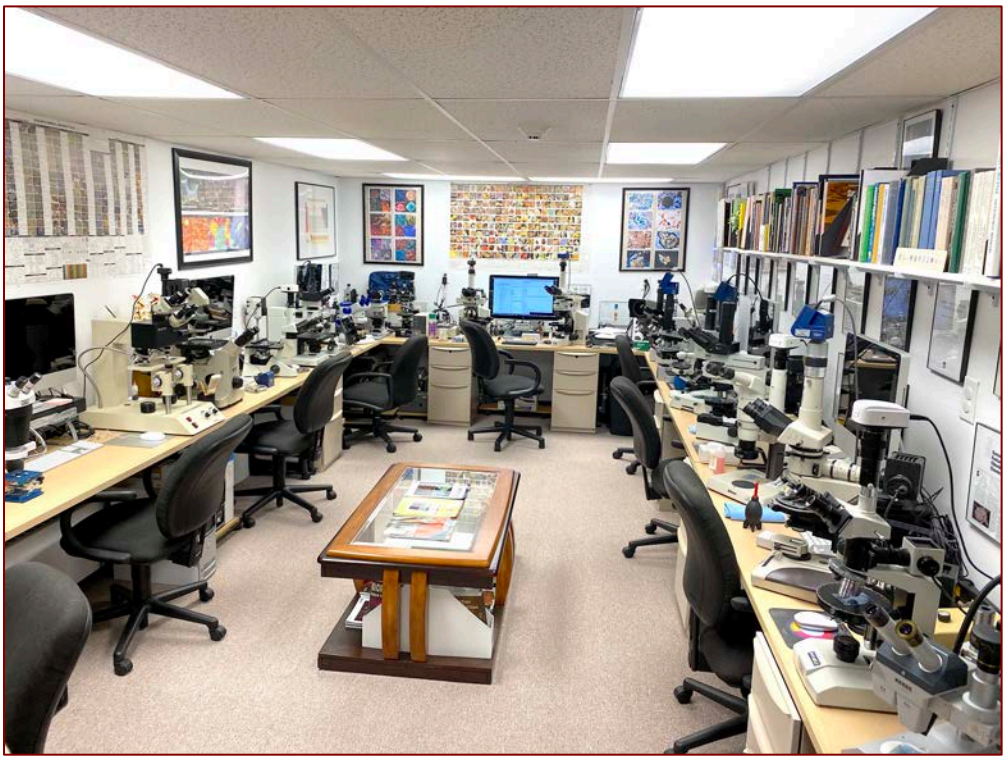

Figure 11: Some of the optical microscopes in the optical microscopy lab that were used for this investigation, from low-power stereo microscope, to high-power transmitted-light stereo-zoom microscope with plane and crossed-polarized light, to epi-fluorescent microscope for observations of florescent dye-mixed epoxy impregnated thin sections and petrographic microscopes for further observations of thin sections of stucco.

Briefly, the steps followed during petrographic examination of the stucco samples include:

i. Visual examinations of the samples, as received, including adequate documentation of dimensions, measurements, condition, physical properties, integrity, etc.;
ii. Low-power stereo microscopical examinations of as-received, saw-cut and freshly fractured sections, and lapped cross sections of samples for evaluation of texture, air-void systems, and compositions;
iii. Examinations of oil immersion mounts in a petrographic microscope for mineralogical compositions of specific areas of interests;
iv. Examinations of fluorescent dye-mixed (to highlight open spaces, cracks, etc.) low-viscosity epoxy-impregnated large area (50 mm × 75 mm) thin sections of stucco in a petrographic microscope for detailed compositional and microstructural analyses;
v. Photographing the samples, as received and at various stages of preparation with a digital camera and a flatbed scanner;
vi. Micrographs of lapped sections and thin sections of stuccos taken with stereomicroscope and petrographic microscope, respectively to provide detailed compositional and mineralogical information of stucco.

Figure 12: CamScan Series 2 scanning electron microscope used for examination of coating failure in a stucco sample.

After optical microcopy, thin section examination was further carried out in a CamScan Series 2 scanning electron microscope (Figure 12) equipped with a high-resolution column 40Å tungsten, 40 kV electron optics zoom condenser 75° focusing lens operating at 20 kV, equipped with a variable geometry secondary electron detector, backscatter electron detector, EDS detector for observations of microstructures at high-resolution, compositional analysis, and quantitative determinations of major element oxides from various areas of interest, respectively. Revolution 4Pi software is used for digital storage of secondary electron and backscatter electron images, elemental mapping, and analysis along a line, a point or an area of interest. A 50 mm × 75 mm thin section of a stucco sample was polished, coated with a gold-palladium alloy, and used with a custom-made aluminum sample holder in the large multiported chamber with the eucentric 50 × 100 mm motorized stage.

X-RAY DIFFRACTION

The stucco samples were pulverized to finer than 44-micron (US 325 sieve) particle size for X-ray diffraction studies. The purpose of this study is to detect: (a) the major and minor minerals in the stucco from the sand used to the binder phases, and, (b) any potentially deleterious minerals in the stucco coats as well as in the failed exterior coating, which might have contributed to the coating failure.

X-ray diffraction was carried out in a Bruker D2 Phaser (2nd Generation) benchtop Powder diffractometer Bragg-Brentano geometry) employing a Cu X-ray tube (Cu k-alpha radiation of 1.54 angstroms), a primary slit of 1 mm, a receiving slit of 3 mm, a position sensitive 1D Lynxeye XE-T detector. Generator settings used are 30 kV and 10mA (300 watt). Sample was placed in a zero background sample holder which is an optically polished 111 plane of silicon wafer attached to a stainless steel sample holder for use in the 6-position sample stage of D2 Phaser. Tests were scanned at 2θ from 8° to 64° with a step of 0.05° 2θ integrated at 0.05 sec. step^{-1} dwell time. The resulting diffraction patterns were collected by Bruker's Diffrac.Measurement software. Phase identification was done with Bruker's Diffrac.EVA software with the search-match database from Crystallographic Open Database (COD). Additional phase identification, and Rietveld quantitative analyses were carried out with Match! software.

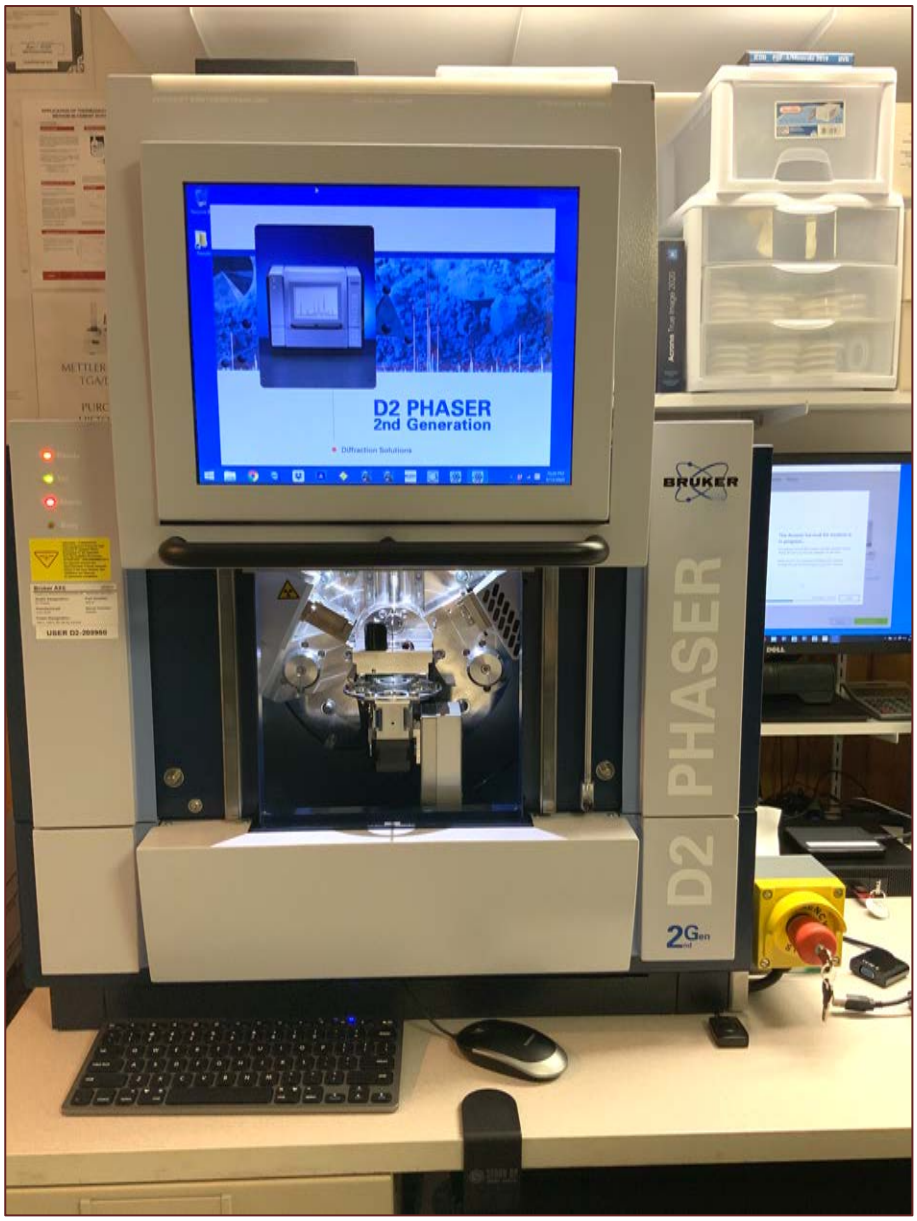

Figure 13: Bruker's D2 Phaser (2nd generation) benchtop X-ray powder diffractometer with Lynxeye 1D position sensitive detector used in X-ray diffraction studies of stucco samples.

X-RAY FLUORESCENCE SPECTROSCOPY

X-ray fluorescence (XRF) was used for determining major element oxide compositions of stucco, which provide clues about the siliceous sand contents of stuccos from silica contents, types of binder used (e.g., a dolomitic lime or natural cement based binder gives a characteristically higher magnesia than a calcitic lime or Portland cement based binder), effect of alterations and deteriorations.

A series of standards from Portland cements, lime, gypsum, to various rocks, and masonry mortars of certified compositions (e.g., from USGS, GSA, NIST, CCRL, Brammer, or measured by ICP) are used to calibrate the instrument for various oxides and empirical calculations are done from such calibrations to determine oxide compositions of stuccos.

Figure 14: Rigaku NEX-CG in CMC, which can perform analyses of 9 pressed pellets or fused beads of sample. Samples are prepared either as pressed pellet (usually the one already prepared for XRD) or can also accommodate fused bead with proper calibration of standard beads

An energy-dispersive bench-top X-ray fluorescence unit from Rigaku Americas Corporation (NEX-CG) was used (Figure 14). Rigaku NEX CG delivers rapid qualitative and quantitative determination of major and minor atomic elements in a wide variety of sample types with minimal standards. Unlike conventional EDXRF analyzers, the NEX CG was engineered with a unique close-coupled Cartesian Geometry (CG) optical kernel that dramatically increases signal-to-noise. By using monochromatic secondary target excitation, instead of conventional direct excitation, sensitivity is further improved. The resulting dramatic reduction in background noise, and simultaneous increase in element peaks, result in a spectrometer capable of routine trace element analysis even in difficult sample types. The instrument is calibrated by using various certified (CCRL, NIST, GSA, and Brammer) reference standards of cements and rocks.

THERMAL ANALYSES

Thermal analyses encompass: (1) thermogravimetric analysis (TGA), which measures the weight loss during heating related to decomposition of a phase of interest at a specific temperature that is characteristic of the phase from which both the phase composition and the abundance can be determined; (2) differential thermal analysis (DTA, or first derivative of TGA i.e. DTG) measuring temperature difference between the sample and an inert standard (Al_2O_3) both are heated at the same rate and time where endothermic peaks are recorded when the standard continues to increase in temperature during heating but the sample does not due to decompositions (e.g., dehydration of hydrous or decarbonation of carbonate phases); the endothermic or exothermic transitions are characteristic of particular phase, which can be identified and quantified using DTA (or DTG); and (3) differential scanning calorimetry (DSC), which follows the same basic principle as DTA, whereas temperature differences are measured in DTA, during heating using DSC energy is added to maintain the same and the reference material (Al_2O_3) at the same temperature; this energy use is recorded and used as a measure of the calorific value of the thermal transitions that the sample experiences; this is particularly useful for detection of quartz that undergoes polymorphic (α to β form) transitions and no weight loss.

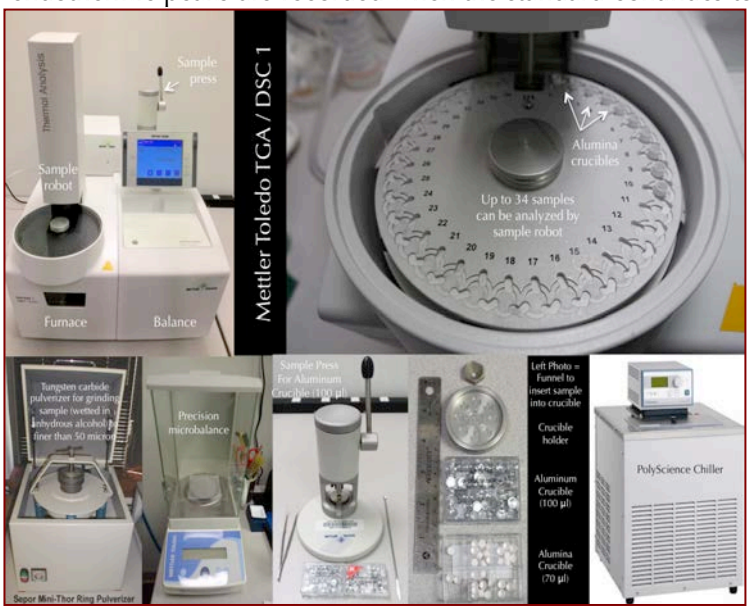

Figure 15: Mettler-Toledo simultaneous TGA/DSC1 unit in CMC that can accommodate 32 samples. The top left photo shows the TGA/DSC1 unit with sample robot for automation as well as the sample holder for pressing aluminum sample holders. Sample is pulverized in a ring pulverizer shown in the bottom left, then a small amount (usually 30-70 mg) is weighed in a precision balance (shown 2nd from left in bottom row) and taken in an alumina sample holder (without lid). For DSC measurements up to 600°C, sometimes sample is taken in an aluminum holder and pressed in sample press (3rd from left in bottom row) and pierced with a needle for release of volatiles from decomposition. A PolyScience chiller (rightmost one in the bottom row) is used to cool the furnace. An ultrapure nitrogen gas is purged through the system during analyses.

Thermal analyses determine the presence and quantitative amounts of: (a) hydrates (e.g., water liberated from paste dehydration during decomposition of calcium-silicate-hydrate component in paste at 180-190ºC); (b) sulfates (gypsum from decompositions at 125ºC, and 185-200ºC, ettringite at 120-130ºC, thaumasite at 150ºC); (c) brucite from its dehydroxylation at 300-400ºC to confirm the presence of dolomitic lime; (d) hydrate water from decomposition of Portlandite component of paste at 400-600ºC; (e) quartz from polymorphic transformation (α to β form) at 573ºC; (f) cryptocrystalline calcite in the carbonated lime matrix from decomposition at 620-690ºC, or magnesite at 450-520ºC, or (g) coarsely crystalline calcite e.g., in limestone by decomposition at 680-800ºC or (h) dolomite at 740-800ºC and 925ºC, and (i) phase transition of belite (C_2S) at 693ºC, etc. Phases are determined from their

characteristic decomposition temperatures occurring mostly as endothermic peaks or polymorphic transition temperatures as for quartz.

Simultaneous TGA and DSC analyses are done in a Mettler Toledo TGA/DSC 1 unit (Figure 15) on 30-70 mg of finely ground (<0.6 mm) sample in alumina crucible (70 µl, no lid) from 30°C to 1000°C at a heating rate of 10°C/min with high purity nitrogen as purge gas at a flow rate of 75.0 ml/min. By using one of the three removable sensor types the TGA/DSC 1 simultaneously measures heat flow in addition to weight change. The instrument offers high resolution (ultra-microgram resolution over the whole measurement range), efficient automation (with a reliable sample robot for high sample throughput), wide measurement range (measure small and large sample masses and volumes) broad temperature scale (analyze samples from ambient to 1100°C), superior ultra-micro balance, simultaneous DSC heat flow measurement (for simultaneous detection of thermal events, e.g., polymorphic alpha-to-beta transition of quartz and quartz content), and a gastight cell (ensures a properly defined measurement environment).

FTIR SPECTROSCOPY OF FINISH COAT OF STUCCO

To determine the possible reasons for coating failure from stucco façade, determinations of compositions of paint applied on the façade are essential. Fourier-transform infrared spectroscopy (FT-IR) is an important technique, which determines the paint compositions, mainly the binder phases of paint, along with the fillers and sometimes pigment used.

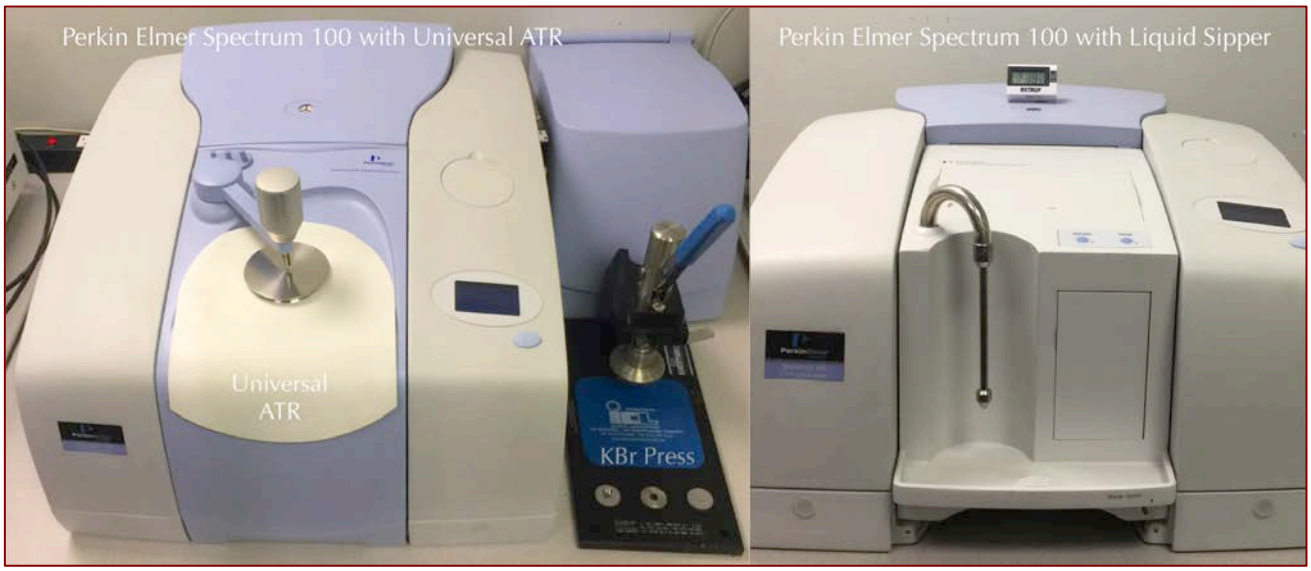

Figure 16: Perkin Elmer Spectrum 100 FT-IR unit with Universal ATR attachment for examinations of paint coats on stucco.

FTIR measures interaction between applied infrared radiation and the molecules in the compounds of interest. Bonds between atoms have distinctive geometrics and natural states of rotation and vibration. Incident infrared radiation will excite these vibrations and rotations when a critical wavelength is reached that can impart energy to the bond. At this point the atomic bond that is being excited will absorb that wavelength of infrared radiation. If the

sample is placed between the source of radiation and a detector these times of absorption of infrared radiation can be recorded as reduced intensity and can be related to specific types of atomic bonds characteristic of particular functional groups in compounds (e.g., CO^{3-}group in carbonates). FT-IR is particularly useful for detection of polymer resins beneath floorings. FT-IR is used mainly to identify various organic components (functional groups) in paint coats on stucco from their characteristic spectral fingerprints in FT-IR spectrum. Organic compounds such as synthetic (e.g., acrylics, polyesters) and natural resins, carbohydrates, colorants, oils and fats, proteins, waxes as well as inorganic compounds, e.g., corrosion products, minerals, pigments, paints, fillers, stone, glass, and ceramics can be detected by this technique.

FT-IR measurements are done in a Perkin Elmer Spectrum 100 FT-IR spectrophotometer (Figure 16) running with Spectrum 10 software. Outermost finish coats of the two samples were measured using attenuated total reflection (ATR) on a single bounce diamond/ZnSe ATR crystal. Samples were measured between a frequency range of 4000 to 650 cm^{-1}. Each run was collected at 4 cm^{-1} resolution with Strong Beer-Norton apodization. Data were collected with a temperature-stabilized deuterated triglycine sulfate (DTGS) detector by placing the sample in contact with the ATR crystal and by applying force from the pressure applicator supplied with the ATR accessory. The application of pressure enabled the sample to be in intimate contact with the ATR crystal, ensuring a high-quality spectrum was achieved.

SAND CONTENTS FROM ACID-INSOLUBLE RESIDUE AND SAND SIZE DISTRIBUTION FROM IMAGE ANALYSES

Sand contents of three stucco samples were determined from hydrochloric-acid insoluble residues, where approximately 1.00 gram of pulverized stucco was digested in diluted (1+3) hydrochloric acid first in near-boiling temperature for 15 minutes followed by an hour long digestion, filtration of sand out of the digested mass and determining residue contents of stuccos. Since sand used in all three stuccos are determined to be siliceous in compositions that are insoluble in acid, the acid-insoluble residue contents are judged similar to the siliceous sand contents of stuccos.

Grain-size distribution of sands are determined from micrographs of thin sections of stucco in plane polarized light modes where ImageJ software was used to determine the grain sizes of individual sand particles for plotting grain-size distributions.

SAMPLES

Figures 17 through 20 show three disc-shaped stucco cores received from north, south, and east elevations that are marked as S4, S7, and S8, respectively. As mentioned, all three cores are 3 inches in nominal diameters and approximately 1 in. in thickness. An additional sample from the west elevation was provided later to check the composition of the paint coat.

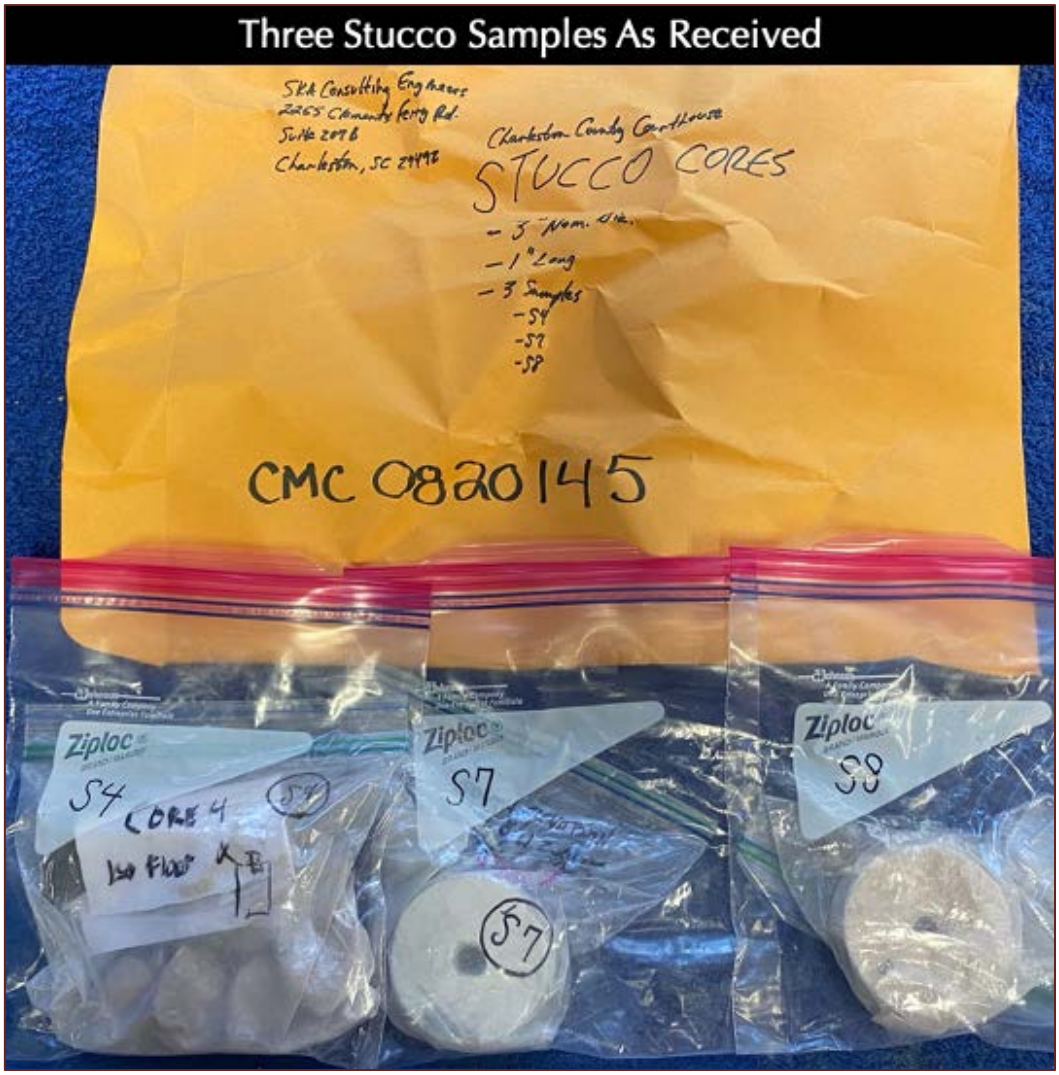

Figure 17: Shown are the drilled 3-in. diameter and approximately 1 in. thick stucco cores from north, south, and east elevations of courthouse that are marked as S4, S7, and S8, respectively.

Sample S4 was received in multiple fragmented pieces even though the sample was reportedly collected from a location away from the location of coating failure in the north elevation (see Figures 2 and 4). By contrast, Samples S7 and S8 from south and east elevations, respectively were received in relatively intact conditions without any fragmentations.

All three samples show a paint coat on the exposed faces which are well-bonded to the underlying stucco. All three samples, however, are very dusty in appearance, which are signatures of use of abundant lime in the binders as determined from subsequent examinations.

All three stucco samples show two prominent coats, a brown coat on which the paint was applied, and an underlying scratch coat. No fiber mesh or expanded metal lath reinforcement are present in the scratch coat.

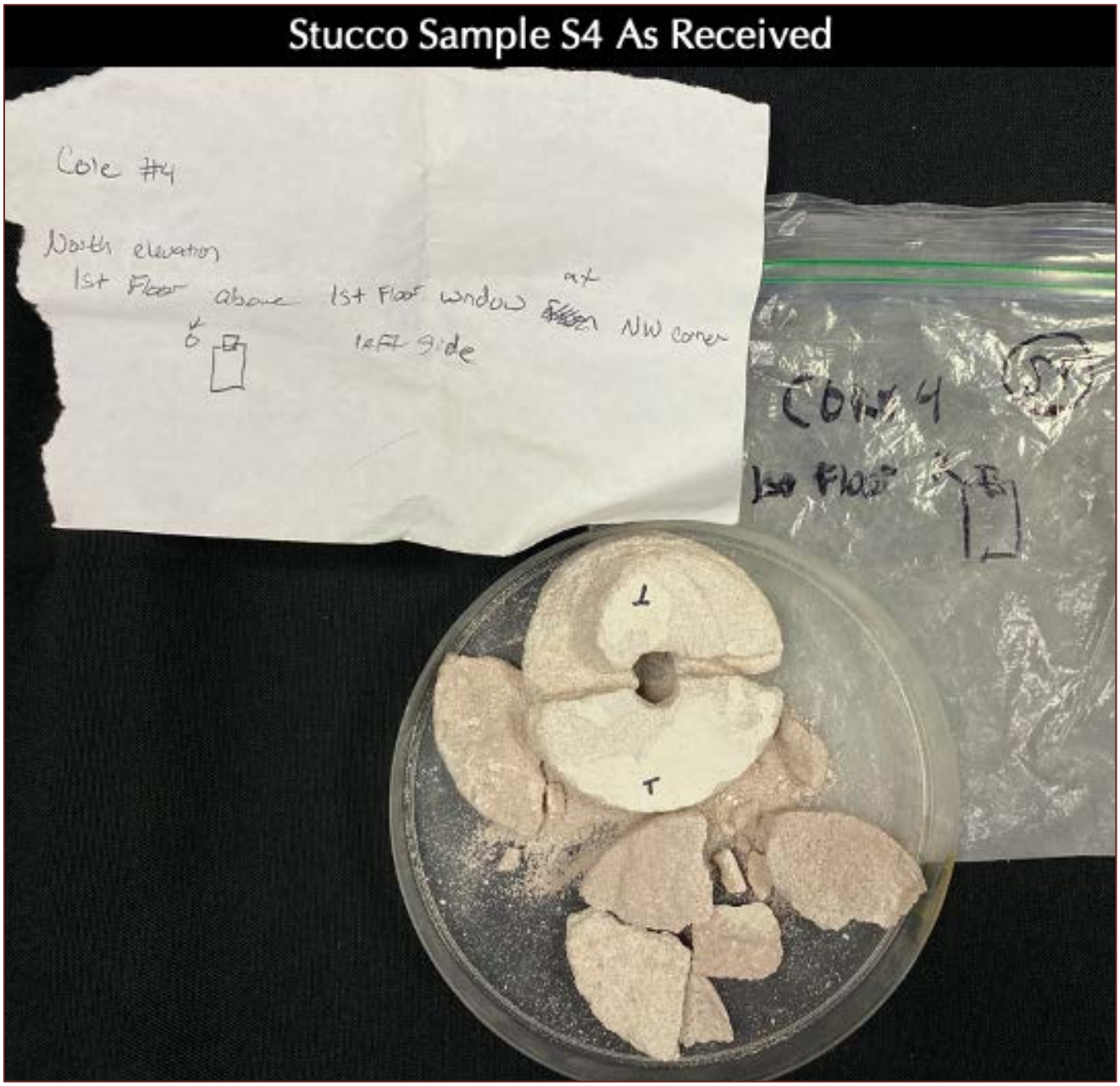

Figure 18: A close-up of stucco from north elevation of courthouse marked as S4 that shows light-colored paint coat remains on some fragmented pieces of stucco. Notice the overall soft, dusty appearance of stucco pieces.

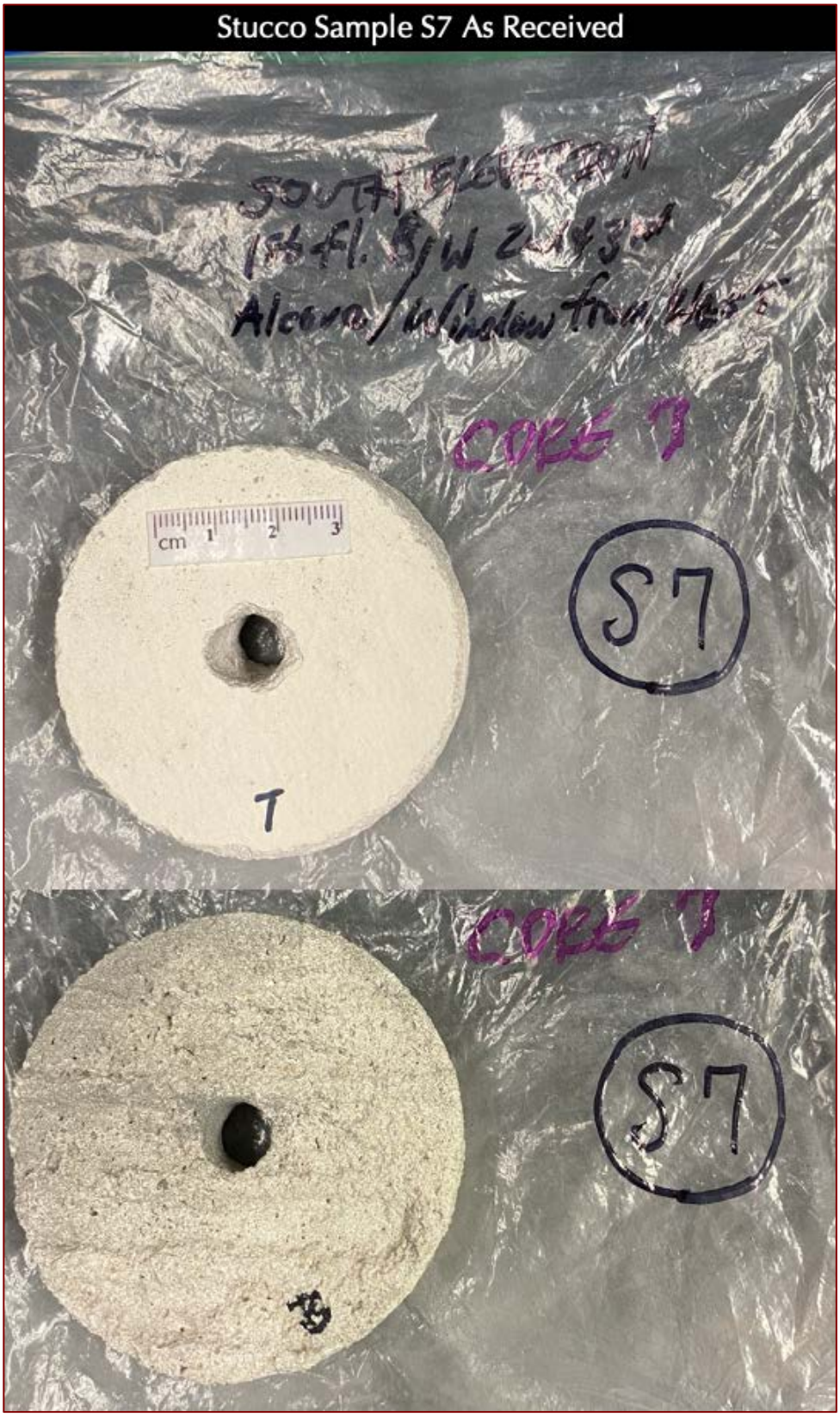

Figure 19: A close-up of stucco from south elevation of courthouse marked as S7 that shows light-colored paint coat remains on the stucco. Notice the overall soft, dusty appearance of stucco, but, overall intact condition of drilled core without any fragmentation as seen in S4.

Figure 20: A close-up of stucco from east elevation of courthouse marked as S8 that shows light-colored paint coat remains on the stucco. Notice the overall soft, dusty appearance of stucco, but, overall intact condition of drilled core without any fragmentation as seen in S4.

PETROGRAPHIC EXAMINATIONS

SAW-CUT CROSS SECTIONS

Figure 21: Saw-cut cross sections of the three stucco samples showing:

(a) At least two discernable coats in each stucco sample benath the paint coat (finish coat) – a brown coat which is approximately 8 mm in S4, 7 mm in S7, and 8 mm in S8, and, a scratch coat, which is approximately 10 mm in S4, 7 mm in S7, and 14 mm in S8;

(b) Overall nominal thickness of stucco range from 18 mm in S4, to 16 mm in S7, to 22 mm in S8;

(c) Overall good bond between two coats of stucco in each sample, the interface between brown and scratch coats are marked with dashed lines;

(d) A very thin (less than 1 mm thickness) light colored paint coat on all three stucco samples;

(e) Well adherence of paint to the stucco base in all three samples; and,

(f) The fragments shown here are impregnated with a fluorescent dye-mixed epoxy for preparaiton of thin sections.

LAPPED CROSS SECTIONS

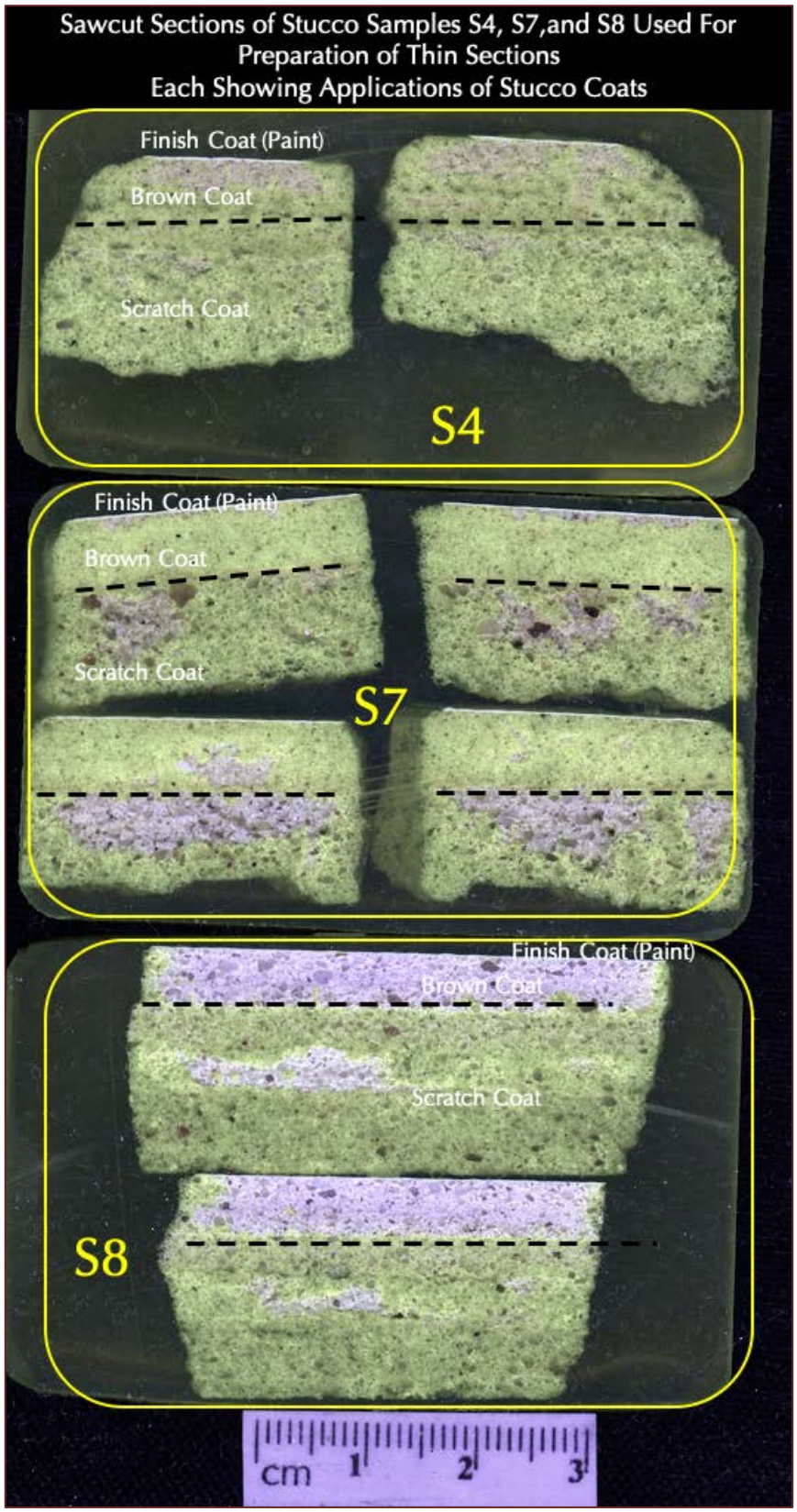

Figure 22: Fluorescent dye-mixed epoxy-impregnated residues of thin sections of stucco samples showing:

(a) At least two discernable coats in each stucco sample beneath the paint (finish) coat – a brown coat which is approximately 8 mm in S4, 7 mm in S7, and 8 mm in S8, and, a scratch coat, which is approximately 10 mm in S4, 7 mm in S7, and 14 mm in S8;

(b) Overall nominal thickness of stucco range from 18 mm in S4, to 16 mm in S7, to 22 mm in S8;

(c) Overall good bond between two coats of stucco in each sample, the interface between brown and scratch coats are marked with dashed lines;

(d) A very thin (less than 1 mm thickness) light colored paint coat on all three stucco samples;

(e) Well adherence of paint to the stucco base in all three samples; and,

(f) Variable porosities of paste in brown and scratch coats of stucco that are revealed from various degrees of absoprtion of fluorecent dye-mixed epoxy in the stucco.

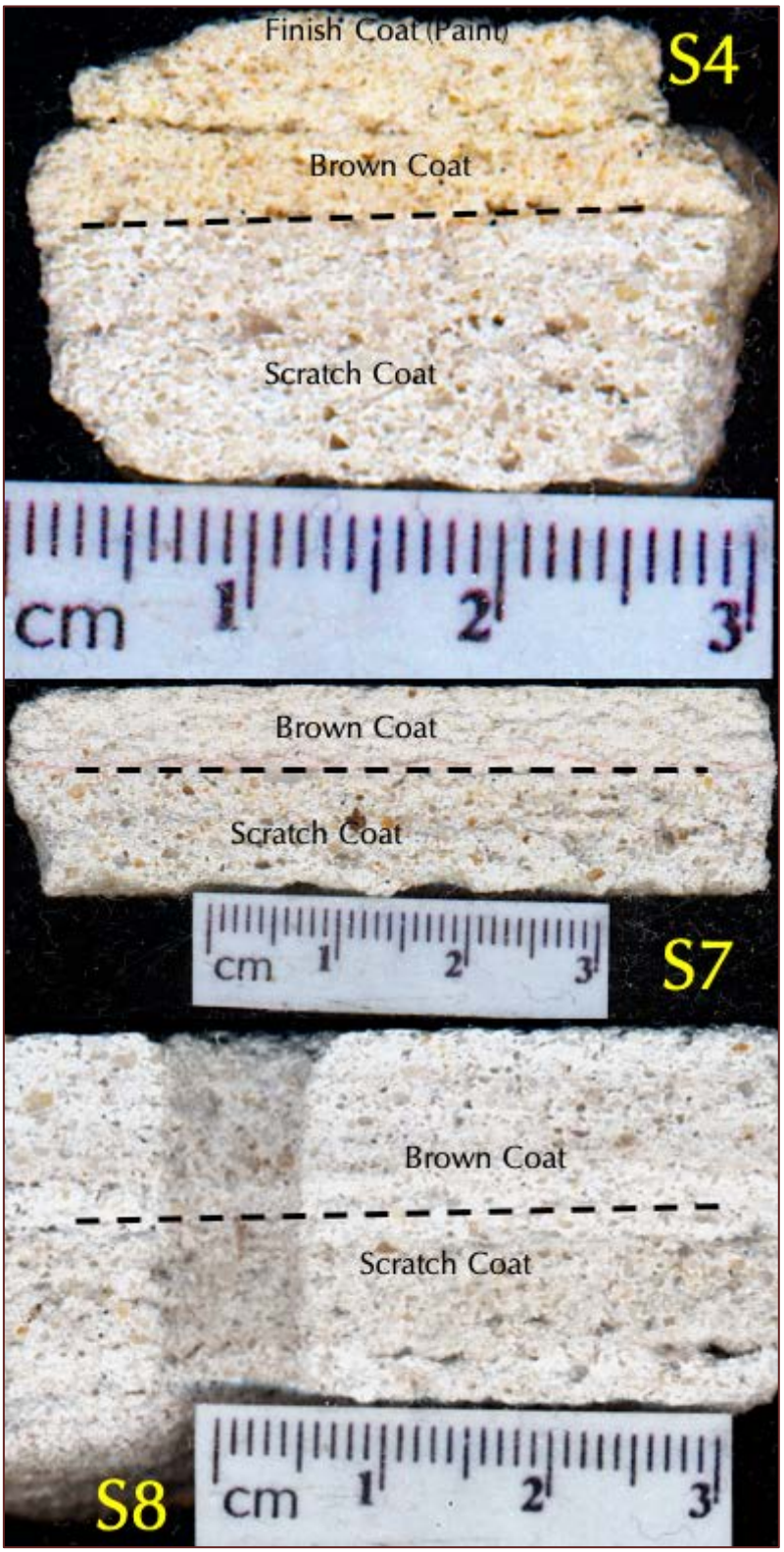

Figure 23: Lapped cross sections of stucco samples showing:

(a) At least two discernable coats in each stucco sample beneath the paint (finish) coat – a brown coat which is approximately 8 mm in S4, 7 mm in S7, and 8 mm in S8, and, a scratch coat, which is approximately 10 mm in S4, 7 mm in S7, and 14 mm in S8;

(b) Overall nominal thickness of stucco range from 18 mm in S4, to 16 mm in S7, to 22 mm in S8;

(c) Overall good bond between two coats of stucco in each sample, the interface between brown and scratch coats are marked with dashed lines; and,

(d) Variable color tones and densities of brown and scratch coats of stucco indicating variations in mix proportions of individual coats across three sample locations.

MICROGRAPHS OF LAPPED CROSS SECTION

Figure 24: Micrographs of lapped cross section of stucco Sample S4 from north elevation showing: (a) the brown and scratch coats of stucco in the top row where relatively denser nature of the brown coat and porous popcorn-type texture of scratch coat are seen; dashed line separates the two coats; (b) higher magnification view of the brown coat showing distribution of fine crushed sand particles in a light gray toned paste and overall dense nature of brown coat; and (c) the porous popcorn-type texture of scratch coat where sand particles are relatively coarser in size than sand in the brown coat. Scale bars are 3 mm in the top row and 1 mm in the middle and bottom rows.

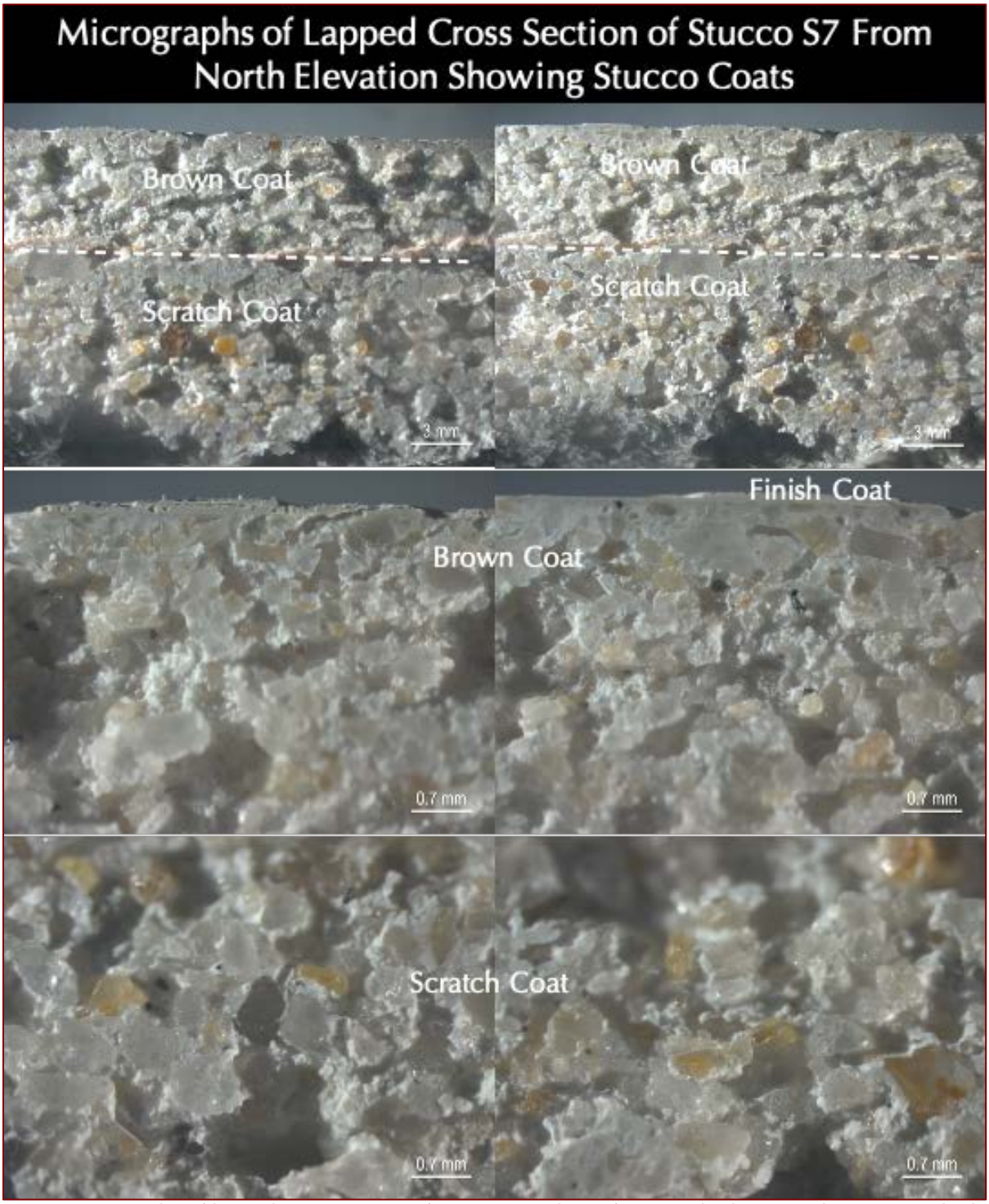

Figure 25: Micrographs of lapped cross section of stucco Sample S7 from south elevation showing: (a) the brown and scratch coats of stucco in the top row where relatively denser nature of the brown coat and porous popcorn-type texture of scratch coat are seen; dashed line separates the two coats; (b) higher magnification view of the brown coat showing distribution of fine crushed sand particles in a light gray toned paste and overall dense nature of brown coat; and (c) the porous popcorn-type texture of scratch coat where sand particles are relatively coarser in size than sand in the brown coat. Scale bars are 3 mm in the top row and 1 mm in the middle and bottom rows.

Figure 26: Micrographs of lapped cross section of stucco Sample S8 from east elevation showing: (a) the brown and scratch coats of stucco in the top row where relatively denser nature of the brown coat and porous popcorn-type texture of scratch coat are seen; dashed line separates the two coats; (b) higher magnification view of the brown coat showing distribution of fine crushed sand particles in a light gray toned paste and overall dense nature of brown coat; and (c) the porous popcorn-type texture of scratch coat where sand particles are relatively coarser in size than sand in the brown coat. Scale bars are 3 mm in the top row and 1 mm in the middle and bottom rows.

THIN SECTIONS

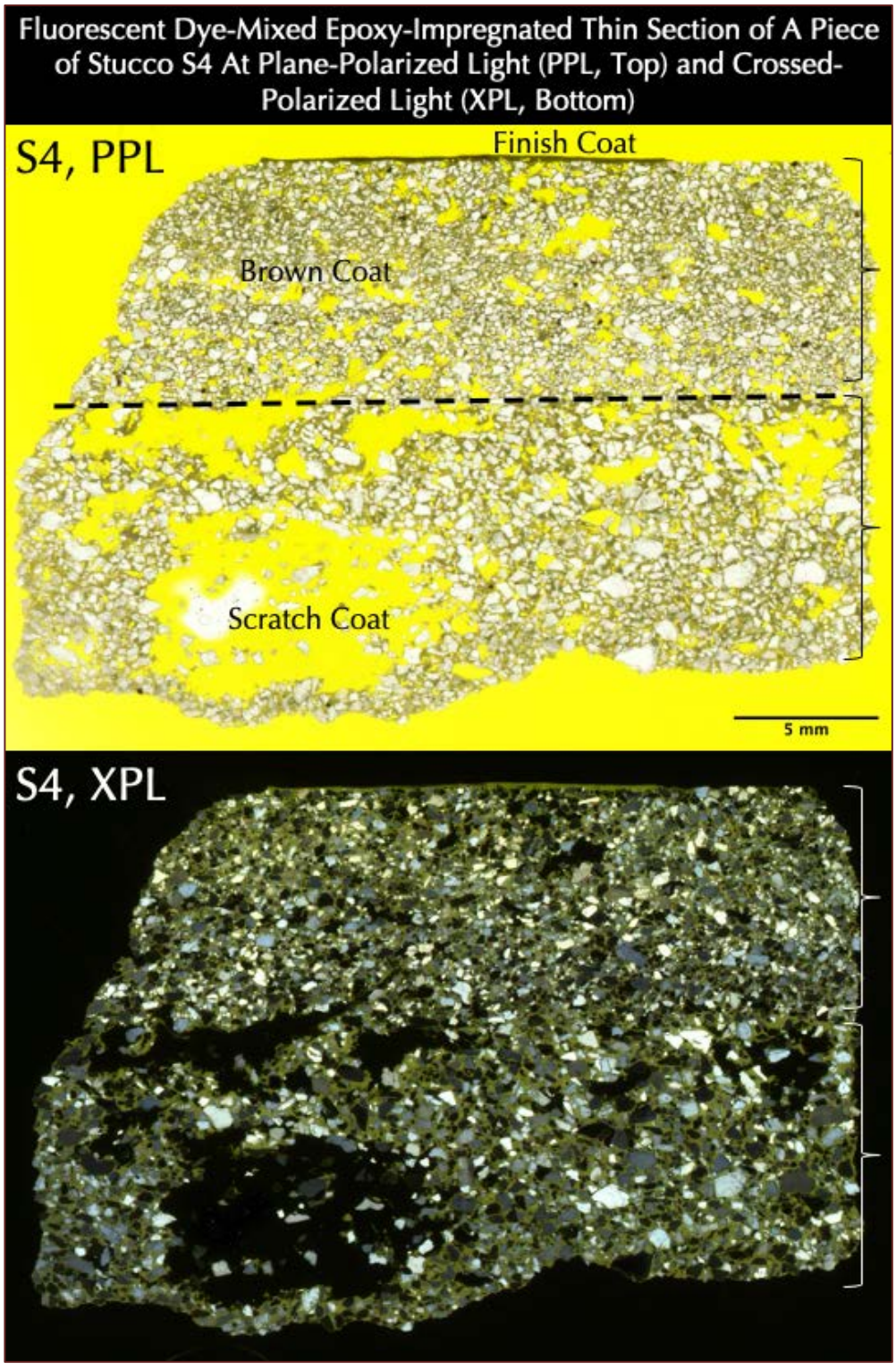

Figure 27: Fluorescent dye-mixed epoxy-impregnated 50 mm x 75 mm size thin section of stucco in Sample S4 scanned on a film scanner in plane (PPL) and crossed (XPL) polarized-light modes with one or two perpendicular polarizing filters, respectively showing:

(a) Size, shape, angularity, gradation, and distribution of sand particles in brown and scratch coats in PPL and XPL images;

(b) A thin paint (finish) coat adhered to the brown coat and seen as a dark brown layer at the top in PPL image;

(c) Relatively finer overall grain-size of sand in the brown coat than sand found in the scratch coat, which is seen in both PPL and XPL images; sand in both coats are angular in nature indicating use of crushed sand;

(d) Siliceous composition of crushed sand revealed in XPL image,

(e) Overall carbonated nature of paste in XPL image,

(f) Overall porous nature of scratch coat relative to the brown coat in PPL image, and,

(g) Overall good bond between the two coats and between the paint and topcoat in PPL image.

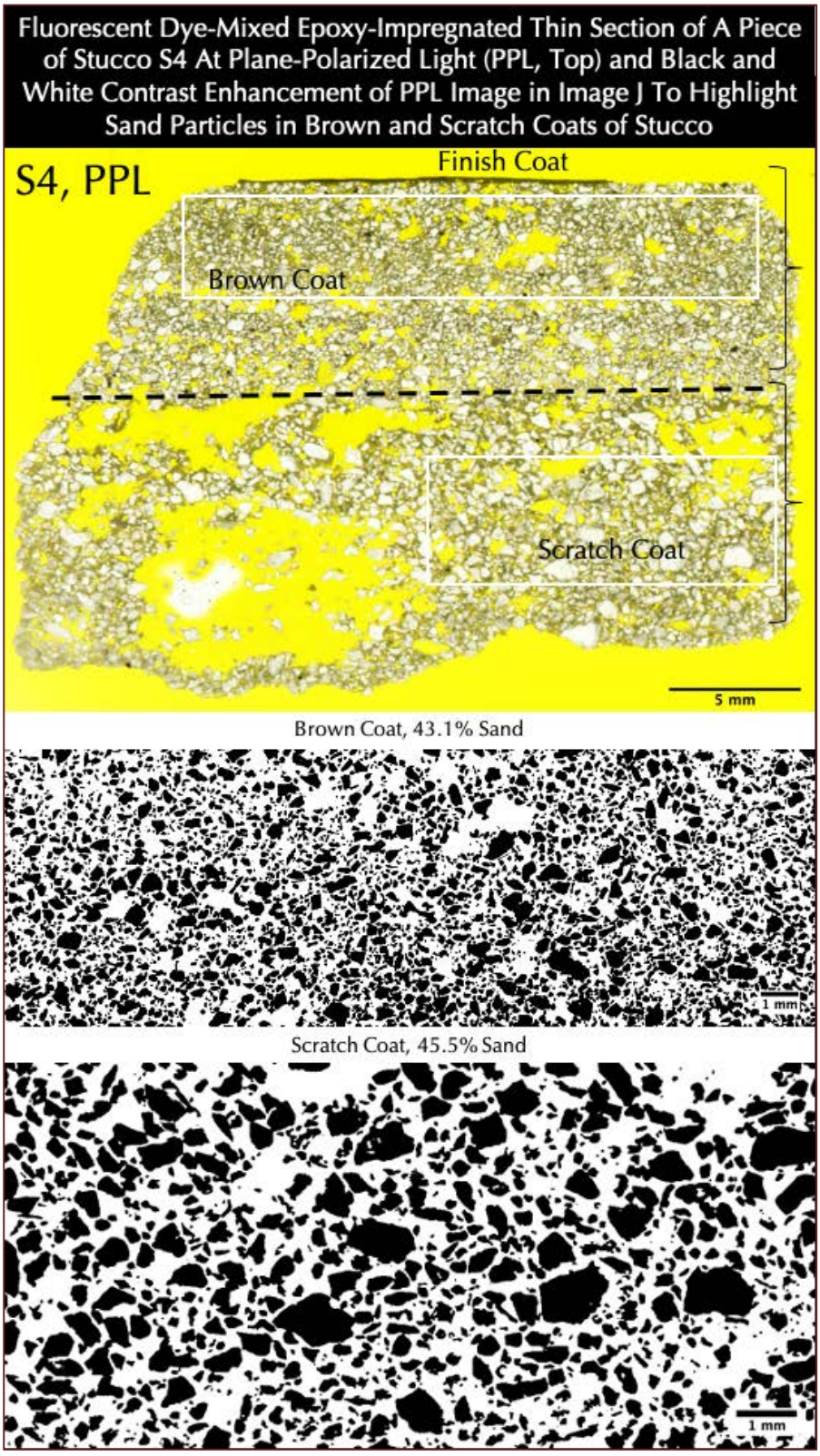

Figure 28: Fluorescent dye-mixed epoxy-impregnated 50 mm x 75 mm size thin section of stucco in Sample S4 scanned on a film scanner in plane (PPL) and crossed (XPL) polarized-light modes with one or two perpendicular polarizing filters, respectively showing:

(a) Size, shape, angularity, gradation, and distribution of sand particles in brown and scratch coats in PPL and XPL images;

(b) A thin paint (finish) coat adhered to the brown coat seen as a dark brown layer at the top in PPL image;

(c) Relatively finer overall grain-size of sand in the brown coat than sand found in the scratch coat, which is seen in both PPL and XPL images; sand in both coats are angular in nature indicating use of crushed sand;

(d) Siliceous composition of crushed sand revealed in XPL image,

(e) Overall carbonated nature of paste in XPL image,

(f) Overall porous nature of scratch coat relative to the brown coat in PPL image,

(g) Overall good bond between the two coats and between the paint and brown coat in PPL image; and,

(h) Boxed areas in brown and scratch coats were selected for image analysis in Image J to determine sand contents (by volume) in each coat, after converting the images to binary black and white contrasts to highlight sand particles in each coat in black, which showed 43.1% sand in brown coat and 45.5% sand in scratch coat and overall coarser sand in the scratch coat as seen in black and white images.

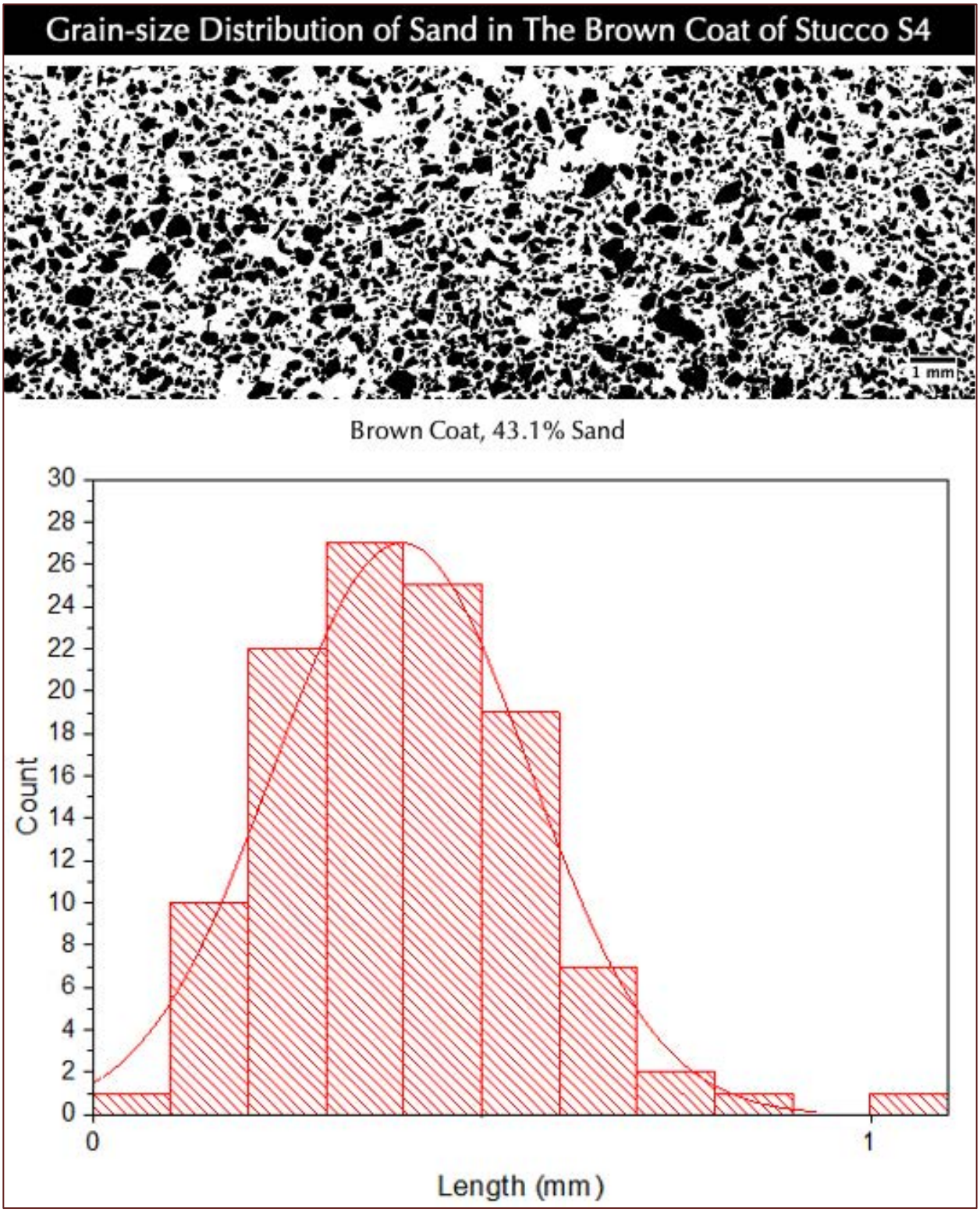

Figure 29: Grain-size distribution of sand in the brown coat from black and white contrast enhancement of boxed area of PPL image of thin section of S4 stucco in Figure 28 showing a normal distribution of sand sizes with a median sand size of around 0.5 mm with almost all of the particles less than a millimeter in grain size. Image analysis of sand sizes were done in Image J.

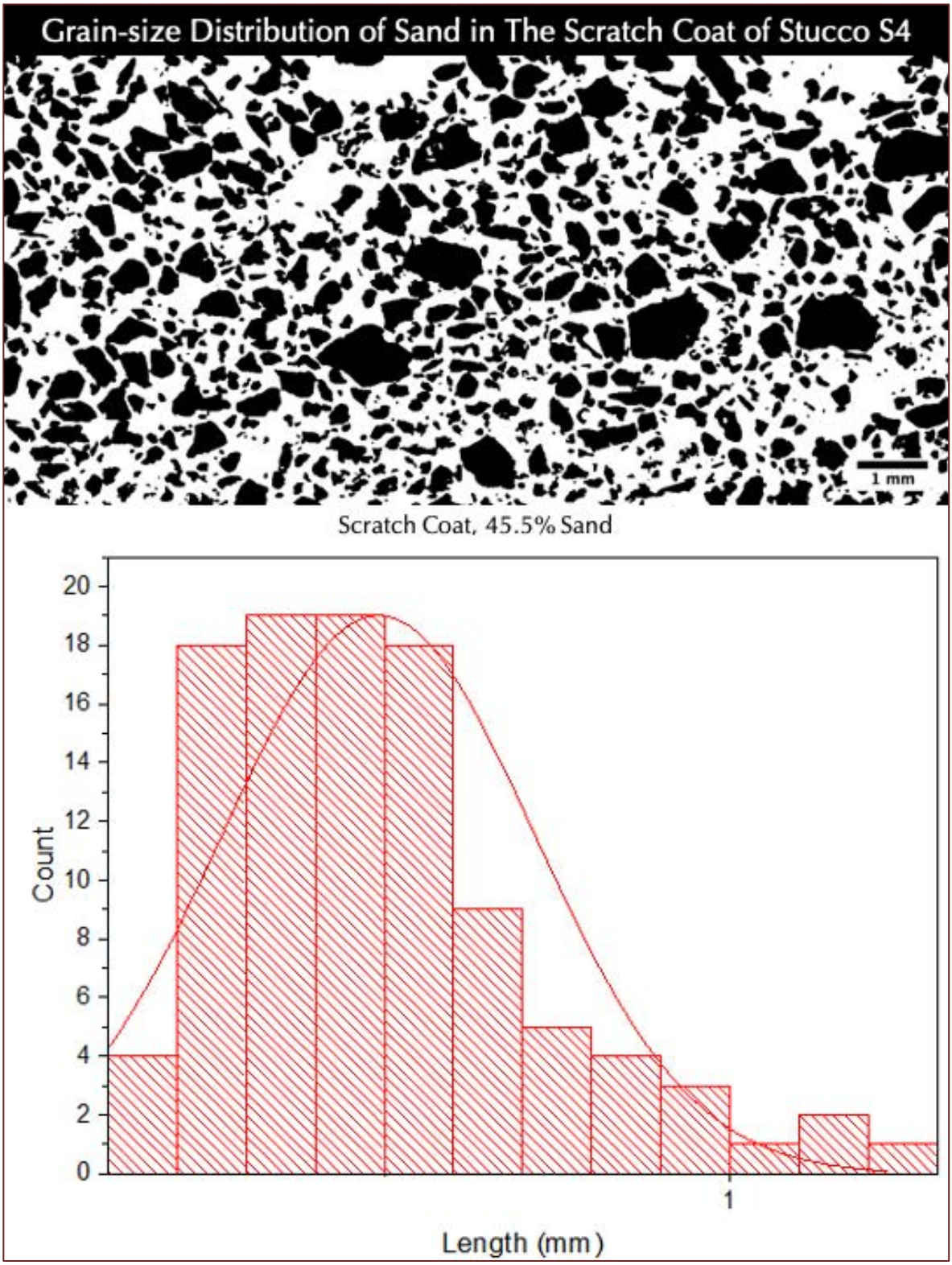

Figure 30: Grain-size distribution of sand in the scratch coat from black and white contrast enhancement of boxed area of PPL image of thin section of S4 stucco in Figure 28 showing a normal distribution of sand sizes with a median sand size of around 0.5 mm with almost all of the particles less than a millimeter in grain size and a fewer particles over 1 mm size which are rare in the brown coat but more in the scratch coat hence giving an overall coarser grain size of sand in the scratch coat. Image analysis of sand sizes were done in Image J.

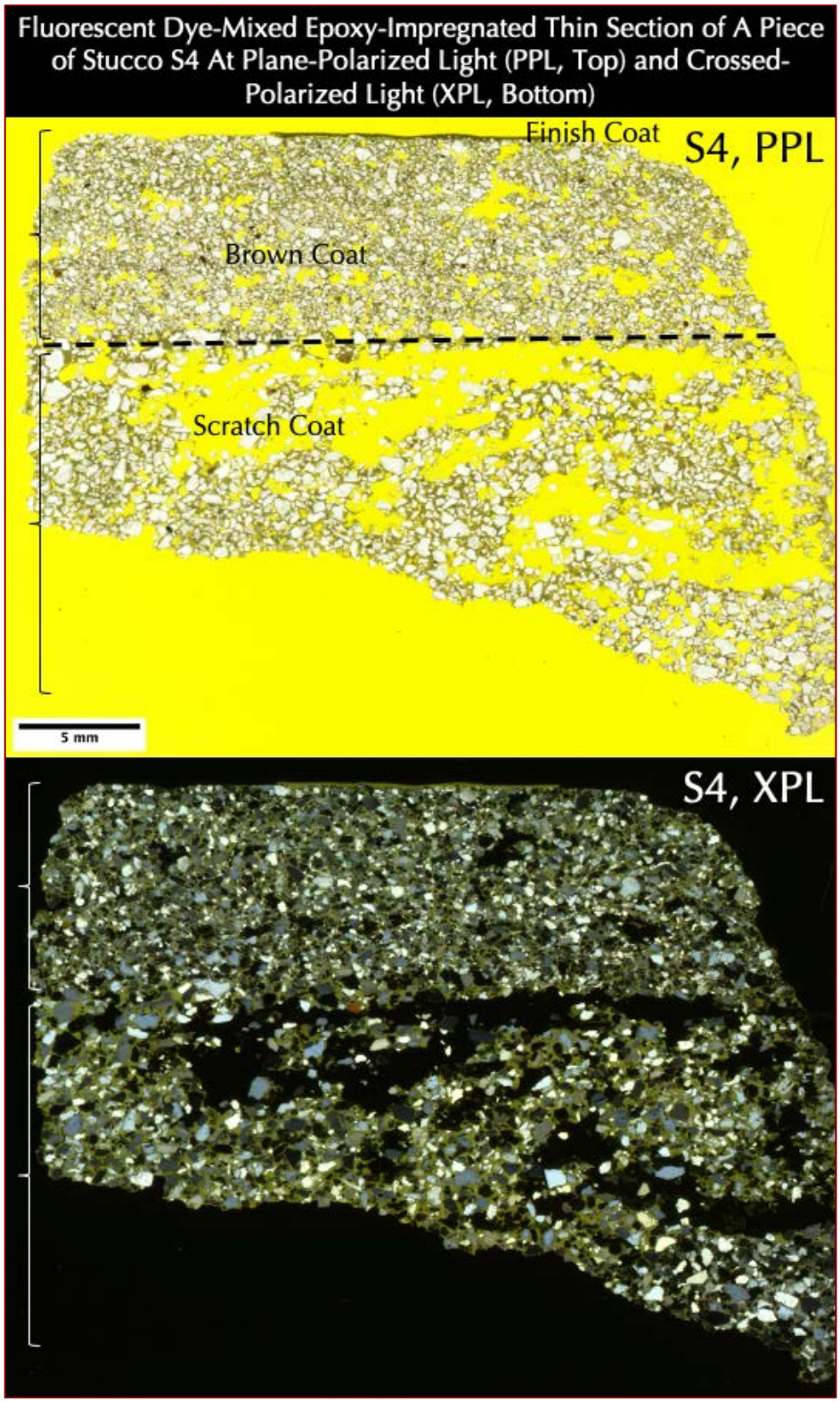

Figure 31: Fluorescent dye-mixed epoxy-impregnated 50 mm x 75 mm size thin section of stucco in Sample S4 scanned on a film scanner in plane (PPL) and crossed (XPL) polarized-light modes with one or two perpendicular polarizing filters, respectively showing:

(a) Size, shape, angularity, gradation, and distribution of sand particles in brown and scratch coats in PPL and XPL images;

(b) A thin paint (finish) coat adhered to the brown coat seen as a dark brown layer at the top in PPL image;

(c) Relatively finer overall grain-size of sand in the brown coat than sand found in the scratch coat, which is seen in both PPL and XPL images; sand in both coats are angular in nature indicating use of crushed sand;

(d) Siliceous composition of crushed sand revealed in XPL image,

(e) Overall carbonated nature of paste in XPL image,

(f) Overall porous nature of scratch coat relative to the brown coat in PPL image, and,

(g) Overall good bond between the two coats and between the paint and topcoat in PPL image.

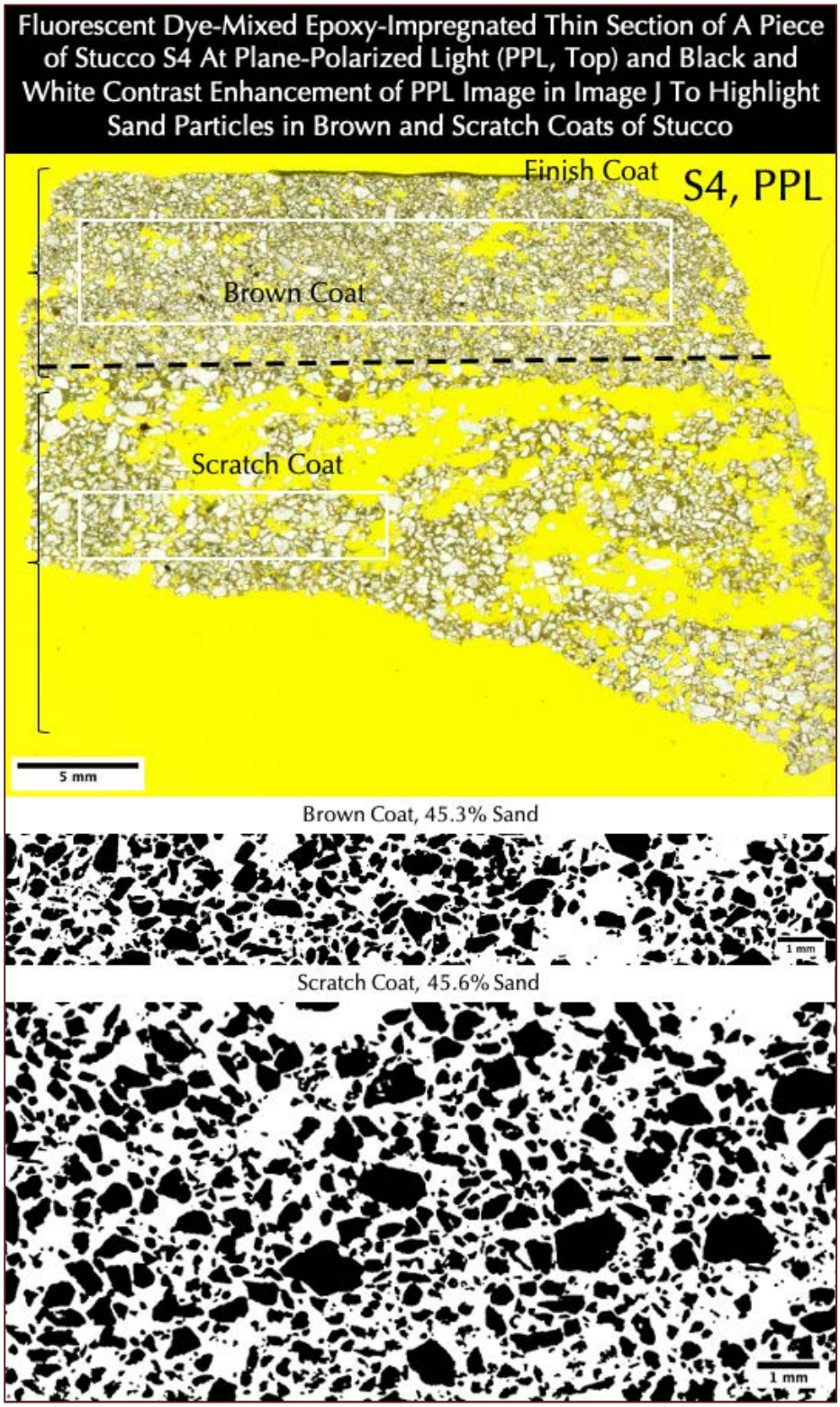

Figure 32: Fluorescent dye-mixed epoxy-impregnated 50 mm x 75 mm size thin section of stucco in Sample S4 scanned on a film scanner in plane (PPL) polarized-light mode with one polarizing filter showing:

(a) Size, shape, angularity, gradation, and distribution of sand particles in brown and scratch coats;

(b) A thin paint (finish) coat adhered to the brown coat seen as a dark brown layer at the top;

(c) Relatively finer overall grain-size of sand in the brown coat than sand found in the scratch coat; sand in both coats are angular in nature indicating use of crushed sand;

(d) Overall porous nature of scratch relative to the brown coat;

(e) Overall good bond between the two coats and between the paint and topcoat; and,

(f) Boxed areas in brown and scratch coats were selected for image analysis in Image J to determine sand contents (by volume) in each coat, after converting the images to binary black and white contrasts to highlight sand particles in each coat in black, which showed 45.3% sand in brown coat and 45.6% sand in scratch coat, and overall coarser sand in the scratch coat as seen in black and white images.

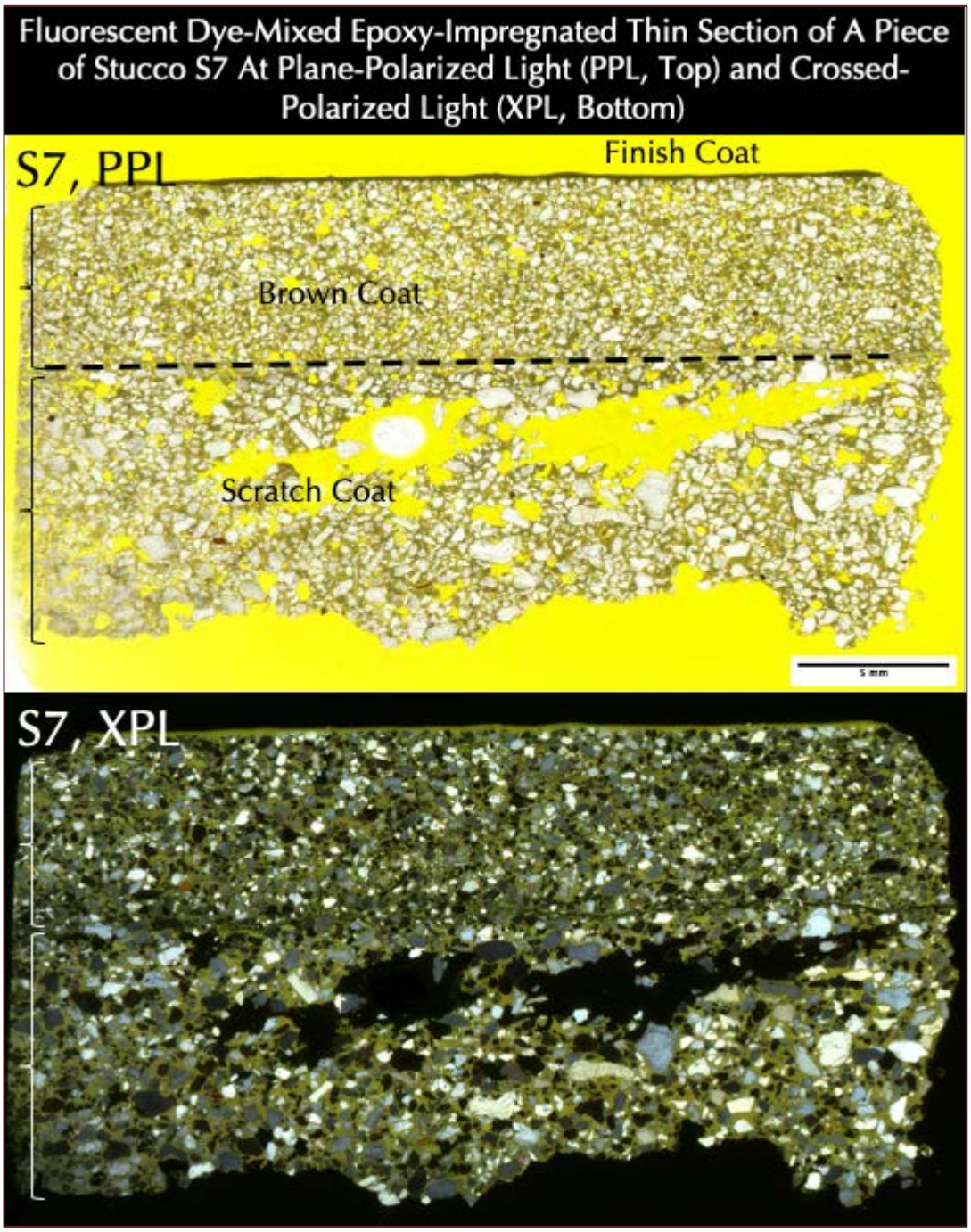

Figure 33: Fluorescent dye-mixed epoxy-impregnated 50 mm x 75 mm size thin section of stucco in Sample S7 scanned on a film scanner in plane (PPL) and crossed (XPL) polarized-light modes with one or two perpendicular polarizing filters, respectively showing:

(a) Size, shape, angularity, gradation, and distribution of sand particles in brown and scratch coats in PPL and XPL images;

(b) A thin paint (finish) coat adhered to the brown coat seen as a dark brown layer at the top in PPL image;

(c) Relatively finer overall grain-size of sand in the brown coat than sand found in the scratch coat, which is seen in both PPL and XPL images; sand in both coats are angular in nature indicating use of crushed sand;

(d) Siliceous composition of crushed sand revealed in XPL image,

(e) Overall carbonated nature of paste in XPL image,

(f) Overall porous nature of scratch coat relative to the brown coat in PPL image, and,

(g) Overall good bond between the two coats and between the paint and topcoat in PPL image.

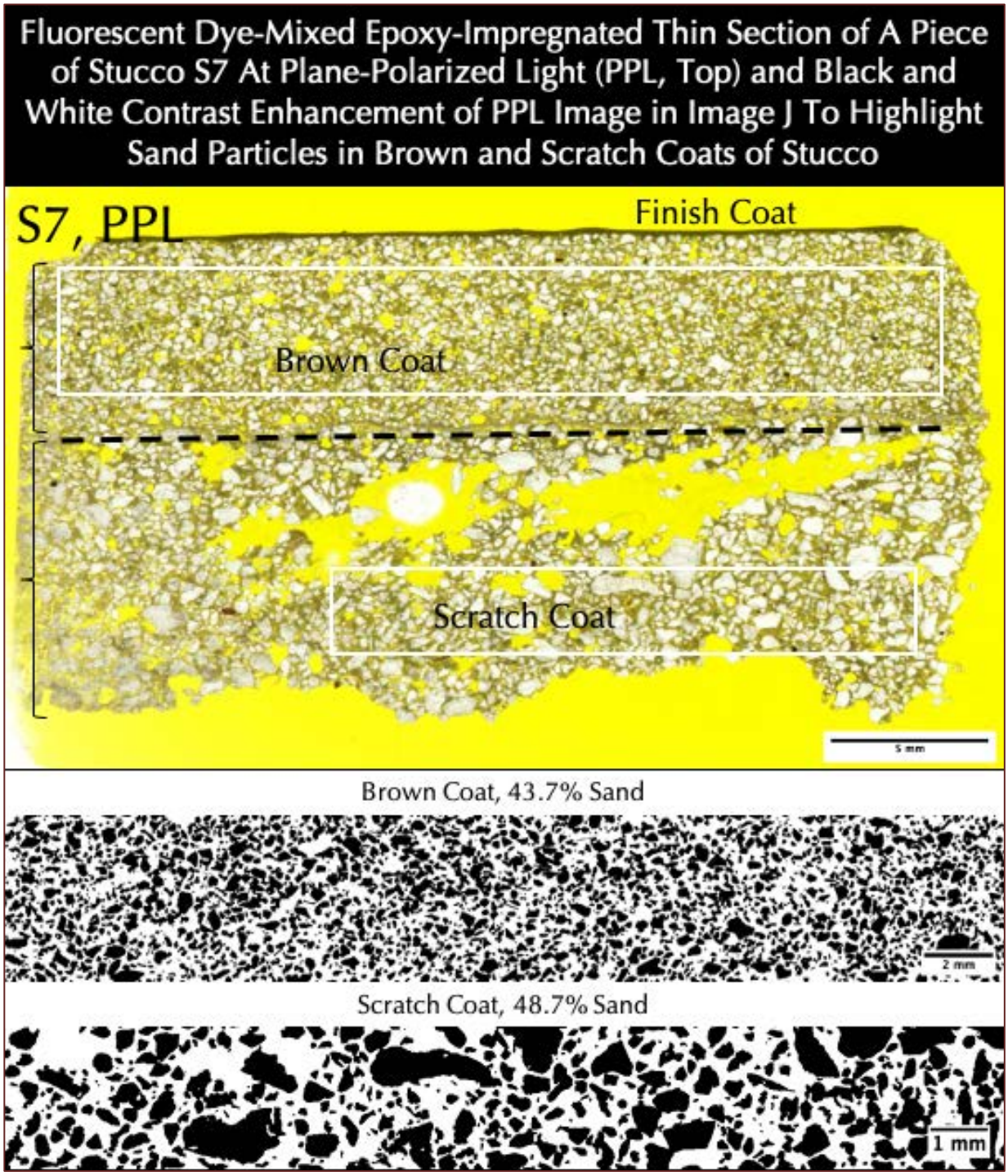

Figure 34: Fluorescent dye-mixed epoxy-impregnated 50 mm x 75 mm size thin section of stucco in Sample S7 scanned on a film scanner in plane (PPL) polarized-light mode showing: (a) size, shape, angularity, gradation, and distribution of sand particles in brown and scratch coats; (b) a thin paint (finish) coat adhered to the brown coat seen as a dark brown layer at the top; (c) relatively finer overall grain-size of sand in the brown coat than sand found in the scratch coat; and sand in both coats are angular in nature indicating use of crushed sand; (d) overall porous nature of scratch coat relative to the brown coat, (e) overall good bond between the two coats and between the paint and brown coat; and, (f) boxed areas in brown and scratch coats were selected for image analysis in Image J to determine sand contents (by volume) in each coat, after converting the images to binary black and white contrasts to highlight sand particles in each coat in black, which showed 43.7% sand in brown coat and 48.7% sand in scratch coat, and overall coarser sand in the scratch coat as seen in black and white images.

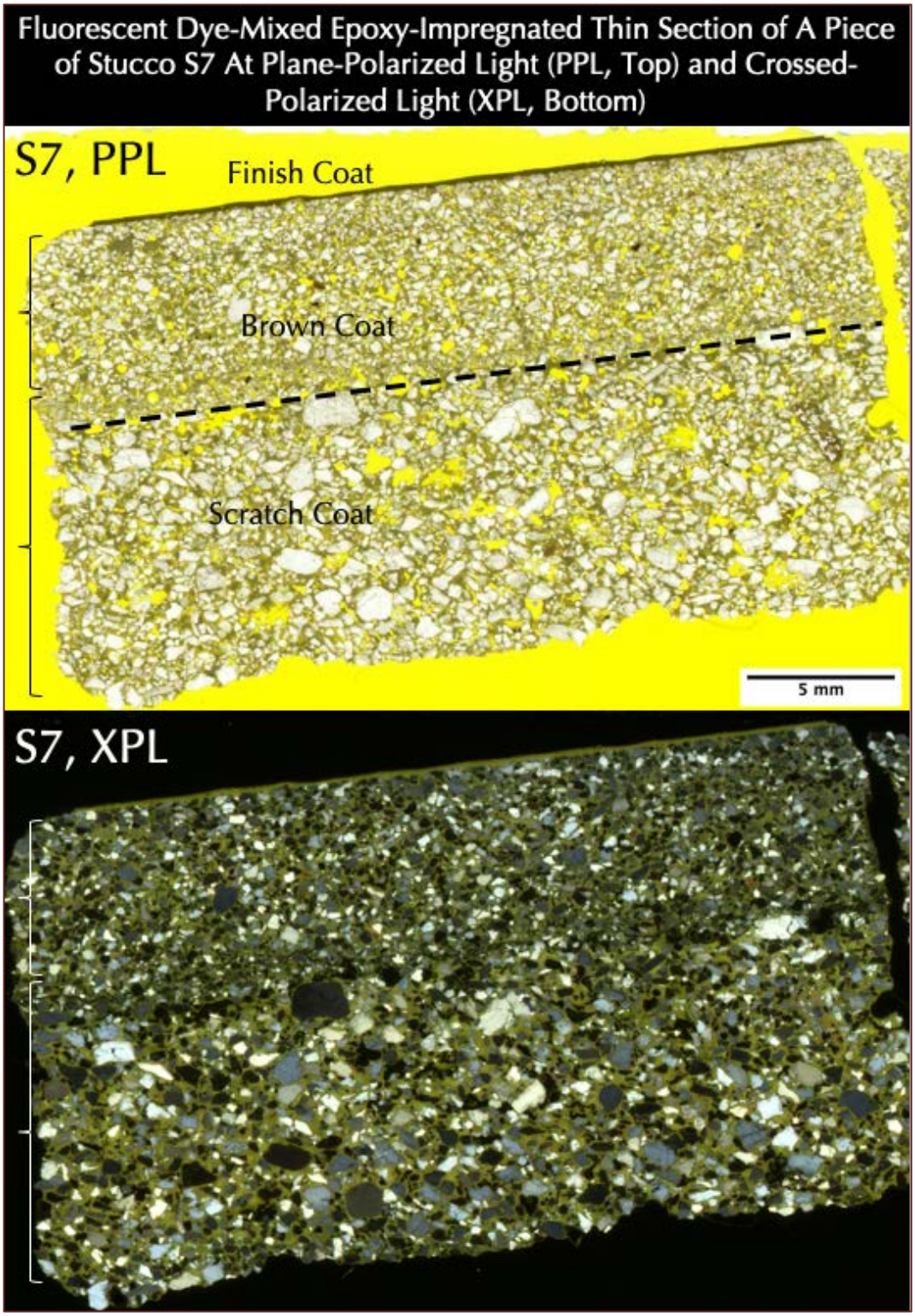

Figure 35: Fluorescent dye-mixed epoxy-impregnated 50 mm x 75 mm size thin section of stucco in Sample S7 scanned on a film scanner in plane (PPL) and crossed (XPL) polarized-light modes with one or two perpendicular polarizing filters, respectively showing:

(a) Size, shape, angularity, gradation, and distribution of sand particles in brown and scratch coats in PPL and XPL images;

(b) A thin paint (finish) coat adhered to the brown coat seen as a dark brown layer at the top in PPL image;

(c) Relatively finer overall grain-size of sand in the brown coat than sand found in the scratch coat, which is seen in both PPL and XPL images; sand in both coats are angular in nature indicating use of crushed sand;

(d) Siliceous composition of crushed sand revealed in XPL image,

(e) Overall carbonated nature of paste in XPL image,

(f) Overall porous nature of scratch coat relative to the brown coat in PPL image, and,

(g) Overall good bond between the two coats and between the paint and topcoat in PPL image.

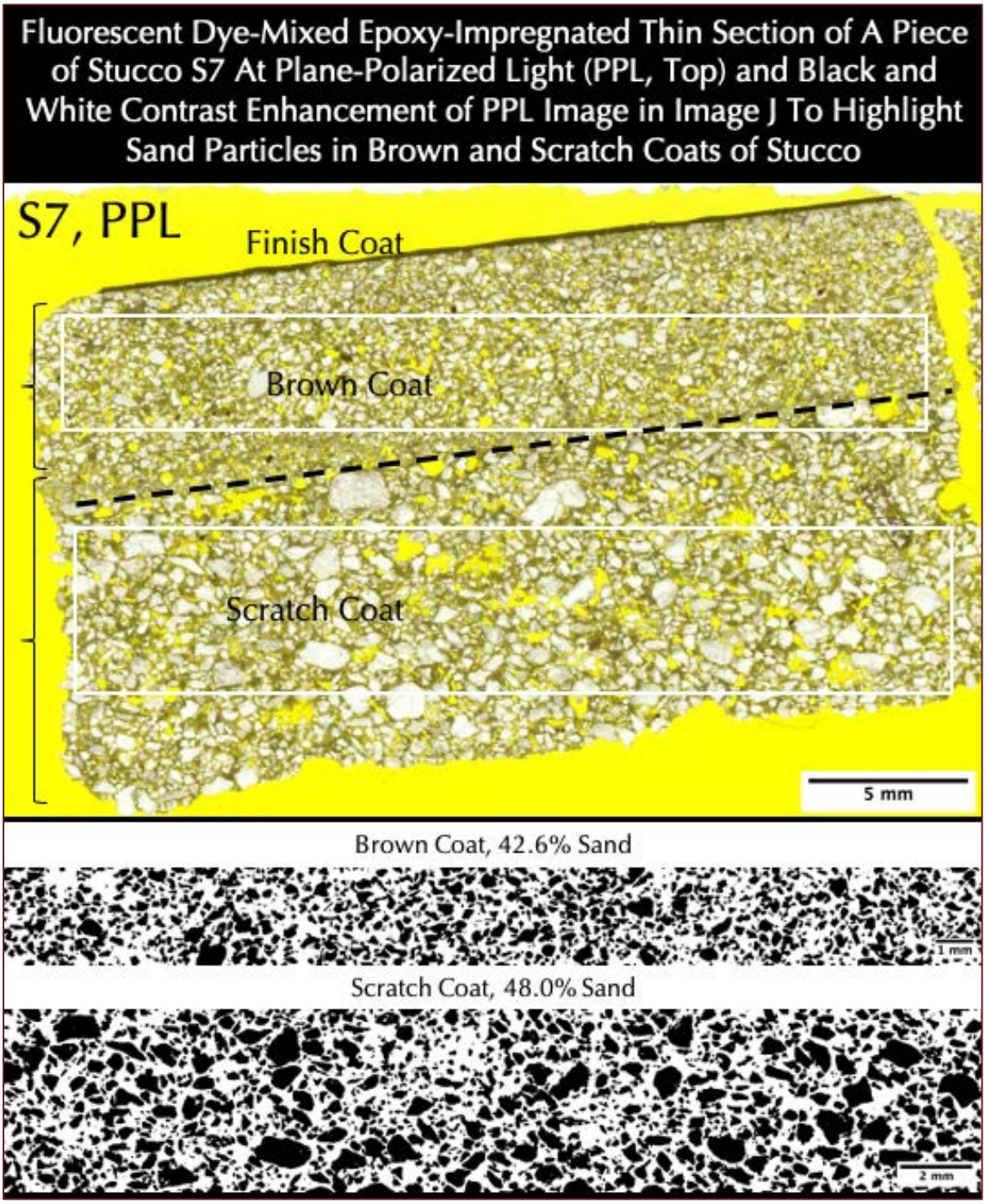

Figure 36: Fluorescent dye-mixed epoxy-impregnated 50 mm x 75 mm size thin section of stucco in Sample S7 scanned on a film scanner in plane (PPL) polarized-light mode showing: (a) size, shape, angularity, gradation, and distribution of sand particles in brown and scratch coats; (b) a thin paint (finish) coat adhered to the brown coat seen as a dark brown layer at the top; (c) relatively finer overall grain-size of sand in the brown coat than sand found in the scratch coat; sand in both coats are angular in nature indicating use of crushed sand; (d) overall porous nature of scratch coat relative to the brown coat, (e) overall good bond between the two coats and between the paint and brown coat; and, (f) boxed areas in brown and scratch coats were selected for image analysis in Image J to determine sand contents (by volume) in each coat, after converting the images to binary black and white contrasts to highlight sand particles in each coat in black, which showed 42.6% sand in brown coat and 48.0% sand in scratch coat, and overall coarser sand in the scratch coat as seen in black and white images.

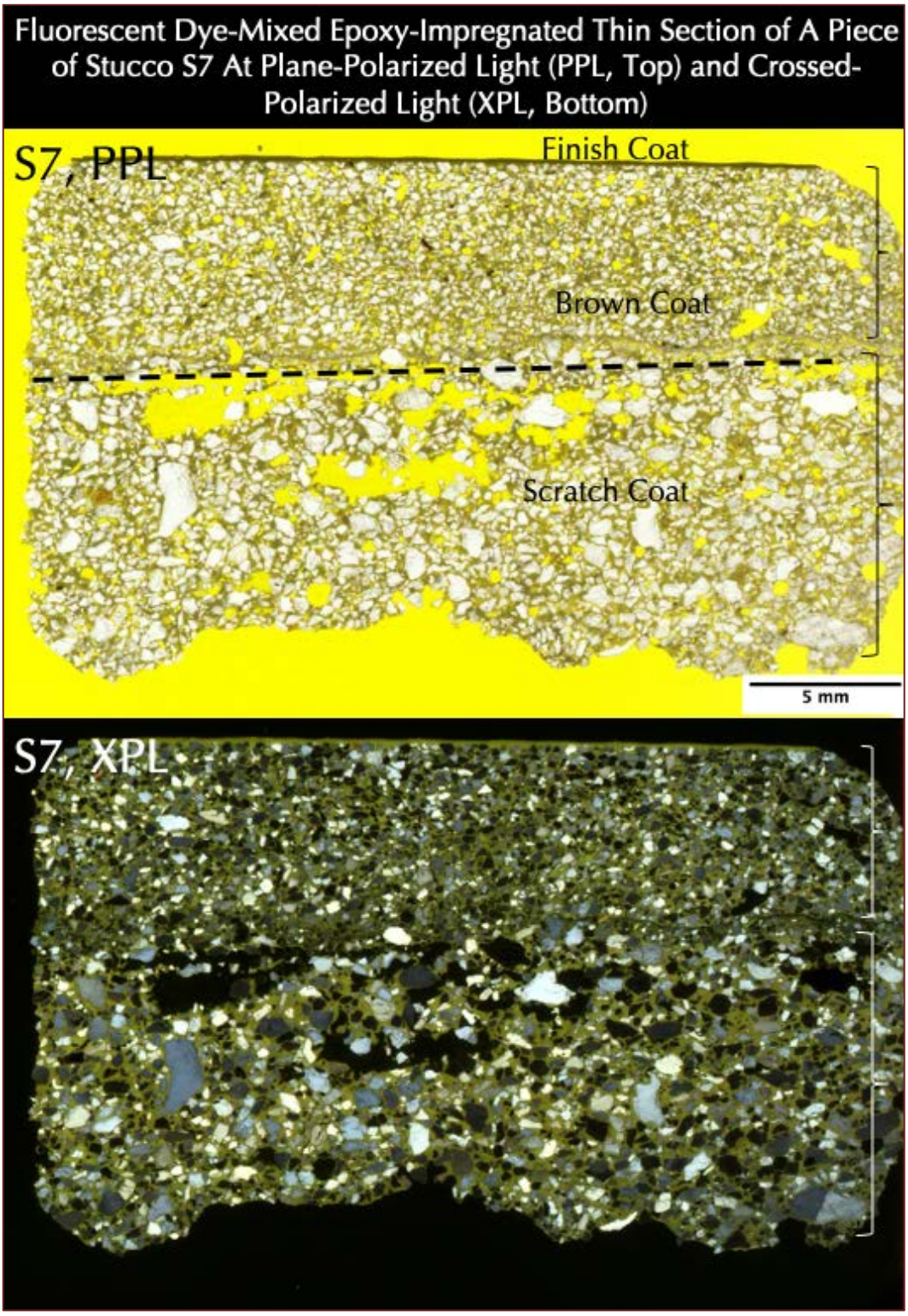

Figure 37: Fluorescent dye-mixed epoxy-impregnated 50 mm x 75 mm size thin section of stucco in Sample S7 scanned on a film scanner in plane (PPL) and crossed (XPL) polarized-light modes with one or two perpendicular polarizing filters, respectively showing:

(a) Size, shape, angularity, gradation, and distribution of sand particles in brown and scratch coats in PPL and XPL images;

(b) A thin paint (finish) coat adhered to the topcoat seen as a dark brown layer at the top in PPL image;

(c) Relatively finer overall grain-size of sand in the brown coat than sand found in the scratch coat, which is seen in both PPL and XPL images; sand in both coats are angular in nature indicating use of crushed sand;

(d) Siliceous composition of crushed sand revealed in XPL image,

(e) Overall carbonated nature of paste in XPL image,

(f) Overall porous nature of scratch coat relative to the brown coat in PPL image, and,

(g) Overall good bond between the two coats and between the paint and topcoat in PPL image.

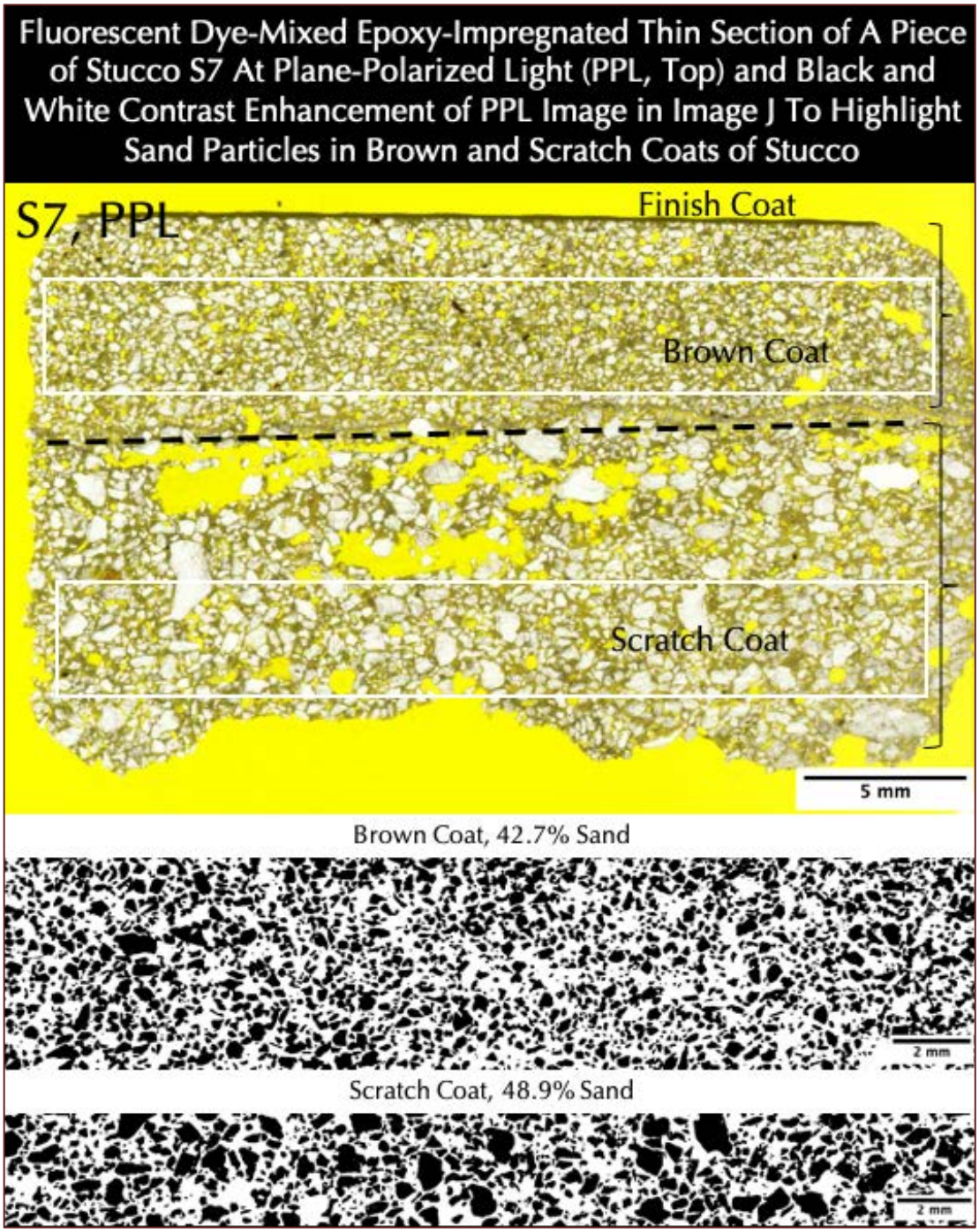

Figure 38: Fluorescent dye-mixed epoxy-impregnated 50 mm x 75 mm size thin section of stucco in Sample S7 scanned on a film scanner in plane (PPL) polarized-light mode showing: (a) size, shape, angularity, gradation, and distribution of sand particles in brown and scratch coats; (b) a thin paint coat adhered to the brown coat seen as a dark brown layer at the top; (c) relatively finer overall grain-size of sand in the brown coat than sand found in the scratch coat; sand in both coats are angular in nature indicating use of crushed sand; (d) overall porous nature of scratch coat relative to the brown coat, (e) overall good bond between the two coats and between the paint and brown coat; and, (f) boxed areas in brown and scratch coats were selected for image analysis in Image J to determine sand contents (by volume) in each coat, after converting the images to binary black and white contrasts to highlight sand particles in each coat in black, which showed 42.7% sand in brown coat and 48.9% sand in scratch coat, and overall coarser sand in the scratch as seen in black and white images.

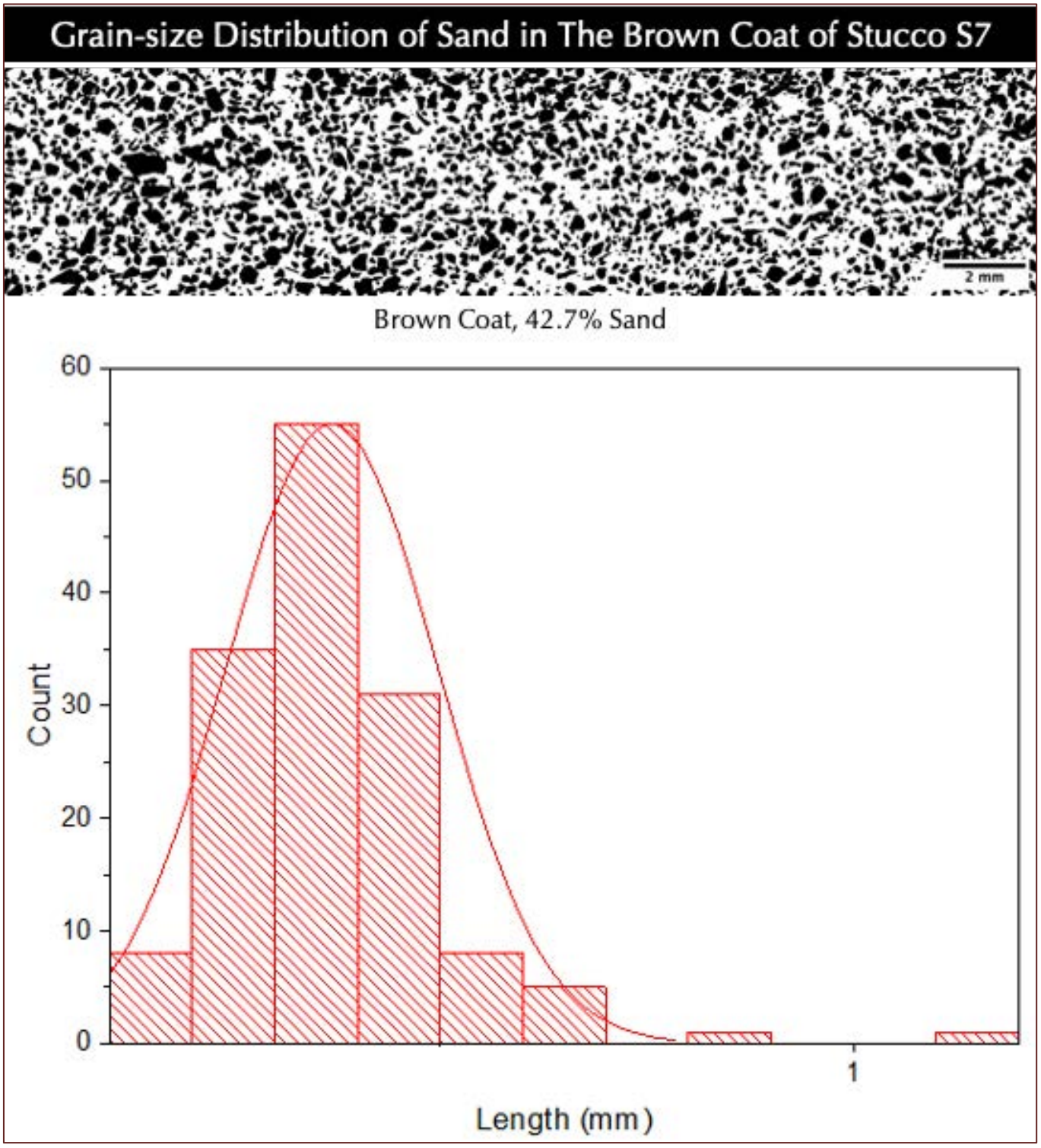

Figure 39: Grain-size distribution of sand in the brown coat from black and white contrast enhancement of boxed area of PPL image of thin section of S7 stucco in Figure 38 showing a normal distribution of sand sizes with a median sand size of around 0.5 mm with almost all of the particles less than a millimeter in grain size. Image analysis of sand sizes were done in Image J.

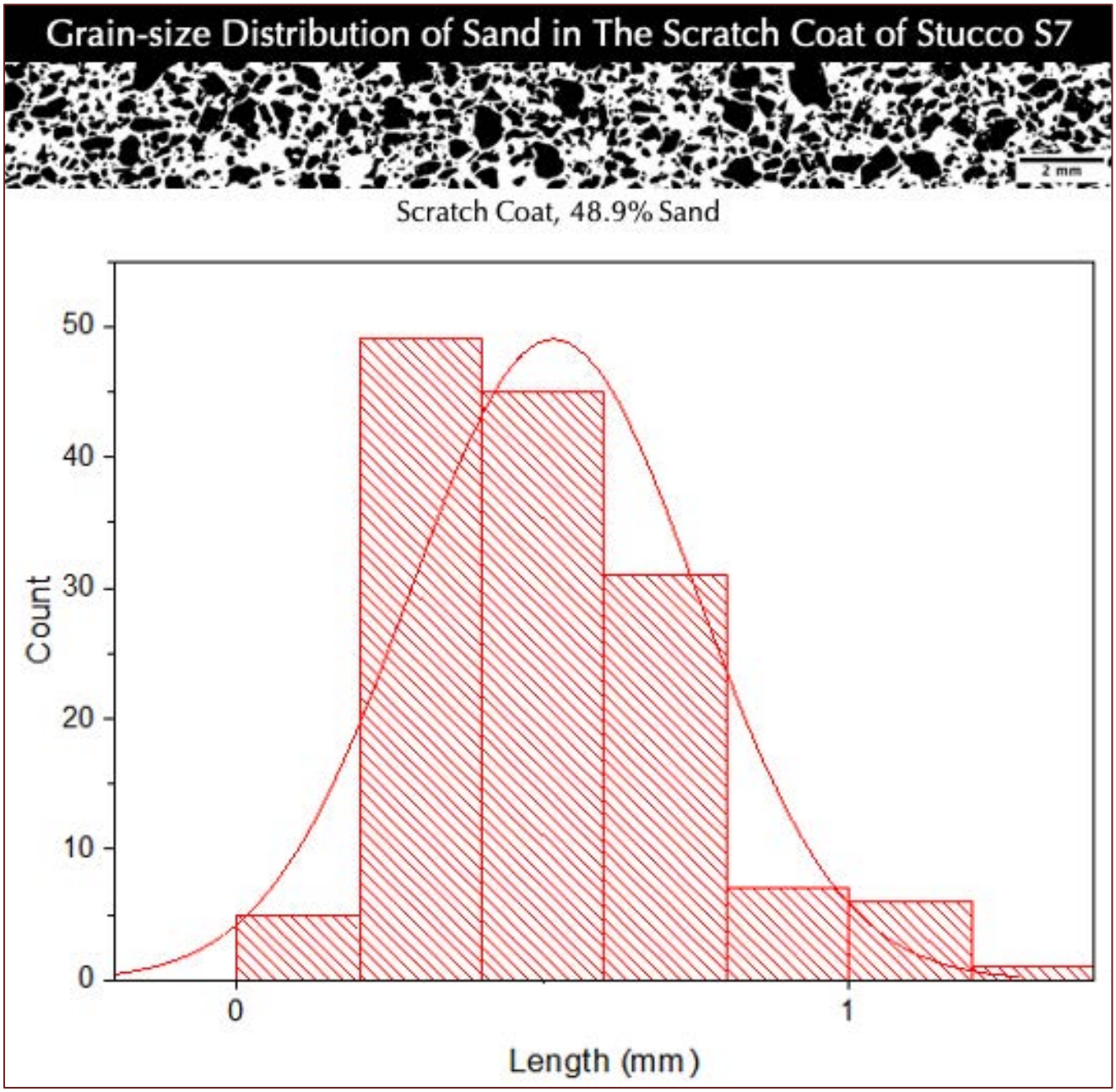

Figure 40: Grain-size distribution of sand in the scratch coat from black and white contrast enhancement of boxed area of PPL image of thin section of S7 stucco in Figure 38 showing a normal distribution of sand sizes with a median sand size of around 0.5 mm with almost all of the particles less than a millimeter in grain size and a few particles over 1 mm size which are rare in the brown coat but more in the scratch coat hence giving an overall coarser grain size of sand in the scratch coat. Image analysis of sand sizes were done in Image J.

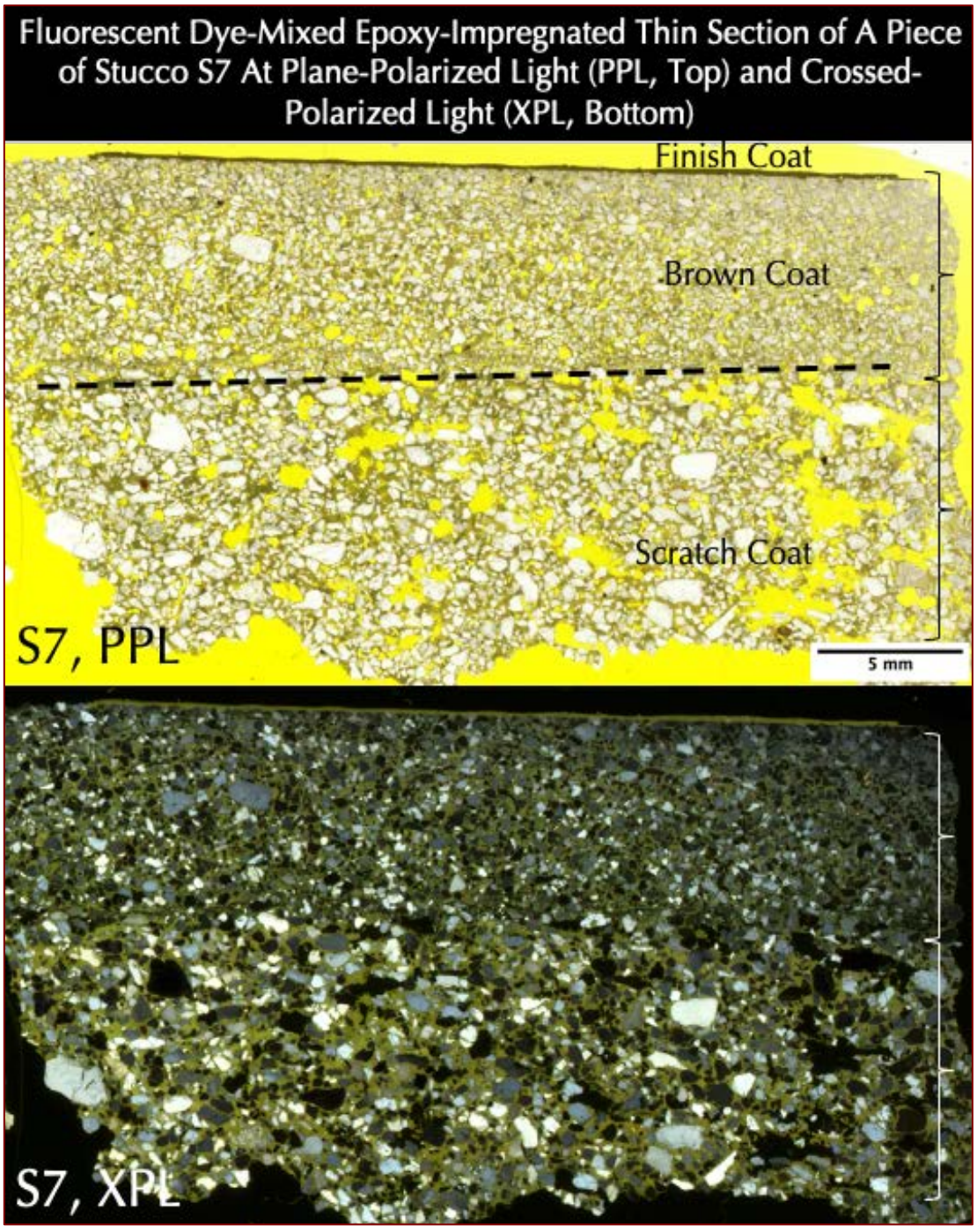

Figure 41: Fluorescent dye-mixed epoxy-impregnated 50 mm x 75 mm size thin section of stucco in Sample S7 scanned on a film scanner in plane (PPL) and crossed (XPL) polarized-light modes with one or two perpendicular polarizing filters, respectively showing:

(a) Size, shape, angularity, gradation, and distribution of sand particles in brown and scratch coats in PPL and XPL images;

(b) A thin paint (finish) coat adhered to the brown coat seen as a dark brown layer at the top in PPL image;

(c) Relatively finer overall grain-size of sand in the brown coat than sand found in the scratch coat, which is seen in both PPL and XPL images; sand in both coats are angular in nature indicating use of crushed sand;

(d) Siliceous composition of crushed sand revealed in XPL image;

(e) Overall carbonated nature of paste in XPL image;

(f) Overall porous nature of scratch coat relative to the brown coat in PPL image; and,

(g) Overall good bond between the two coats and between the paint and topcoat in PPL image.

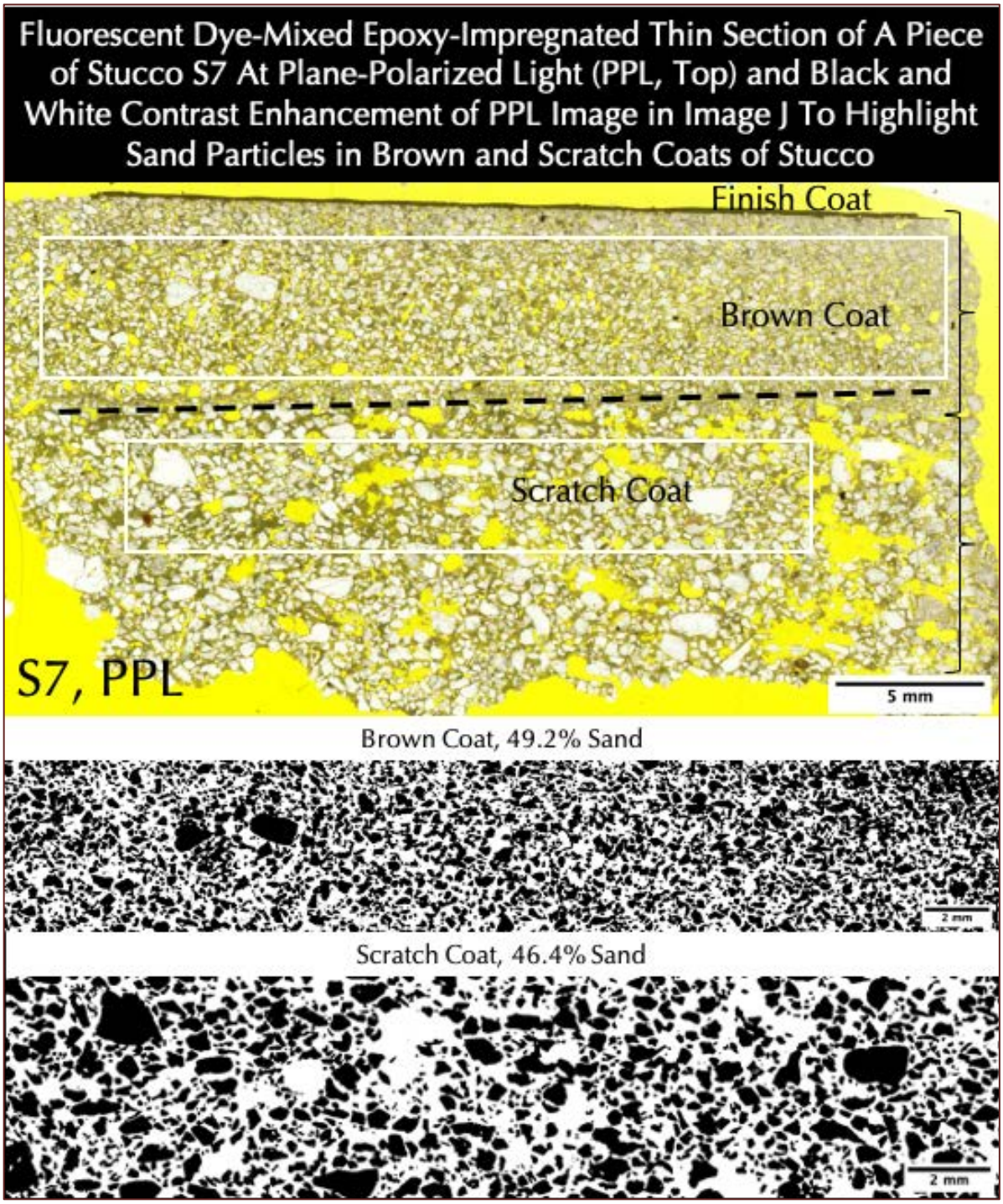

Figure 42: Fluorescent dye-mixed epoxy-impregnated 50 mm x 75 mm size thin section of stucco in Sample S7 scanned on a film scanner in plane (PPL) polarized-light mode showing: (a) size, shape, angularity, gradation, and distribution of sand particles in brown and scratch coats; (b) a thin paint (finish) coat adhered to the brown coat seen as a dark brown layer at the top; (c) relatively finer overall grain-size of sand in the brown coat than sand found in the scratch coat; sand in both coats are angular in nature indicating use of crushed sand; (d) overall porous nature of scratch coat relative to the brown coat, (e) overall good bond between the two coats and between the paint and brown coat; and, (f) boxed areas in brown and scratch coats were selected for image analysis in Image J to determine sand contents (by volume) in each coat, after converting the images to binary black and white contrasts to highlight sand particles in each coat in black, which showed 49.2% sand in brown coat and 46.4% sand in scratch coat, and overall coarser sand in the scratch coat as seen in black and white images.

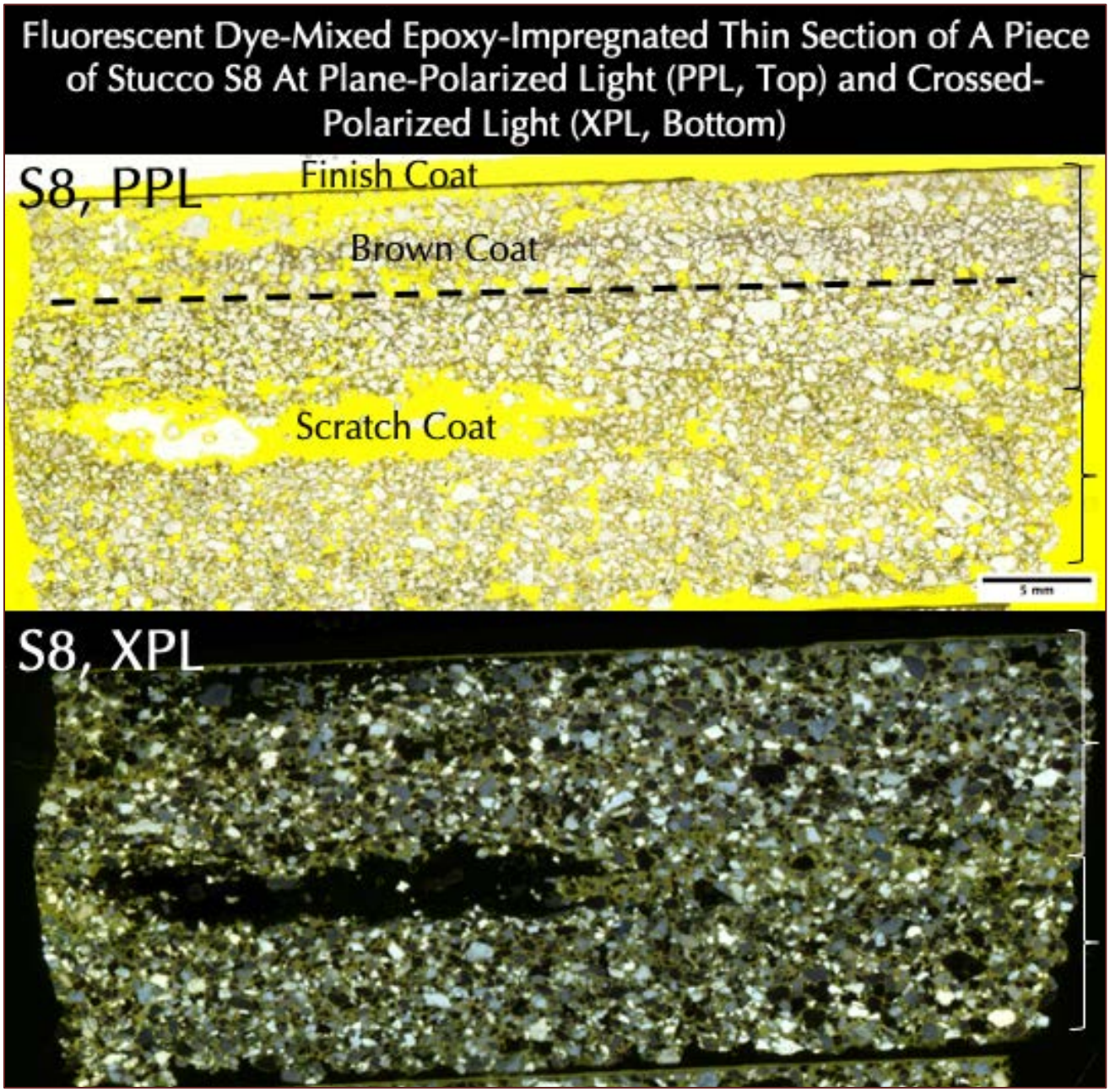

Figure 43: Fluorescent dye-mixed epoxy-impregnated 50 mm x 75 mm size thin section of stucco in Sample S8 scanned on a film scanner in plane (PPL) and crossed (XPL) polarized-light modes with one or two perpendicular polarizing filters, respectively showing: (a) size, shape, angularity, gradation, and distribution of sand particles in brown and scratch coats in PPL and XPL images; (b) a thin paint (finish) coat adhered to the brown coat seen as a dark brown layer at the top in PPL image; (c) relatively finer overall grain-size of sand in the brown coat than sand found in the scratch coat, which is seen in both PPL and XPL images; sand in both coats are angular in nature indicating use of crushed sand; (d) siliceous composition of crushed sand revealed in XPL image, (e) overall carbonated nature of paste in XPL image, (f) overall porous nature of scratch coat relative to the brown coat in PPL image, and, (g) overall good bond between the two coats and between the paint and topcoat in PPL image.

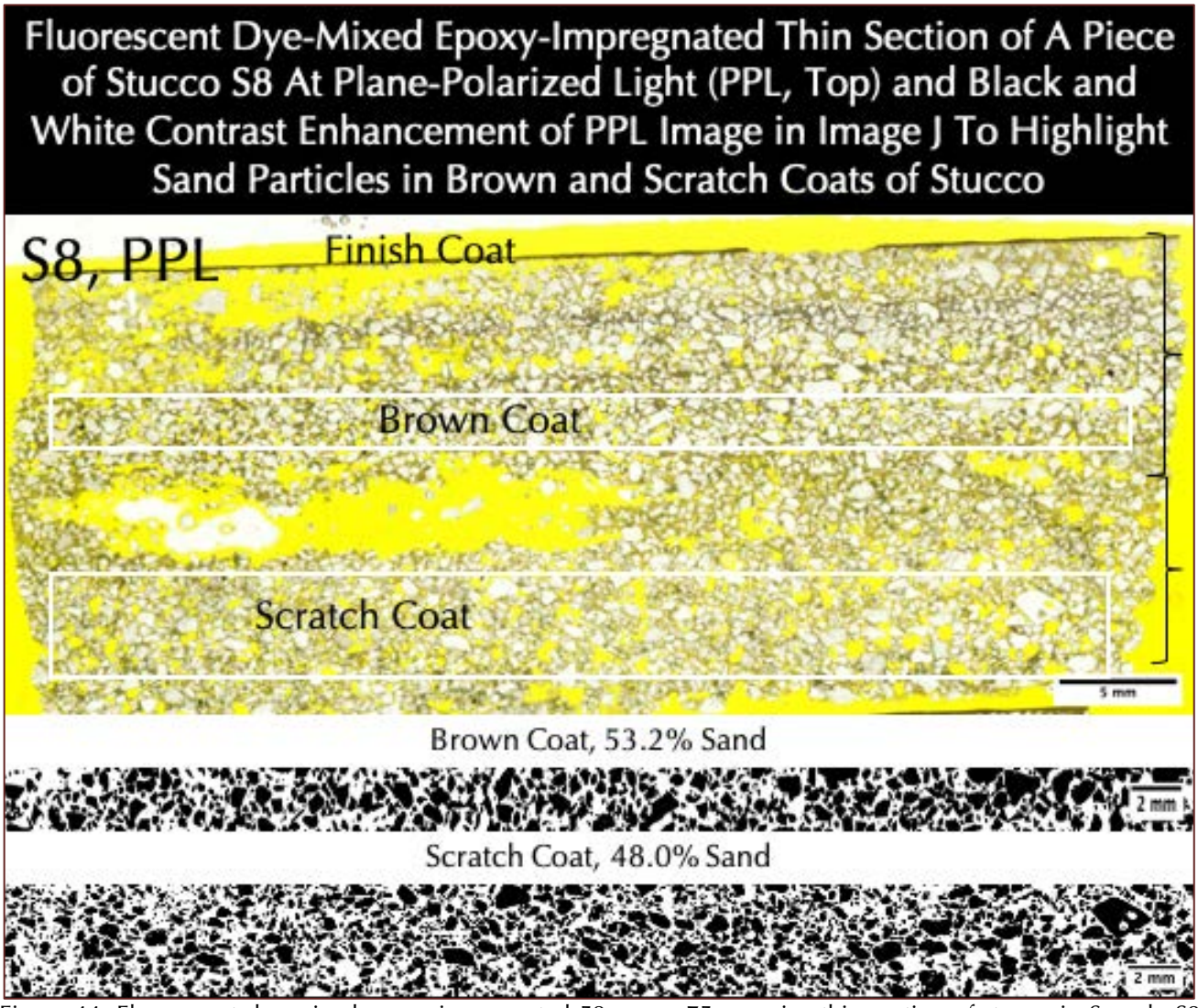

Figure 44: Fluorescent dye-mixed epoxy-impregnated 50 mm x 75 mm size thin section of stucco in Sample S8 scanned on a film scanner in plane (PPL) polarized-light mode showing: (a) size, shape, angularity, gradation, and distribution of sand particles in brown and scratch coats; (b) a thin paint (finish) coat adhered to the brown coat seen as a dark brown layer at the top; (c) relatively finer overall grain-size of sand in the brown coat than sand found in the scratch coat; sand in both coats are angular in nature indicating use of crushed sand; (d) overall porous nature of scratch coat relative to the brown coat, (e) overall good bond between the two coats and between the paint and brown coat; and, (f) boxed areas in brown and scratch coats were selected for image analysis in Image J to determine sand contents (by volume) in each coat, after converting the images to binary black and white contrasts to highlight sand particles in each coat in black, which showed 53.2% sand in brown coat and 48.0% sand in scratch coat, and overall coarser sand in the scratch coat as seen in black and white image.

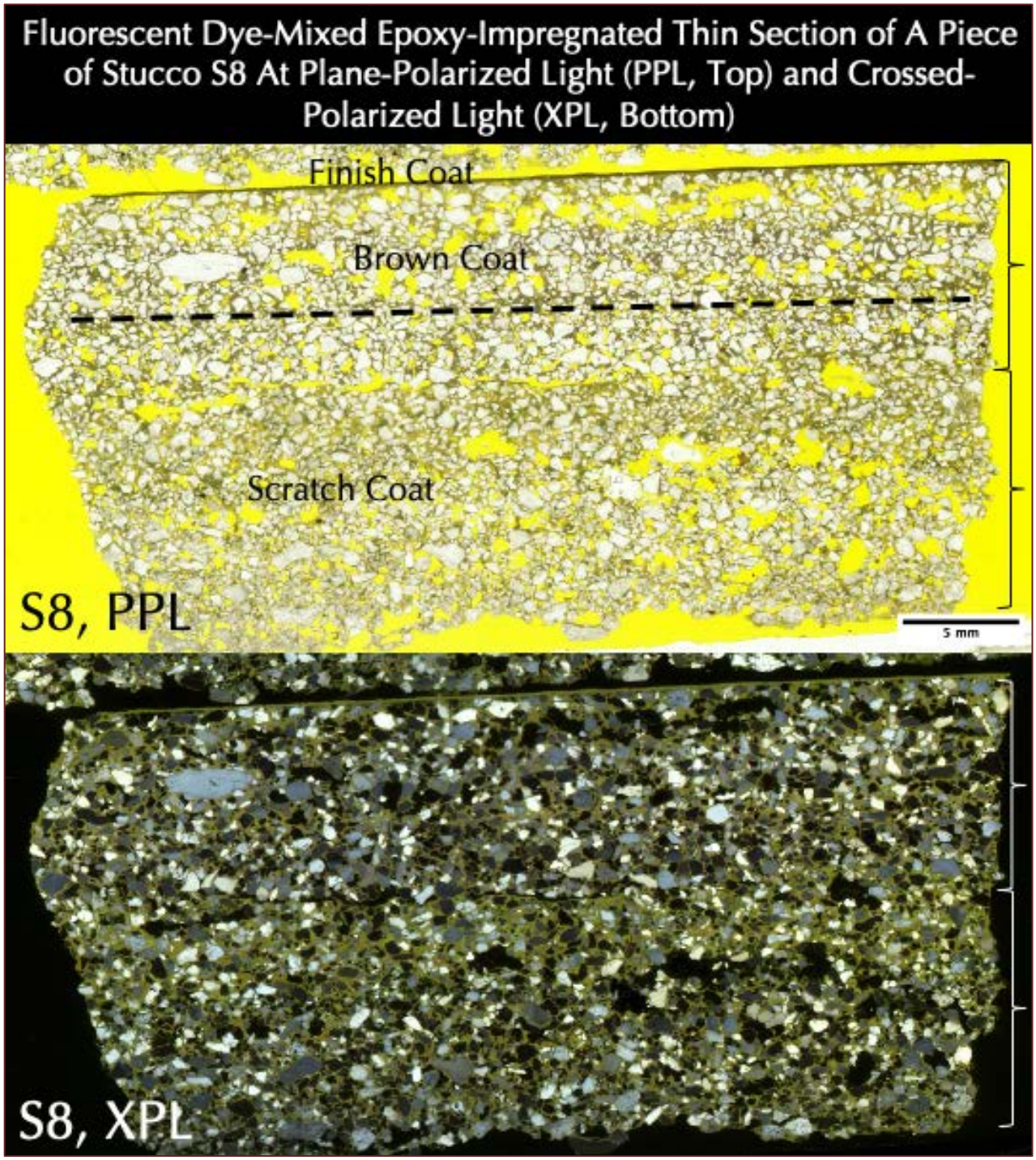

Figure 45: Fluorescent dye-mixed epoxy-impregnated 50 mm x 75 mm size thin section of stucco in Sample S8 scanned on a film scanner in plane (PPL) and crossed (XPL) polarized-light modes with one or two perpendicular polarizing filters, respectively showing: (a) size, shape, angularity, gradation, and distribution of sand particles in brown and scratch coats in PPL and XPL images; (b) a thin paint (finish) coat adhered to the brown coat seen as a dark brown layer at the top in PPL image; (c) relatively finer overall grain-size of sand in the brown coat than sand found in the scratch coat, which is seen in both PPL and XPL images; sand in both coats are angular in nature indicating use of crushed sand; (d) siliceous composition of crushed sand revealed in XPL image, (e) overall carbonated nature of paste in XPL image, (f) overall porous nature of scratch coat relative to the brown coat in PPL image, and, (g) overall good bond between the two coats and between the paint and topcoat in PPL image.

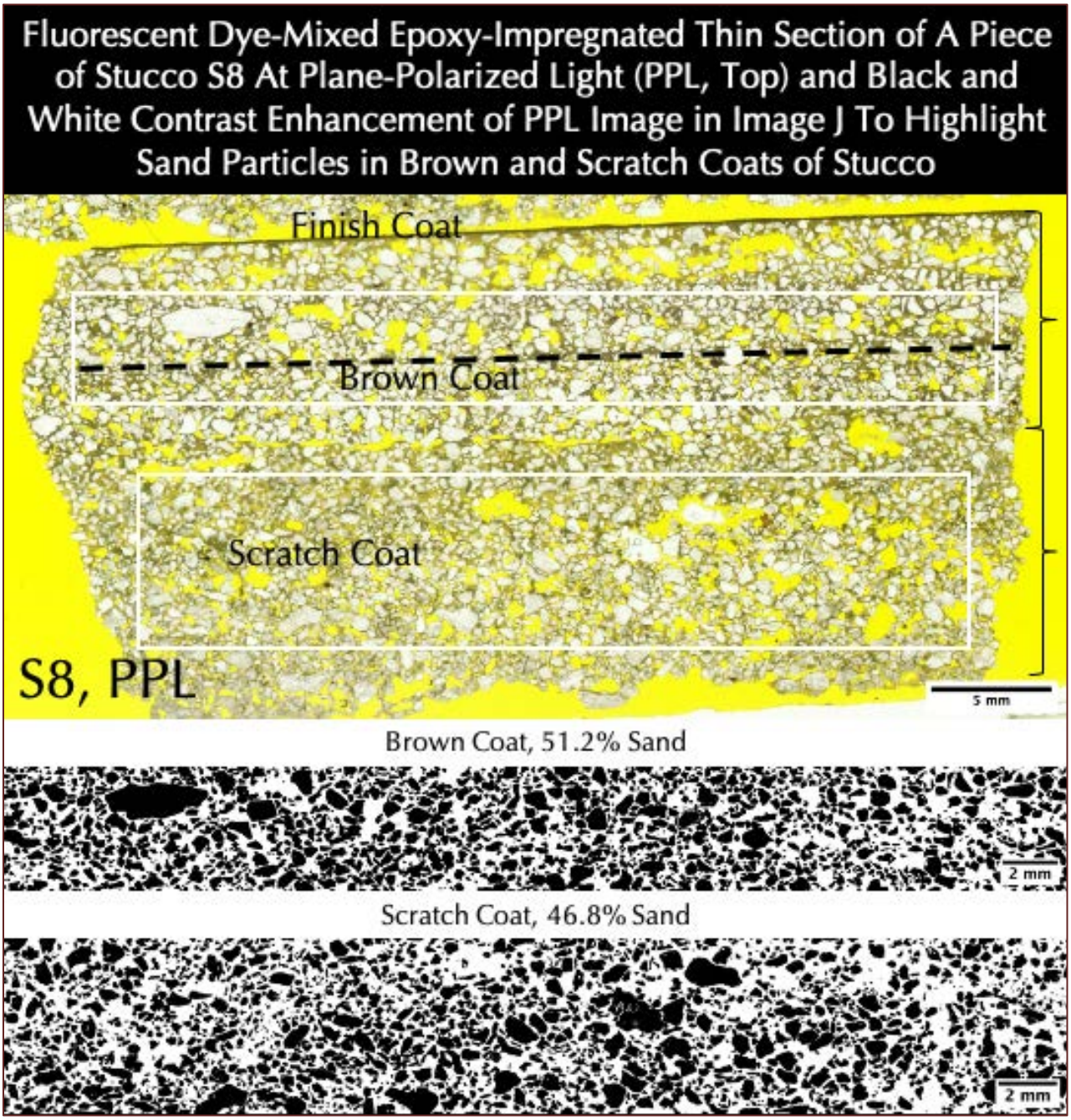

Figure 46: Fluorescent dye-mixed epoxy-impregnated 50 mm x 75 mm size thin section of stucco in Sample S8 scanned on a film scanner in plane (PPL) polarized-light mode showing: (a) size, shape, angularity, gradation, and distribution of sand particles in brown and scratch coats; (b) a thin paint (finish) coat adhered to the brown coat seen as a dark brown layer at the top; (c) relatively finer overall grain-size of sand in the brown coat than sand found in the scratch coat; sand in both coats are angular in nature indicating use of crushed sand; (d) overall porous nature of scratch coat relative to the brown coat, (e) overall good bond between the two coats and between the paint and brown coat; and, (f) boxed areas in brown and scratch coats were selected for image analysis in Image J to determine sand contents (by volume) in each coat, after converting the images to binary black and white contrasts to highlight sand particles in each coat in black, which showed 51.2% sand in brown coat and 46.8% sand in scratch coat, and overall coarser sand in the scratch coat as seen in black and white image.

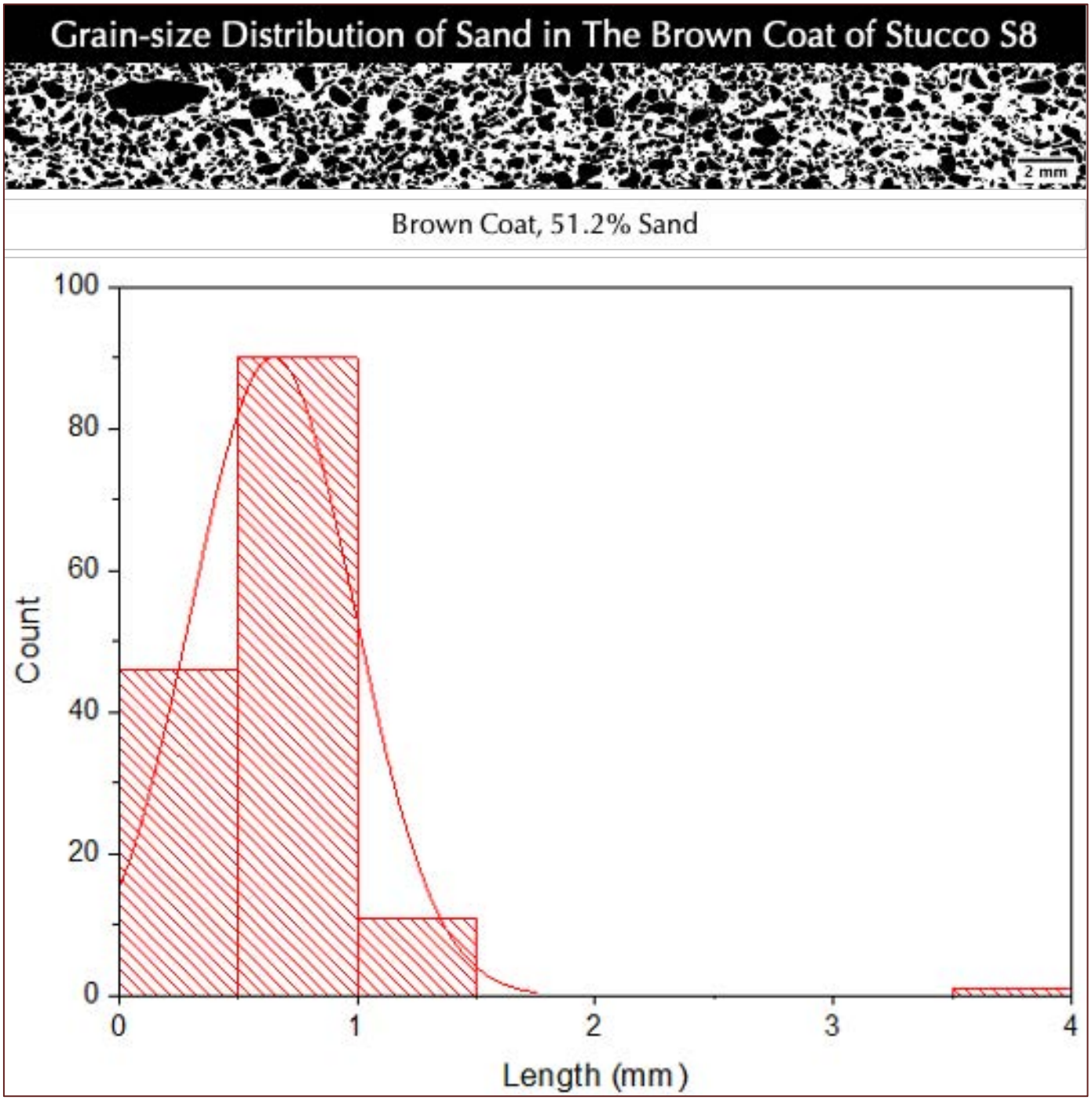

Figure 47: Grain-size distribution of sand in the brown coat from black and white contrast enhancement of boxed area of PPL image of thin section of S8 stucco in Figure 46 showing a normal distribution of sand sizes with a median sand size of around 0.5 mm with almost all of the particles less than a millimeter in grain size. Image analysis of sand sizes were done in Image J.

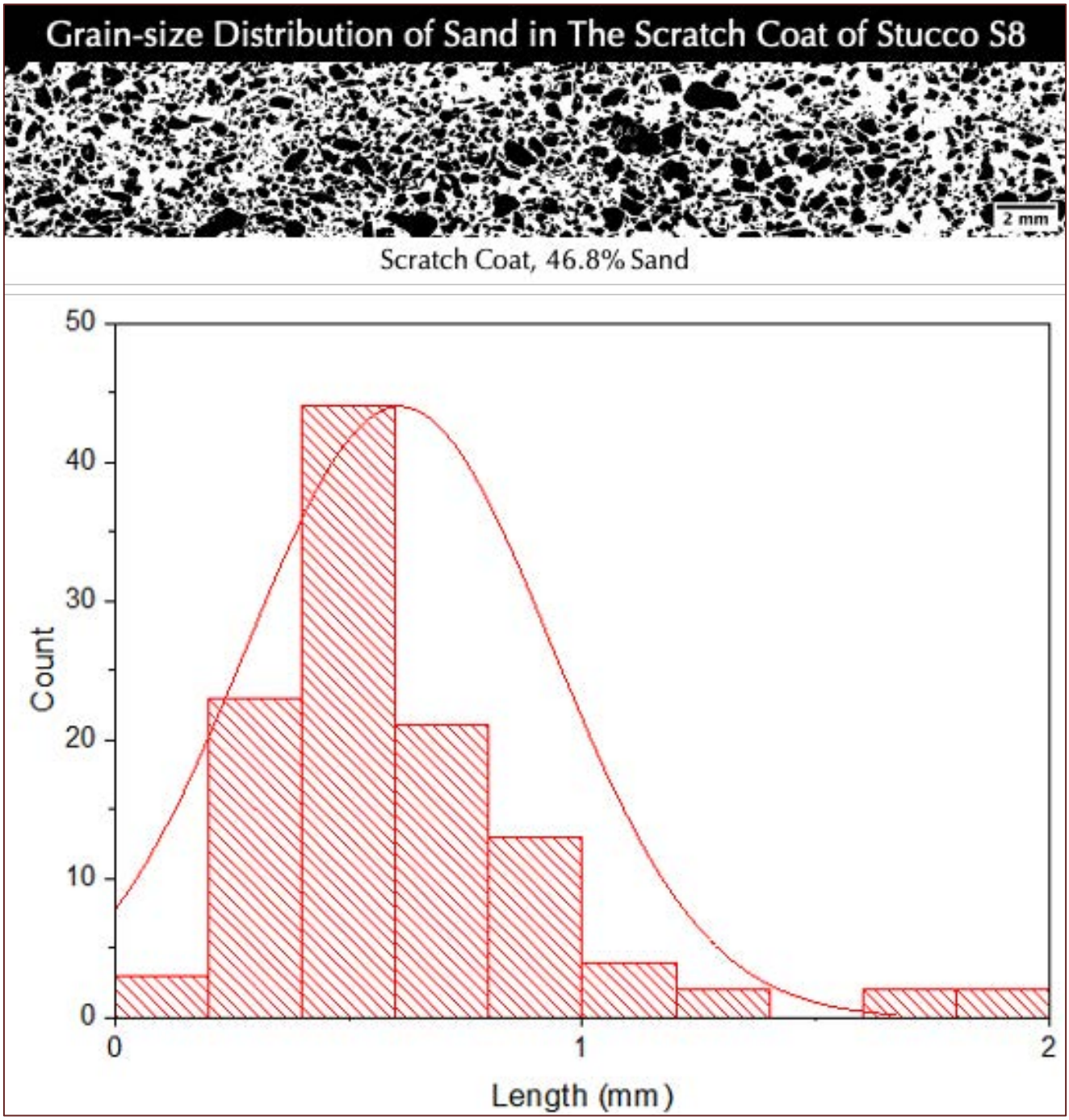

Figure 48: Grain-size distribution of sand in the scratch coat from black and white contrast enhancement of boxed area of PPL image of thin section of S8 stucco in Figure 46 showing a normal distribution of sand sizes with a median sand size of around 0.5 mm with almost all of the particles less than a millimeter in grain size and a fewer particles over 1 mm size which are rare in the brown coat, but more in the scratch coat hence giving an overall coarser grain size of sand in the scratch coat. Image analysis of sand sizes were done in Image J.

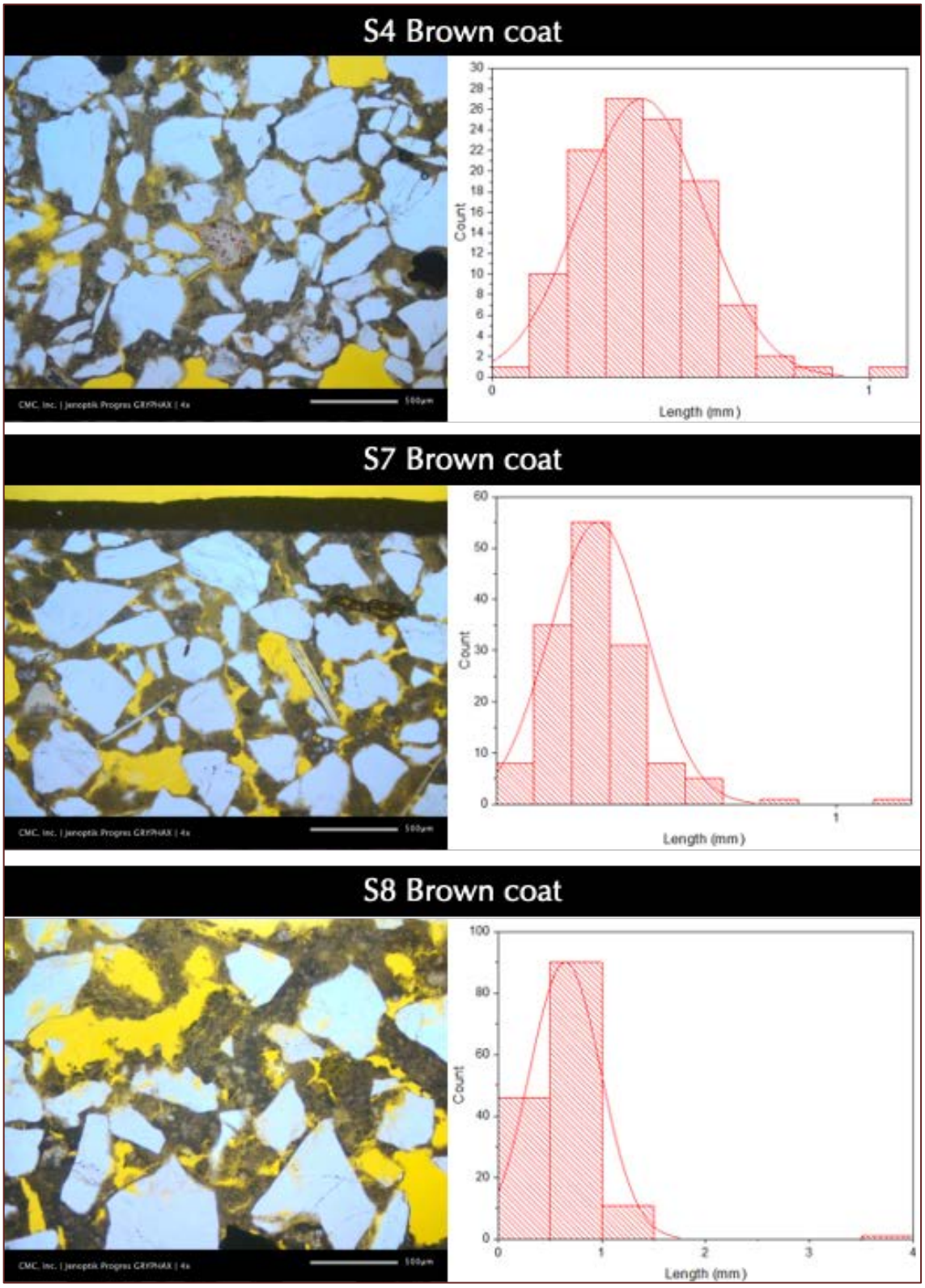

Figure 49: Grain-size distribution of sand in the brown coats from three stucco samples showing a normal distribution of sand sizes with a median sand size of around 0.5 mm with almost all of the particles less than a millimeter in grain size.

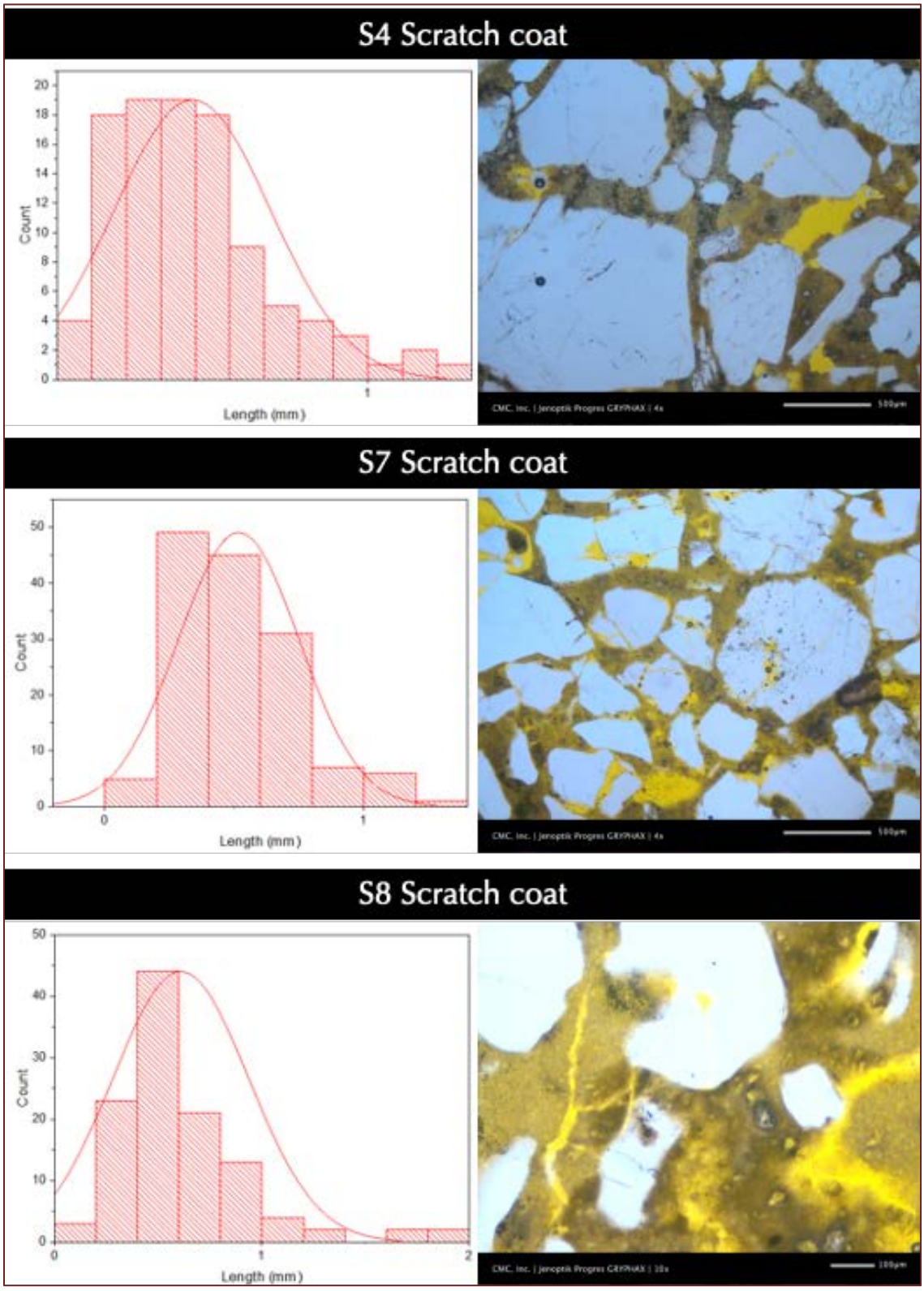

Figure 50: Grain-size distribution of sand in the scratch coats from three stucco samples showing a normal distribution of sand sizes with a median sand size of around 0.5 mm with few sand particles coarser than a millimeter in grain size which are rare in the brown coat, but more in the scratch coat hence giving an overall coarser grain size of sand in the scratch coat.

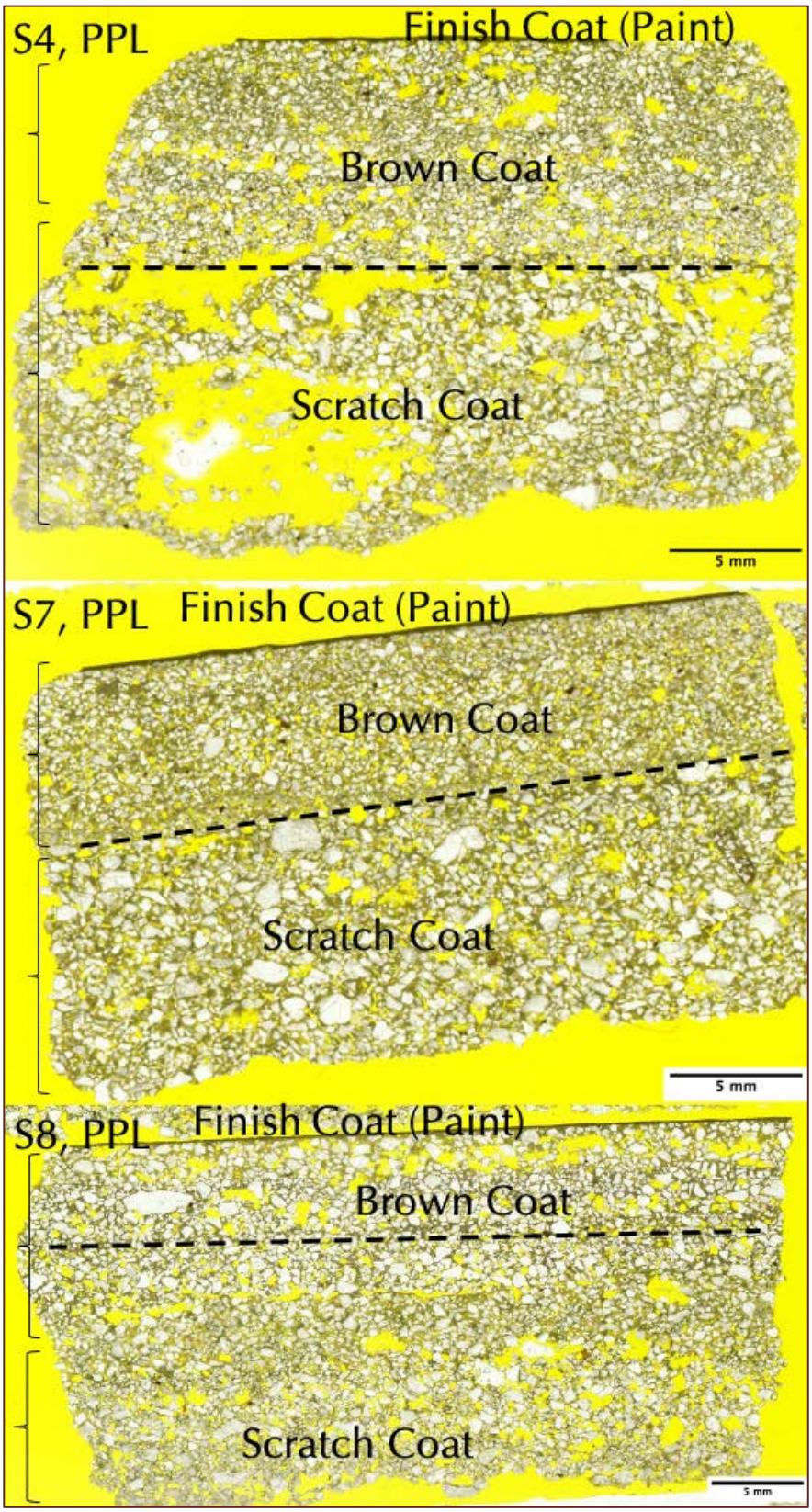

Figure 51: Fluorescent dye-mixed epoxy-impregnated 50 mm x 75 mm size thin sections of three stucco samples scanned on a film scanner in plane (PPL) polarized-light mode showing:

(a) Size, shape, angularity, gradation, and distribution of sand particles in brown and scratch coats;

(b) A thin paint (finish) coat adhered to the brown coat seen as a dark brown layer;

(c) Relatively finer overall grain-size of sands in the brown coats than sand found in the scratch coats;

(d) Sand in both coats are angular in nature indicating use of crushed sand;

(e) Overall porous natures of scratch coats relative to the brown coats, and,

(f) Overall good bonds between the two coats and between the paint and brown coats.

MICROGRAPHS OF THIN SECTIONS

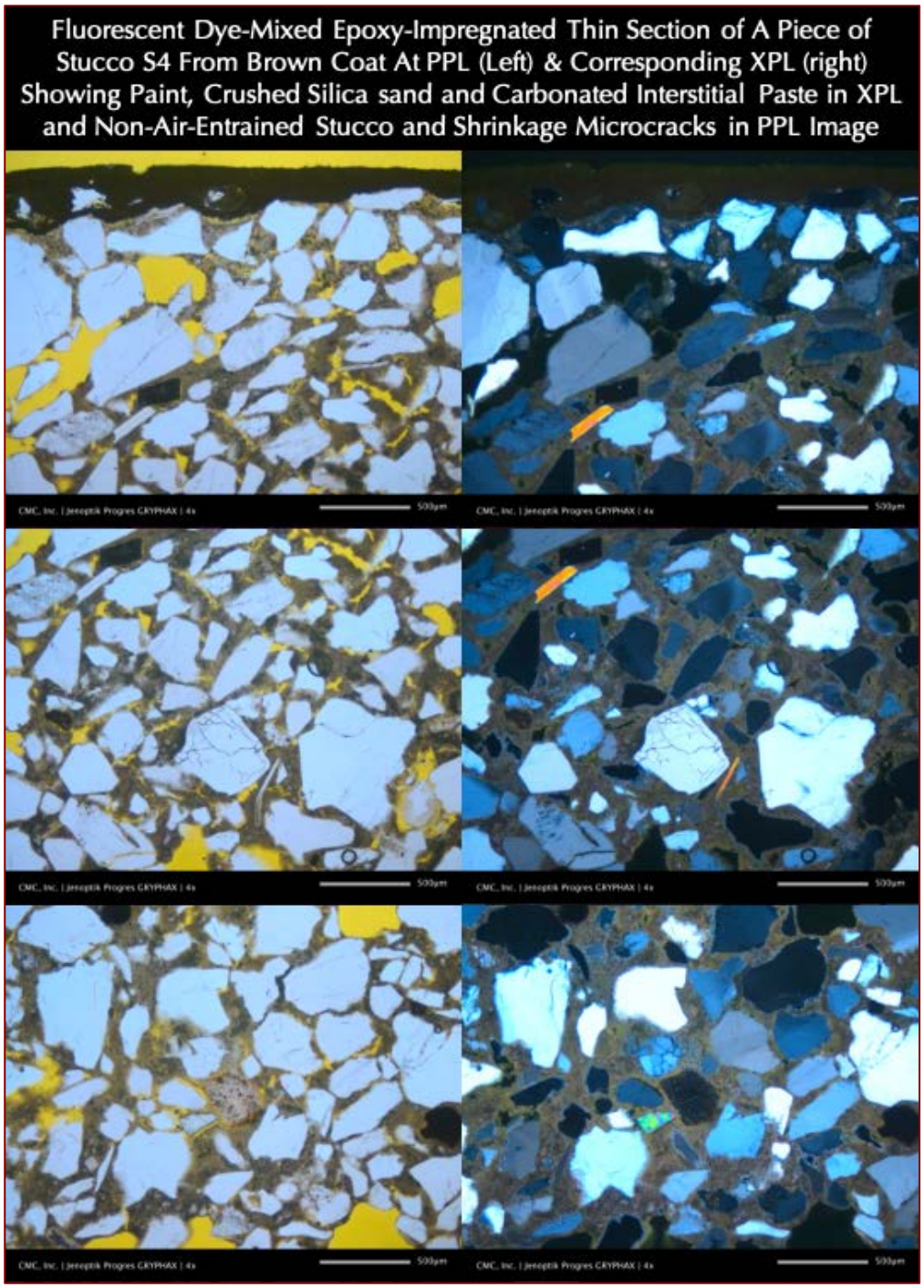

Figure 52: Micrographs of thin section of stucco S4 from north elevation in PPL (left) and corresponding XPL images, showing:

(a) The thin (< 0.25 mm) paint (finish) coat on top of brown coat in top row;

(b) Crushed silica sand particles in brown coat;

(c) Fine-grained, porous, carbonated lime paste of brown coat;

(c) Fine, hair-line, discontinuous elongated shrinkage microcracks in lime paste in brown coat; and,

(d) Dominance of quartz sand in the brown coat's sand.

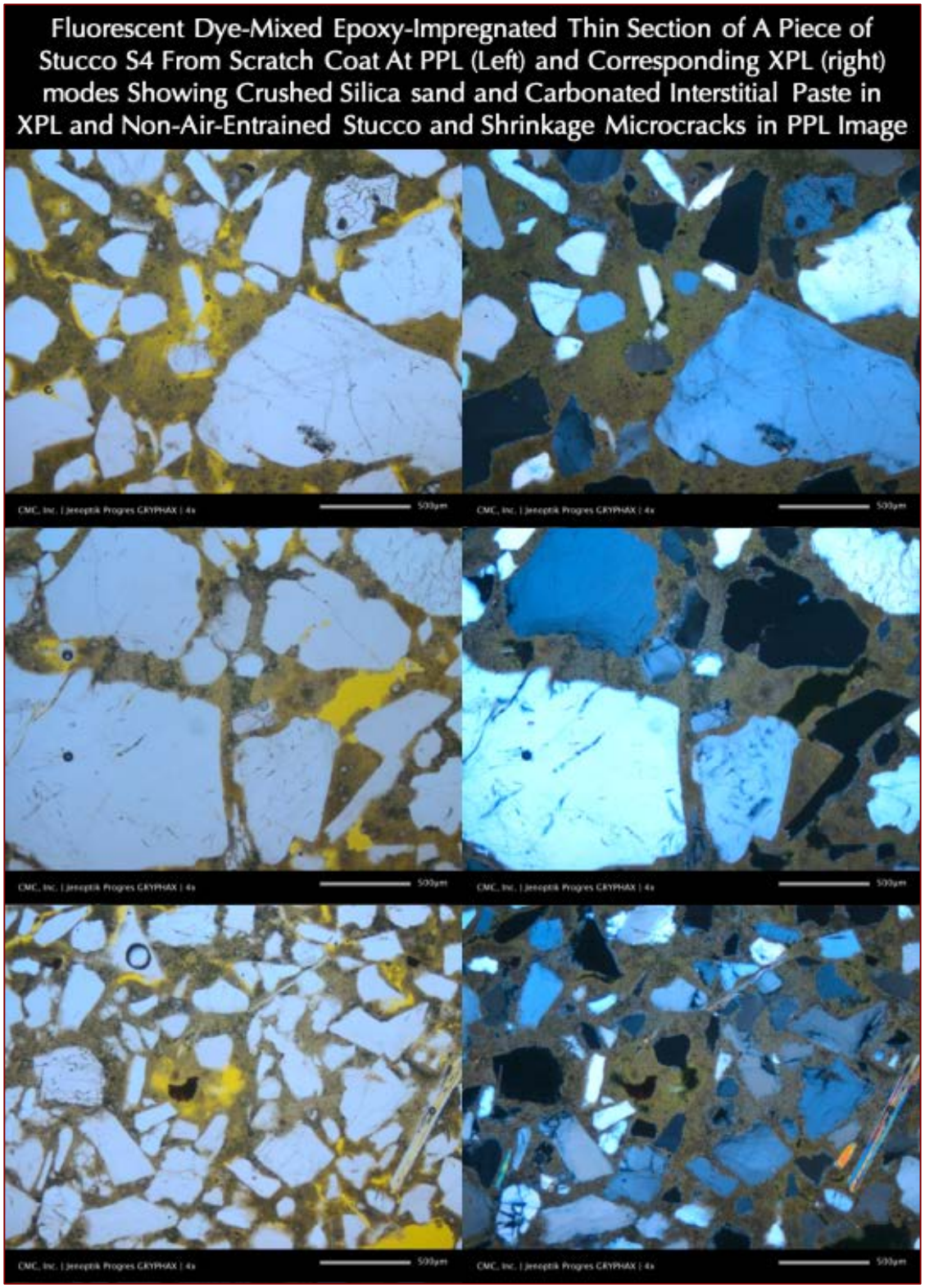

Figure 53: Micrographs of thin section of stucco S4 from north elevation in PPL (left) and corresponding XPL images, showing: (a) crushed silica sand particles in scratch coat in top and middle rows and finer crushed sand in the brown coat in the bottom row; (b) fine-grained, porous, carbonated lime paste of brown and scratch coats having fine, hair-line, discontinuous elongated shrinkage microcracks in lime paste; and (c) dominance of quartz sand in the sand in both brown and scratch coats. Notice the absence of any Portland cement particles in the paste.

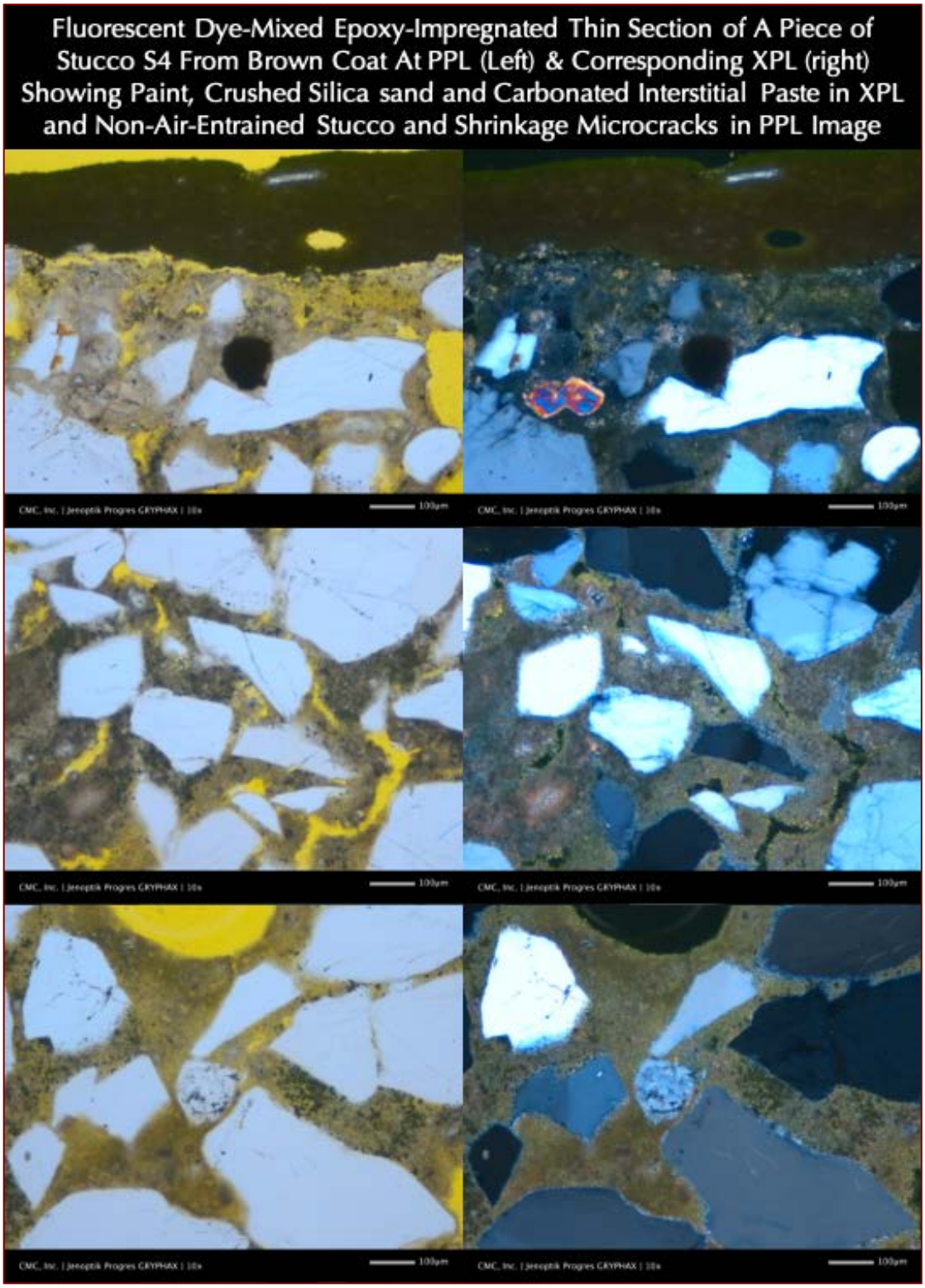

Figure 54: Micrographs of thin section of stucco S4 from north elevation in PPL (left) and corresponding XPL images, showing: (a) finer crushed silica sand particles in brown coat in top and middle rows and coarser crushed sand in the scratch coat in the bottom row; (b) fine-grained, porous, carbonated lime paste of brown and scratch coats having fine, hair-line, discontinuous elongated shrinkage microcracks in lime paste; and (c) dominance of quartz sand in the sand in both brown and scratch coats. Notice the absence of any Portland cement particles in the paste.

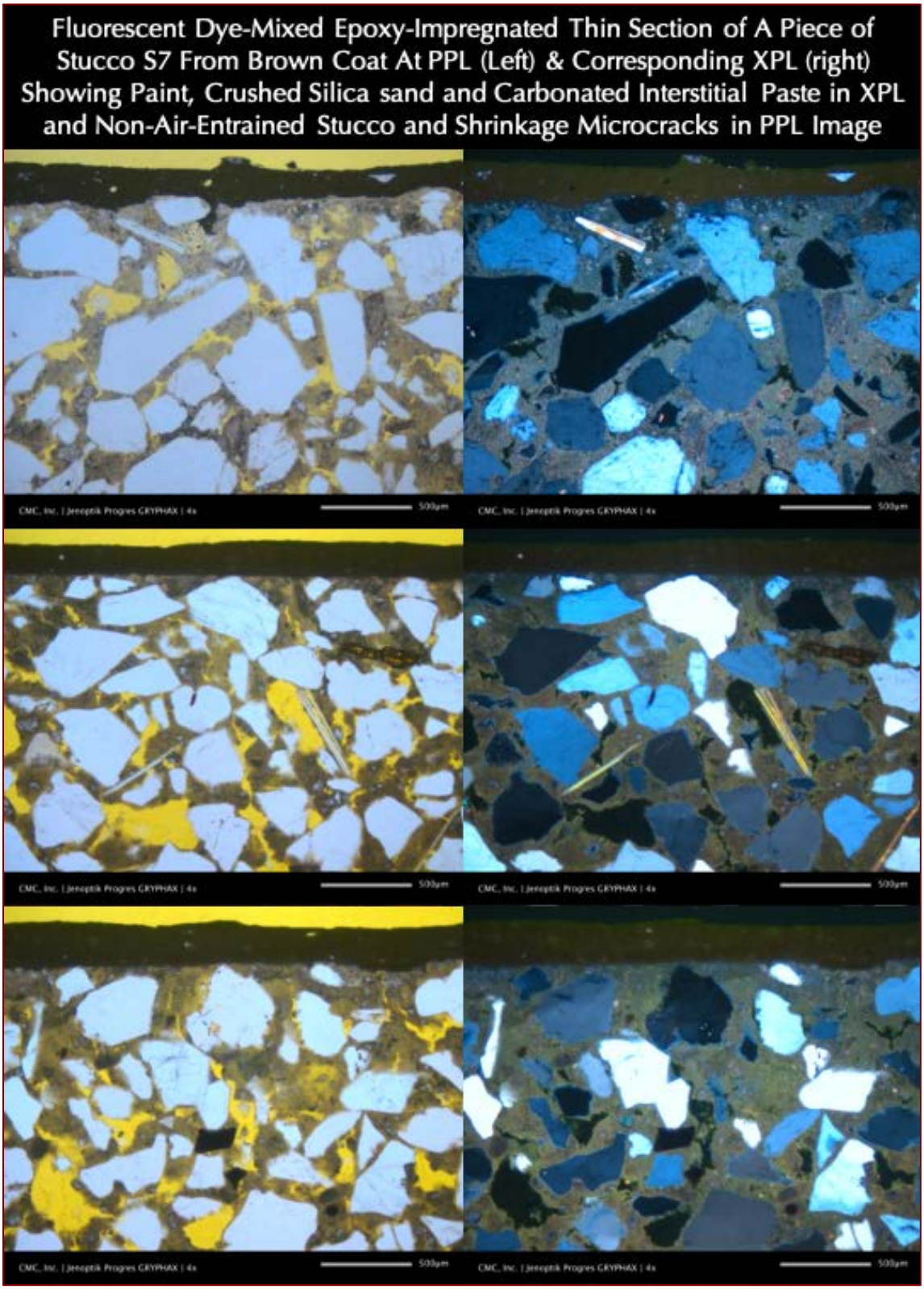

Figure 55: Micrographs of thin section of stucco S7 from south elevation in PPL (left) and corresponding XPL images, showing: (a) the thin (< 0.25 mm) paint (finish) coat on top of brown coat; (b) crushed silica sand particles in brown coat; (c) fine-grained, porous, carbonated lime paste of brown coat; (d) fine, hair-line, discontinuous elongated shrinkage microcracks in lime paste in brown coat; and (e) dominance of quartz sand in the brown coat's sand.

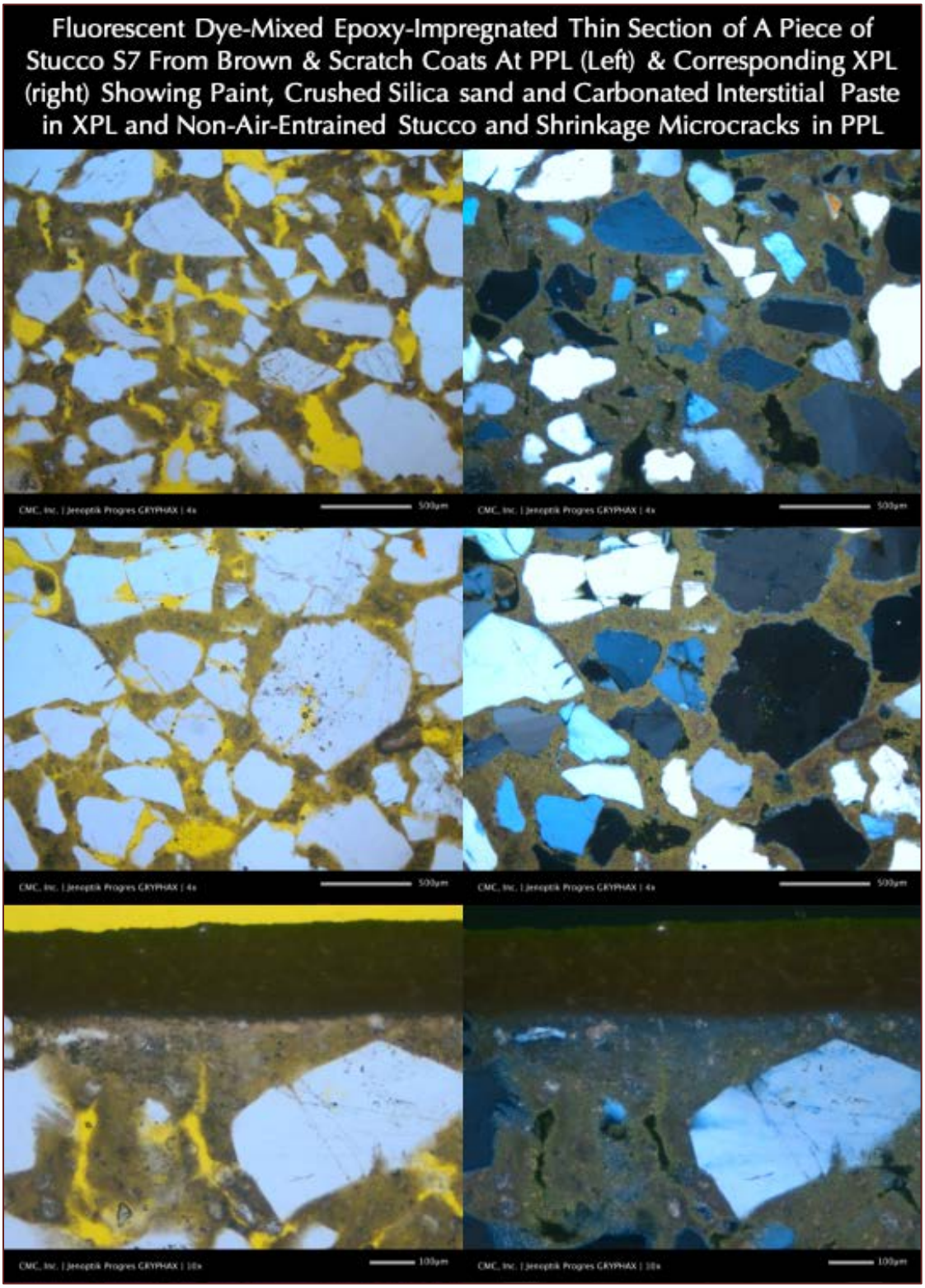

Figure 56: Micrographs of thin section of stucco S7 from south elevation in PPL (left) and corresponding XPL images, showing: (a) finer crushed silica sand particles in brown coat in top and middle rows and coarser crushed sand in the scratch coat in the bottom row; (b) fine-grained, porous, carbonated lime paste of brown and scratch coats having fine, hair-line, discontinuous elongated shrinkage microcracks in lime paste; and (c) dominance of quartz sand in the sand in both brown and scratch coats. Notice the absence of any Portland cement particles in the paste.

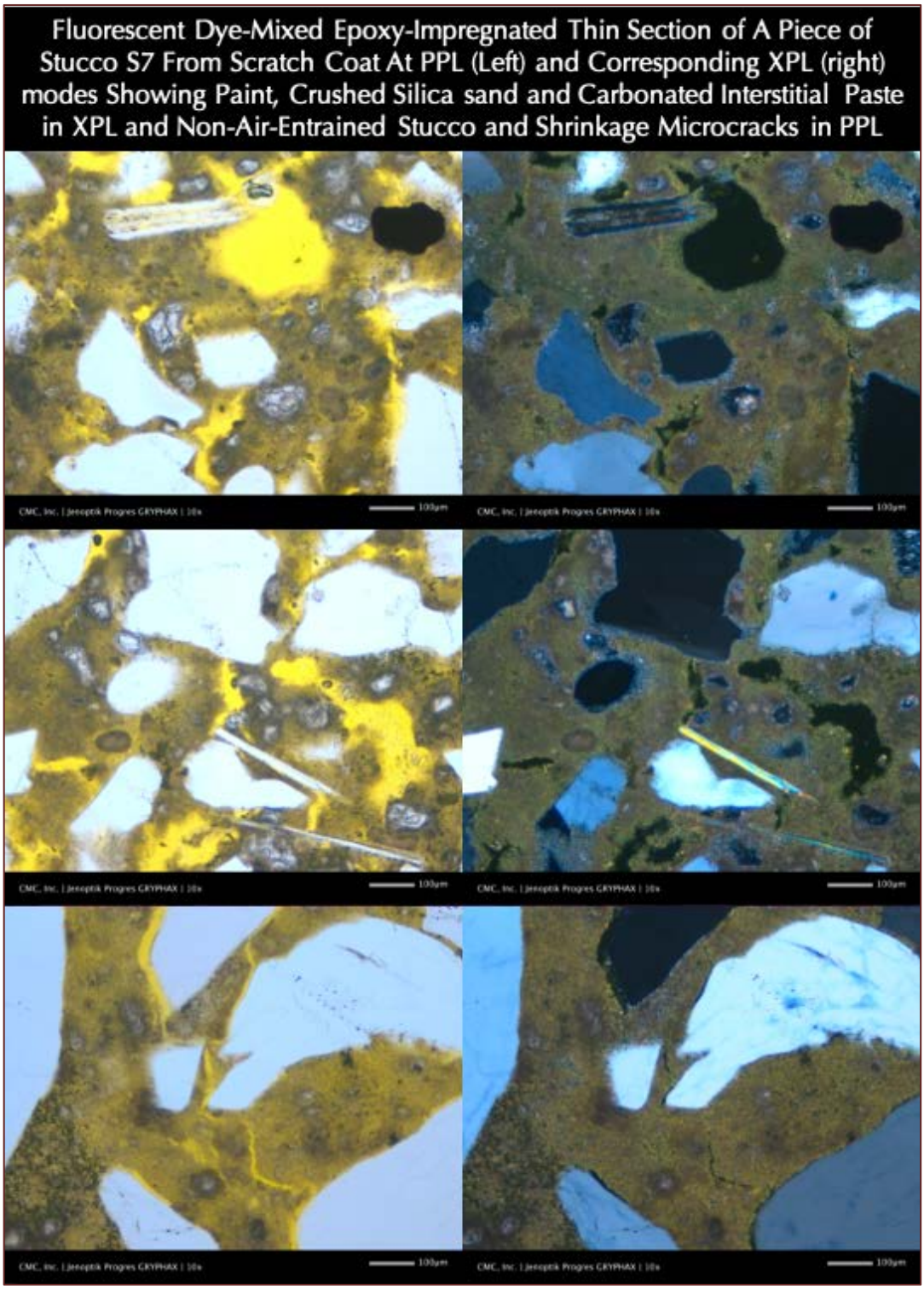

Figure 57: Micrographs of thin section of stucco S7 from south elevation in PPL (left) and corresponding XPL images, showing: (a) crushed sand in the scratch coat; (b) fine-grained, porous, carbonated lime paste of scratch coat having fine, hair-line, discontinuous elongated shrinkage microcracks in lime paste; and (c) dominance of quartz sand in the sand in scratch coat. Notice the absence of any Portland cement particles in the paste.

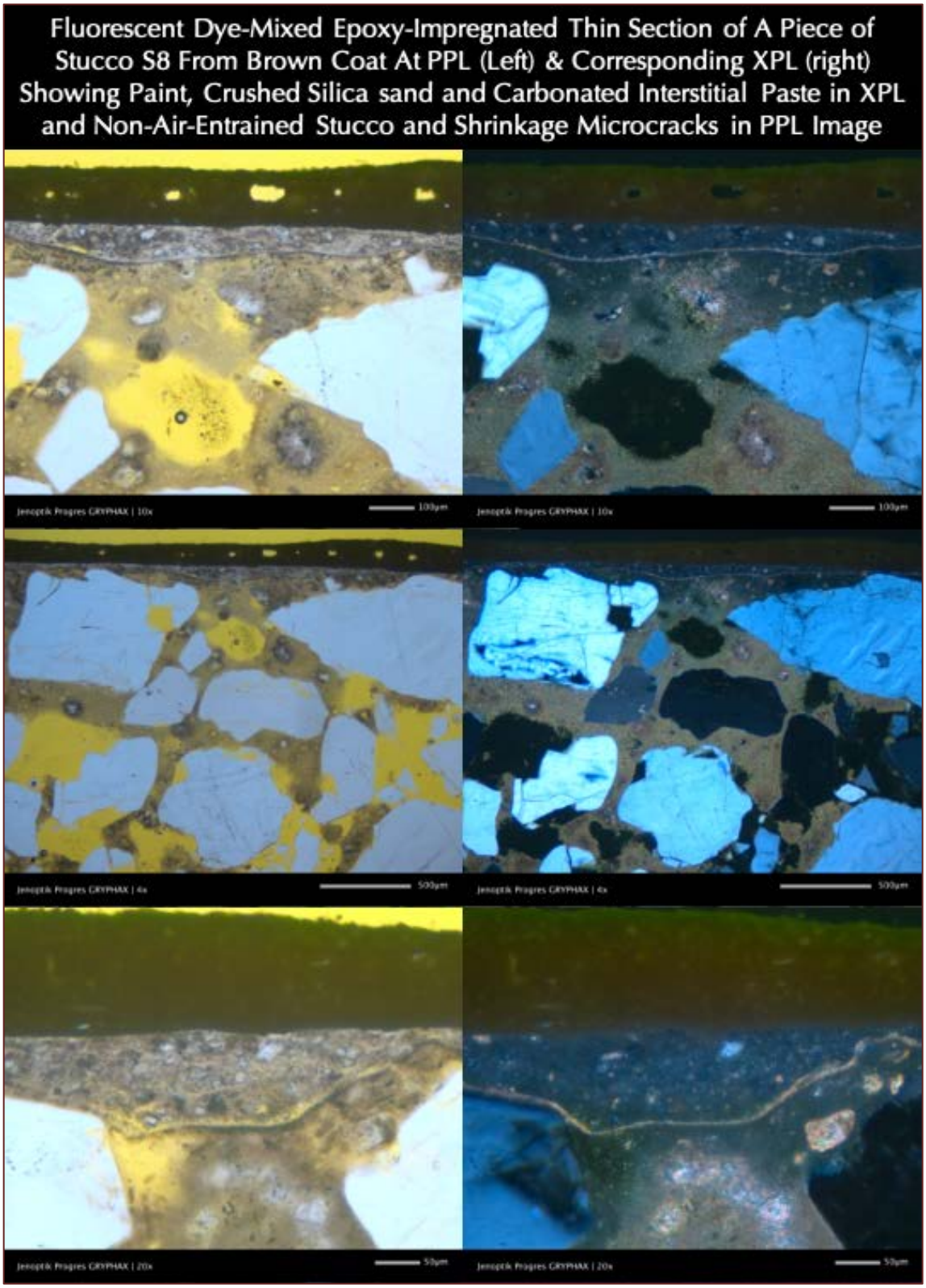

Figure 58: Micrographs of thin section of stucco S8 from east elevation in PPL (left) and corresponding XPL images, showing: (a) the thin (< 0.25 mm) paint (finish) coat and a distinct bonding agent coat on top of brown coat; (b) crushed silica sand particles in brown coat; (c) fine-grained, porous, carbonated lime paste of brown coat; (d) fine, hair-line, discontinuous elongated shrinkage microcracks in lime paste in brown coat; and (e) dominance of quartz sand in the brown coat's sand.

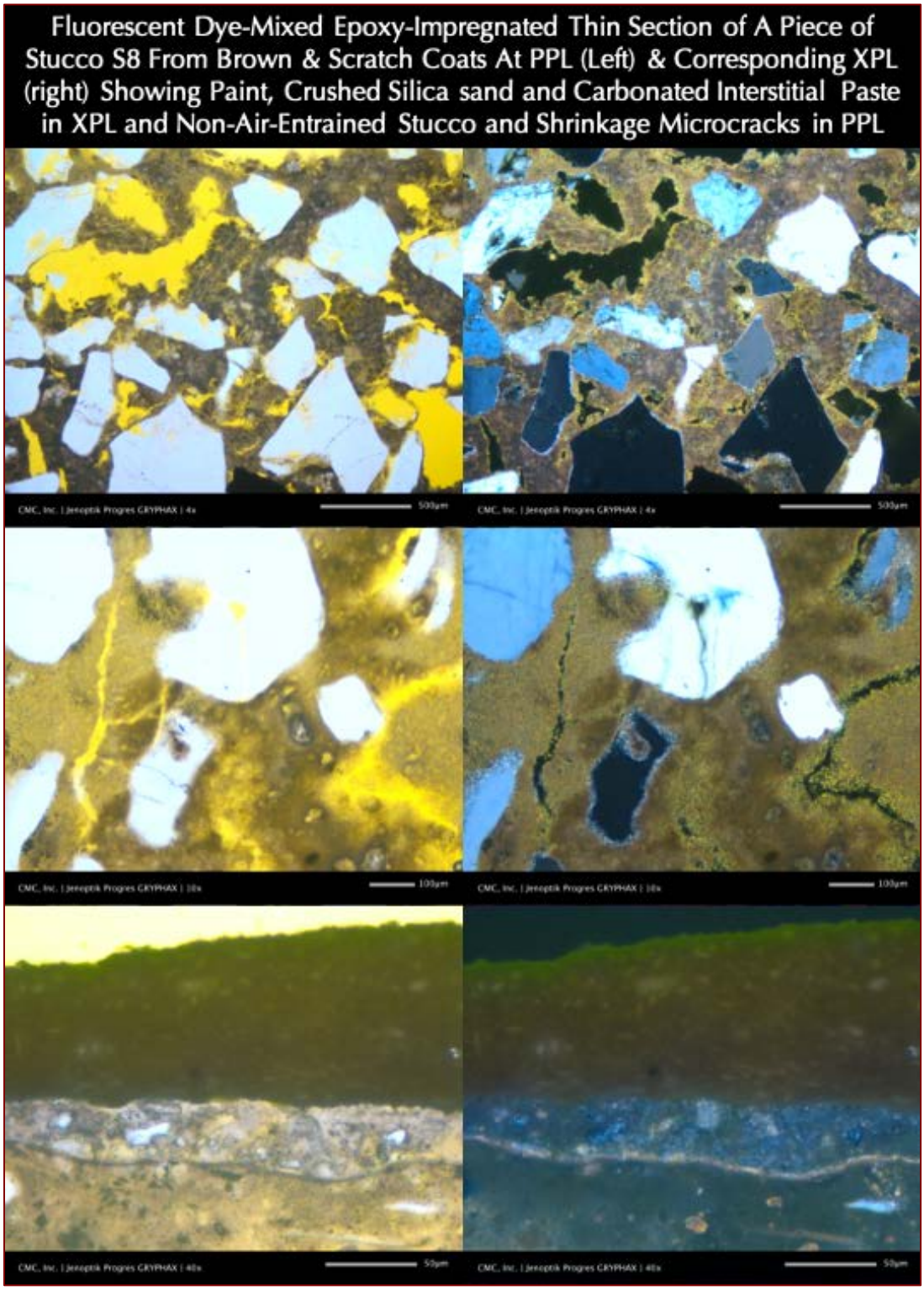

Figure 59: Micrographs of thin section of stucco S8 from east elevation in PPL (left) and corresponding XPL images, showing: (a) the thin (< 0.25 mm) paint (finish) coat and a distinct bonding agent coat on top of brown coat in the bottom row; (b) crushed silica sand particles in brown coat in the top row and relatively coarser crushed sand in the scratch coat in middle row; (c) fine-grained, porous, carbonated lime paste of brown coat; (d) fine, hair-line, discontinuous elongated shrinkage microcracks in lime paste in brown coat; and (e) dominance of quartz sand in the brown coat's sand.

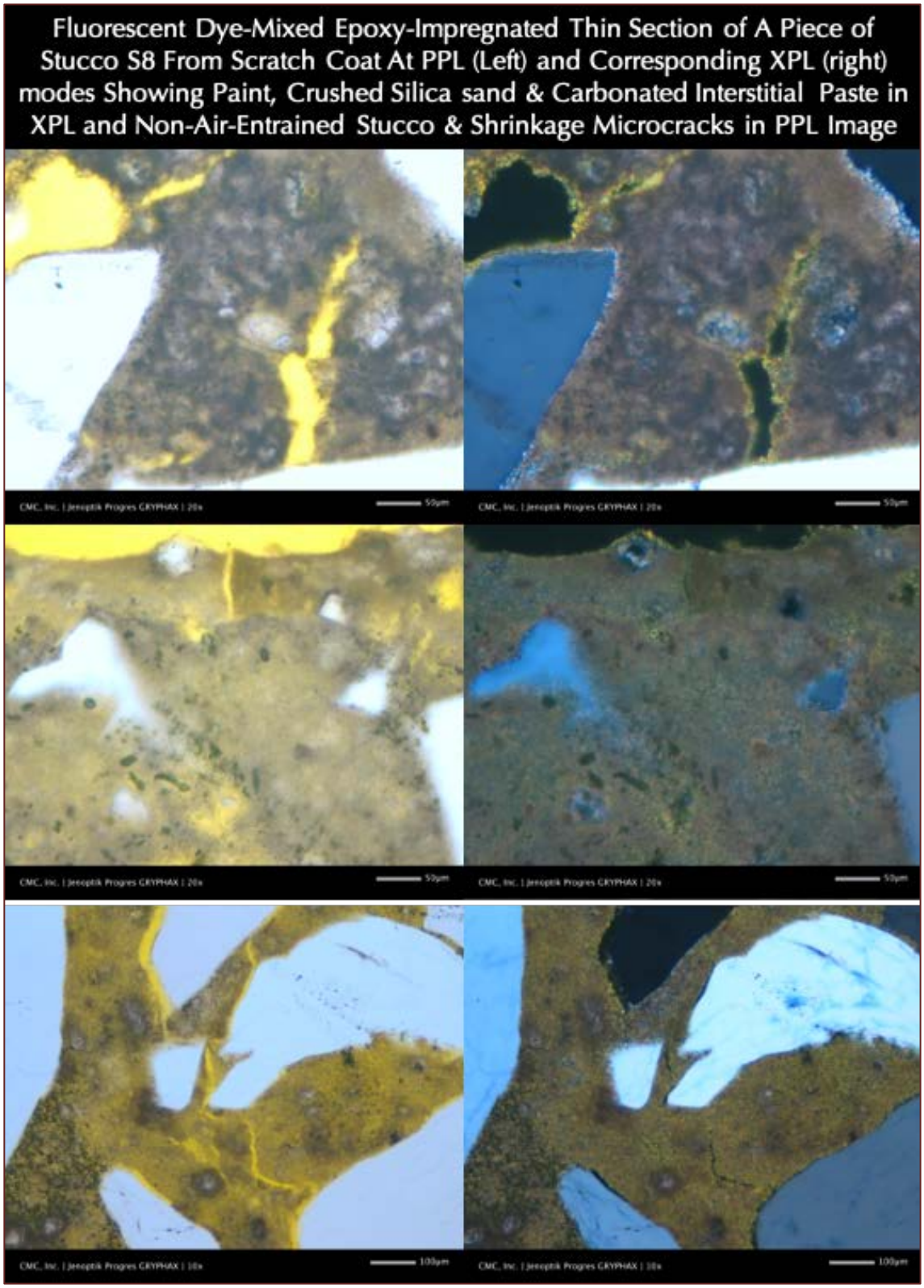

Figure 60: Micrographs of thin section of stucco S8 from east elevation in PPL (left) and corresponding XPL images, showing: (a) crushed sand in the scratch coat; (b) fine-grained, porous, carbonated lime paste of scratch coat having fine, hair-line, discontinuous elongated shrinkage microcracks in lime paste; and (c) dominance of quartz sand in the sand in scratch coat. Notice the absence of any Portland cement particles in the paste.

MICROGRAPHS OF PAINT COATS

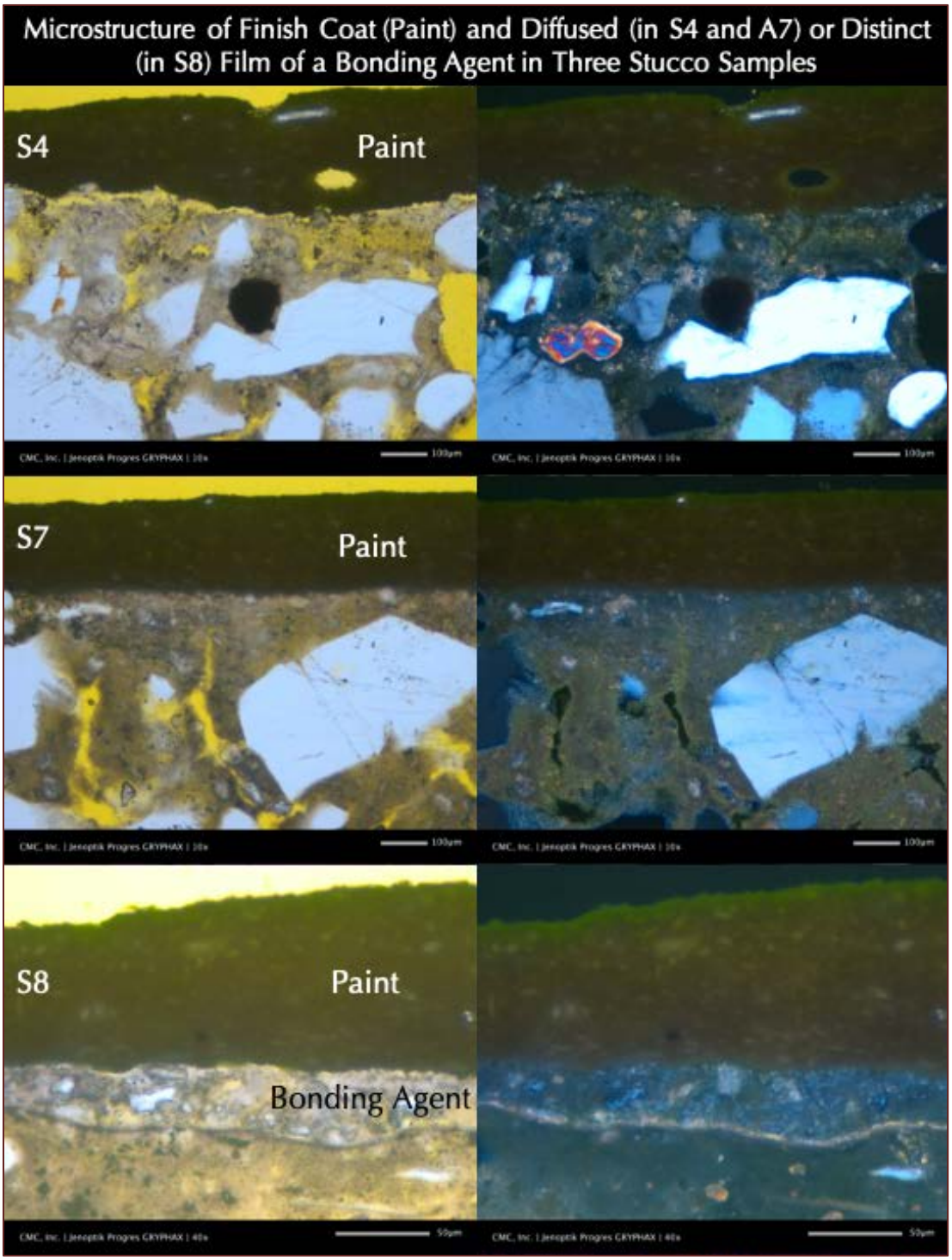

Figure 61: Micrographs of fluorescent dye-mixed epoxy-impregnated thin sections of all three stucco samples showing the details of the paint (finish) coat, which are 0.1 to 0.25 mm in thickness and show no distinct bonding agent in S4 and S7 even though it's presence is detected as diffused one in next two figures, but a distinct bonding agent in S8. The paint is dark brown and dense in PPL which has fine talc filler and titanium oxide pigment that are identified from SEM-EDS and FTIR studies. The bonding agent has fine residual alite and belite particles in a porous carbonated polymer medium which appears dark gray in XPL image.

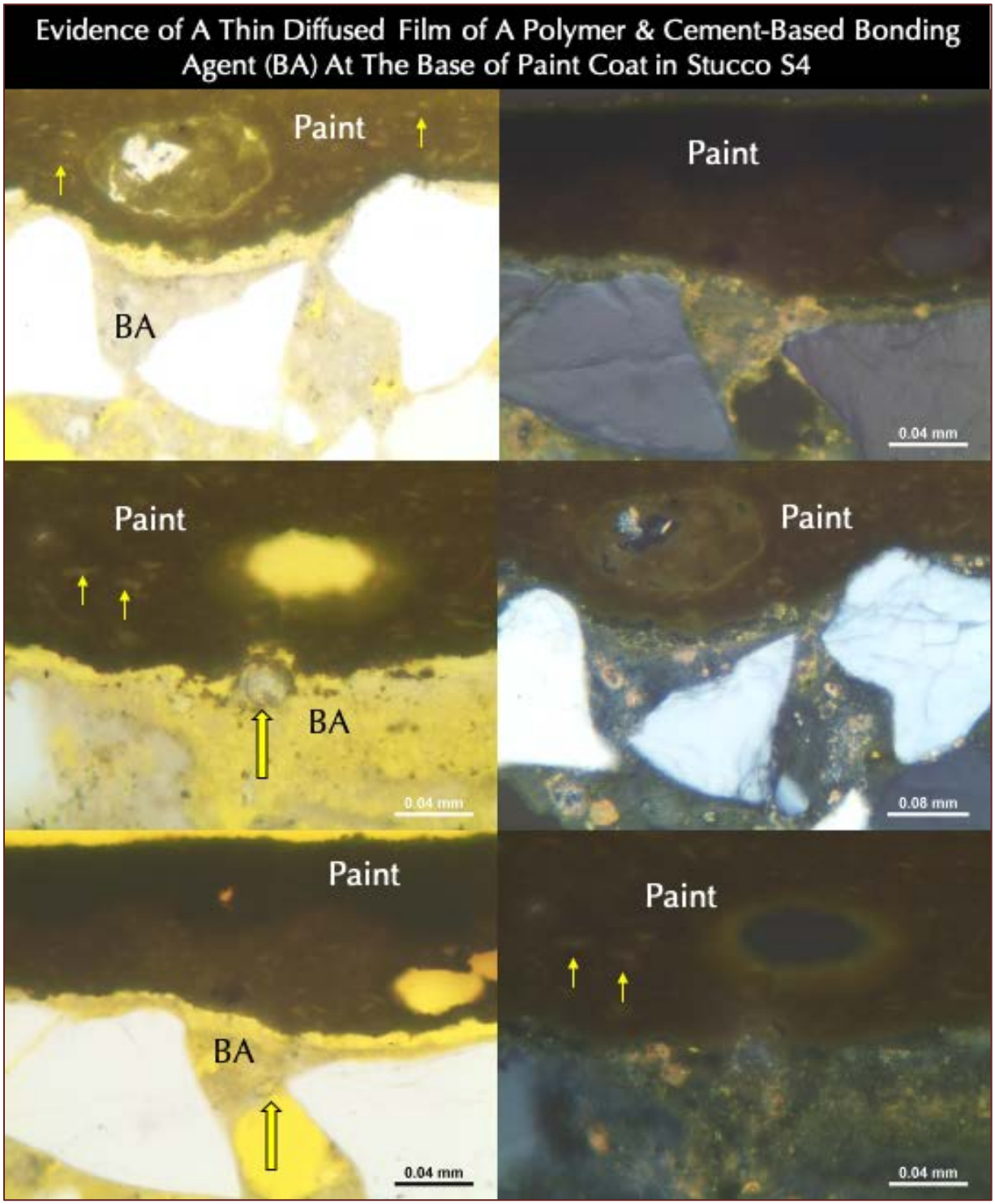

Figure 62: Micrographs of fluorescent dye-mixed epoxy-impregnated thin section of stucco S4 from north elevation showing details of paint coat, which has very fine talc filler (some are shown by fine vertical arrows) and titanium oxide pigment both of which are better detected from SEM-EDS and FTIR studies, an alkyd-based binder detected from FTIR studies, a thin porous diffused bonding agent beneath the paint containing fine residual cement particles (some are marked with thick vertical arrows) in a polymer binder which shows dark gray semi-isotropic appearance in XPL image with some fine carbonate fillers, somehow diffused into the stucco mass.

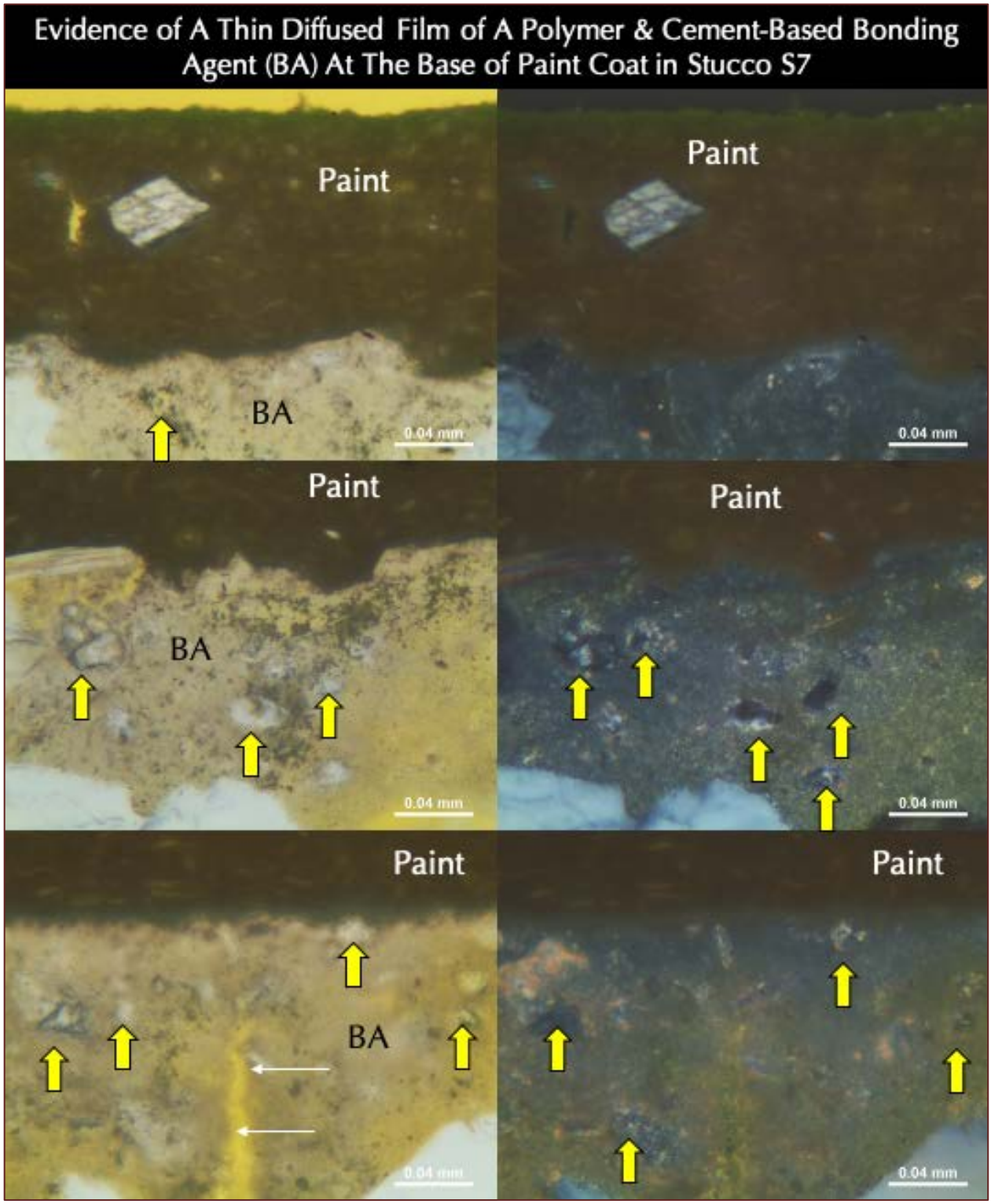

Figure 63: Micrographs of fluorescent dye-mixed epoxy-impregnated thin section of stucco S7 from south elevation showing details of paint coat, which has very fine talc filler (some are shown by fine vertical arrows) and titanium oxide pigment both of which are better detected from SEM-EDS and FTIR studies, an alkyd-based binder detected from FTIR studies, a thin porous diffused bonding agent beneath the paint containing fine residual cement particles (some are marked with thick vertical arrows) in a polymer binder which shows dark gray semi-isotropic appearance in XPL image with some fine carbonate fillers, somehow diffused into the stucco mass. Notice a vertical shrinkage microcrack in stucco that is truncated against the paint coat indicating its formation before application of paint.

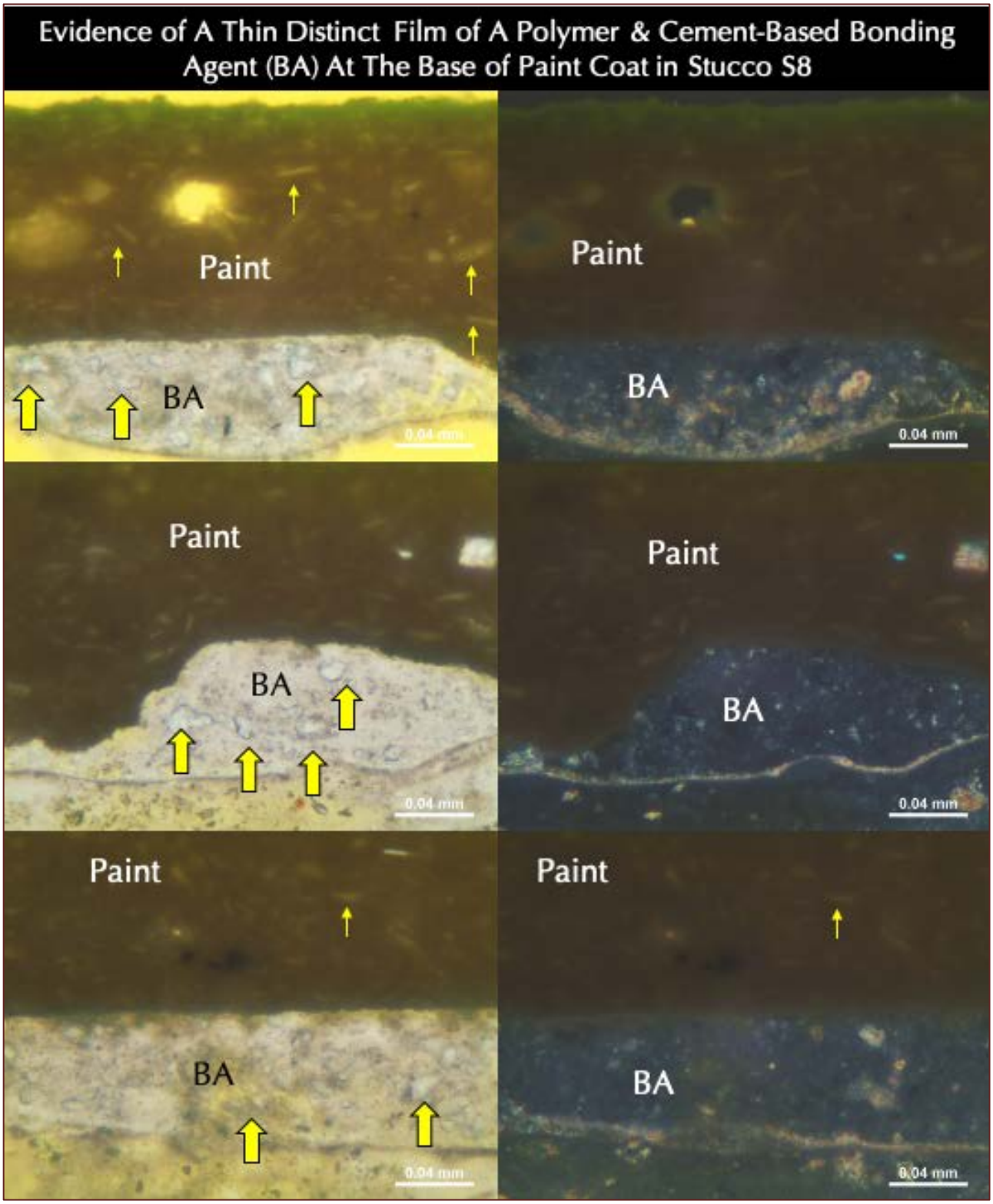

Figure 64: Micrographs of fluorescent dye-mixed epoxy-impregnated thin section of stucco S8 from east elevation showing details of paint coat, which has very fine talc filler (some are shown by fine vertical arrows) and titanium oxide pigment both of which are better detected from SEM-EDS and FTIR studies, an alkyd-based binder detected from FTIR studies, a thin distinct bonding agent beneath the paint containing fine residual cement particles (some are marked with thick vertical arrows) in a polymer binder which shows dark gray semi-isotropic appearance in XPL image with some fine carbonate fillers, which is not diffused into the stucco mass as in other two stuccos.

SEM-EDS

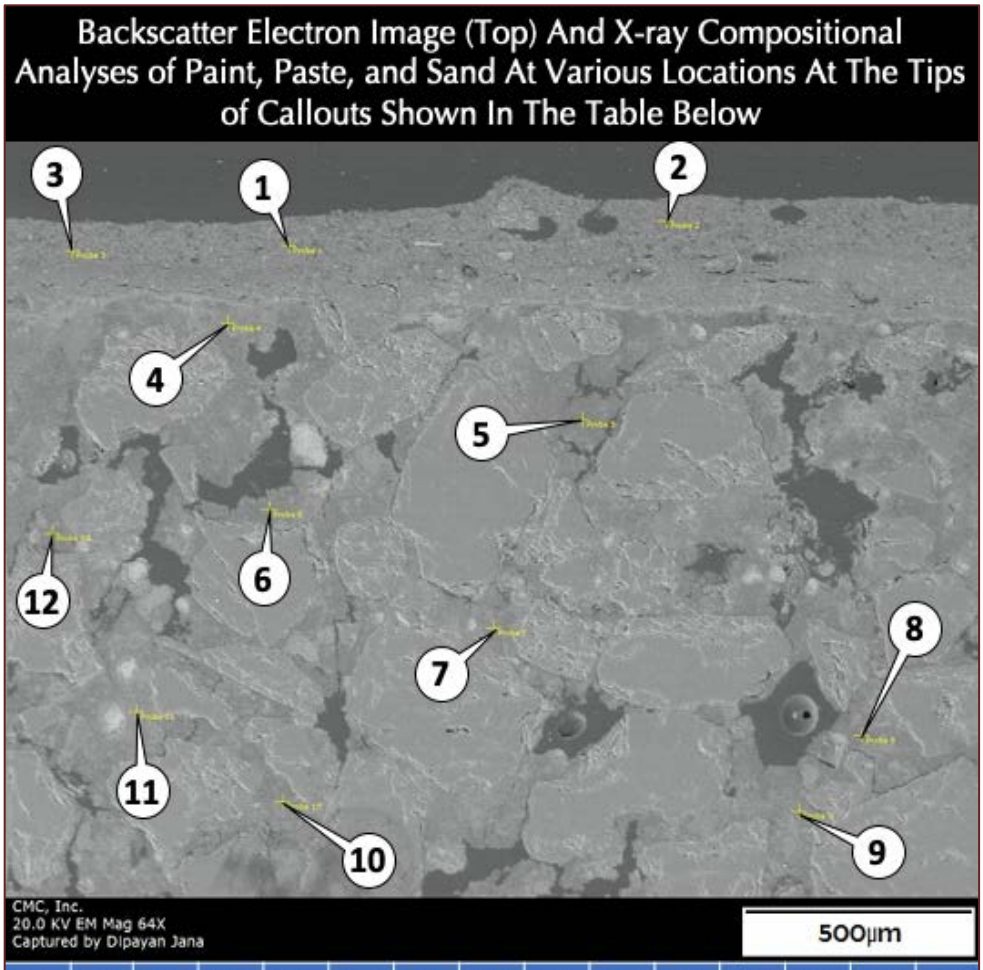

Probe	CaO	SiO_2	Al_2O_3	Na_2O	MgO	SO_3	K_2O	TiO_2	FeO	P_2O_5	CO_2	Total	Phase	Paste CI
1	0.55	**33.43**	**17.57**	5.58	1.08	0.17	2.84	**20.81**	0.10	1.22	16.66	100.0	Paint	-
2	0.32	**36.04**	**11.57**	1.85	0.04	0.35	1.38	**22.00**	0.02	0.85	25.59	100.0	Paint	-
3	0.39	**34.36**	**6.78**	0.44	1.38	0.73	5.18	**30.30**	0.25	1.14	19.05	100.0	Paint	-
4	**64.89**	**9.39**	1.71	0.12	**8.01**	2.28	0.07	0.04	0.04	0.40	13.06	100.0	Paste	**0.37**
5	**59.17**	**8.43**	1.42	0.00	**10.91**	1.71	0.04	0.08	0.39	1.05	16.80	100.0	Paste	**0.34**
6	**64.81**	**7.78**	1.59	0.04	**9.23**	1.22	0.00	0.02	0.18	0.20	14.94	100.0	Paste	**0.30**
7	**63.24**	**5.31**	1.19	0.00	**12.29**	1.80	0.01	0.00	0.59	0.91	14.67	100.0	Paste	**0.21**
8	**40.56**	**10.70**	1.32	0.02	**9.75**	2.39	0.00	0.30	0.00	1.07	33.89	100.0	Paste	**0.58**
9	**42.85**	**12.06**	2.10	0.10	**9.31**	2.41	0.02	0.00	0.03	0.49	30.63	100.0	Paste	**0.65**
10	0.02	**94.99**	0.02	0.00	0.00	0.66	0.00	0.02	0.07	0.91	3.31	100.0	Sand	-
11	**60.50**	**12.80**	1.39	0.06	**11.26**	1.61	0.00	0.21	0.27	1.00	10.91	100.0	Paste	**0.49**
12	**54.80**	**7.99**	5.04	0.00	**10.47**	1.89	0.00	0.15	0.50	1.27	17.88	99.99	Paste	**0.41**

Figure 65: Backscatter electron image (top) and X-ray elemental (oxide compositional) analyses of paste, sand, and paint coat of stucco in S4 showing:

(a) Distinct compositions of paint coat, sand, and interstitial paste in the stucco that are represented by oxide compositional variations in the Table from measurements at the tips of callouts in the backscatter image;

(b) High titanium in the paste from titanium oxide pigment, along with high silica and alumina from use of talc fillers in paint that are detected from FTIR studies;

(c) Characteristic lime-based composition of paste consistent with porous, fine-grained carbonated nature of lime paste seen in optical micrographs, but with some silica in paste indicating use of a hydraulic lime binder in the stucco;

(d) Absence of any Portland cement particles in the paste, which is consistent with its absence in the optical micrographs, hence all silica in the paste came from the hydraulic lime binder;

(e) Measurable magnesium content of paste indicating use of a dolomitic lime binder; and,

(f) Cementitious indices (CI after Eckel, 1922) of paste are all less than 1 which are consistent with hydraulic lime composition of the binder without any cement.

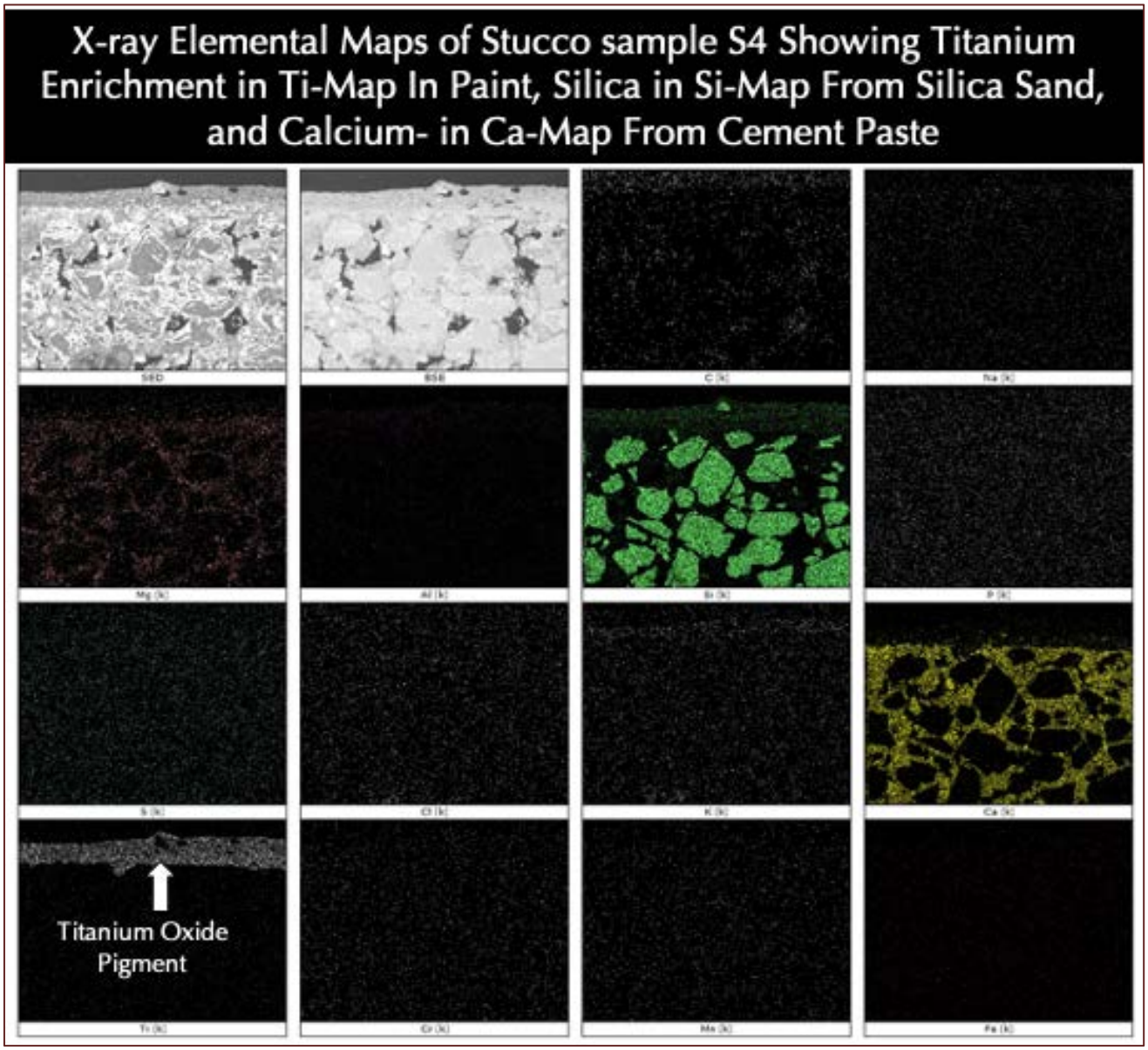

Figure 66: X-ray elemental maps of stucco S4 in SEM-EDS studies showing: (a) titanium enrichment in the paint coat from use of titanium oxide pigment in the paint, (b) characteristic lime-based composition of lime paste in the Ca map, along with (c) some magnesium in the paste detected in the Mg-map indicating use of dolomitic lime binder in stucco; (d) silica sand composition indicated by detection of sand in Si map; and (e) the absence of any other elements to be detected in EDS studies.

X-RAY DIFFRACTION

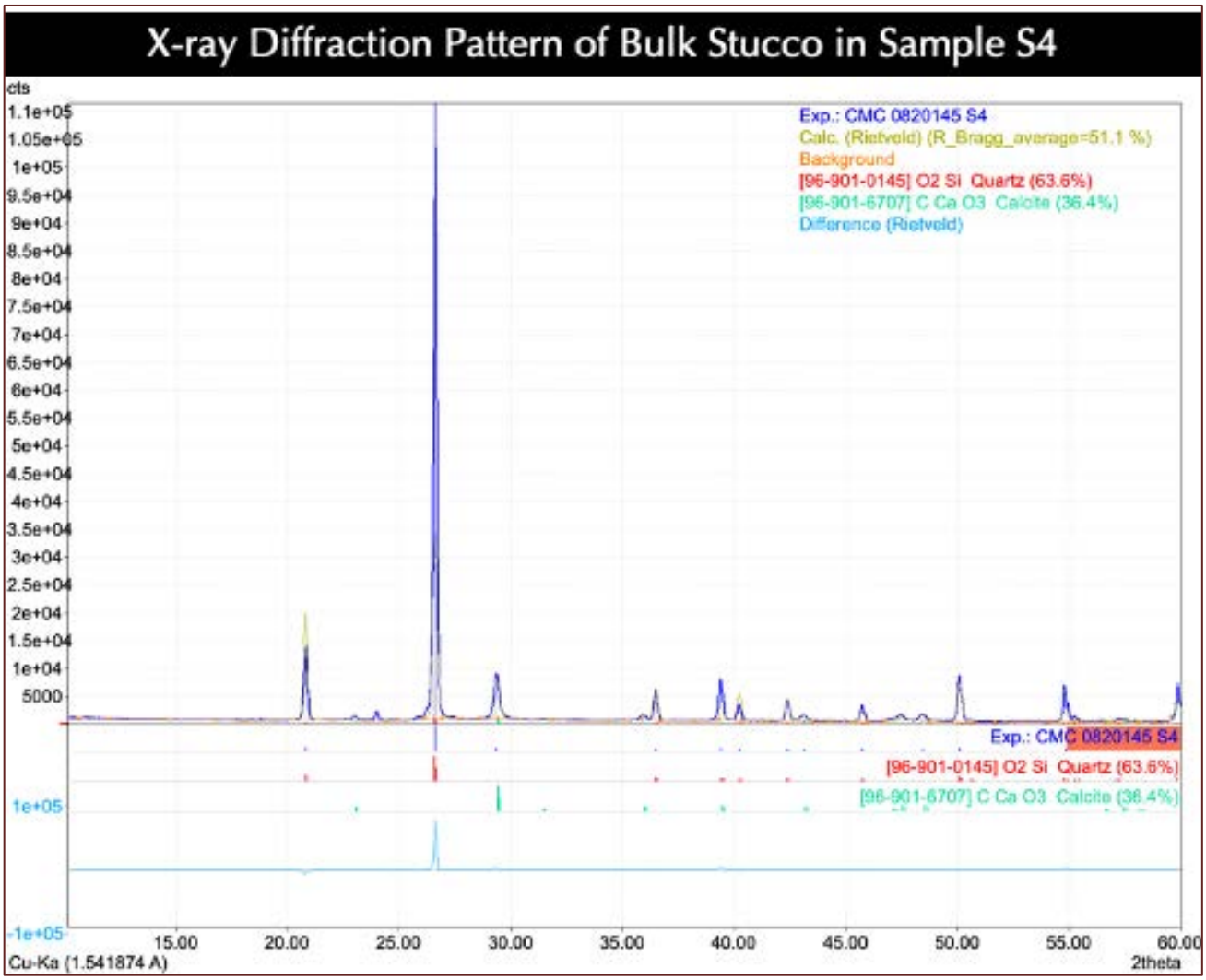

Figure 67: X-ray diffraction pattern of the entire stucco in S4 including both scratch and brown coats showing the dominance of crushed silica sand seen in optical micrographs of both coats as the dominant quartz peak followed by subordinate calcite from the overwhelming carbonated lime paste of lime binder.

XRD studies showed 63.6 percent quartz from quartz sand and 36.4 percent calcite from fine-grained carbonated lime paste.

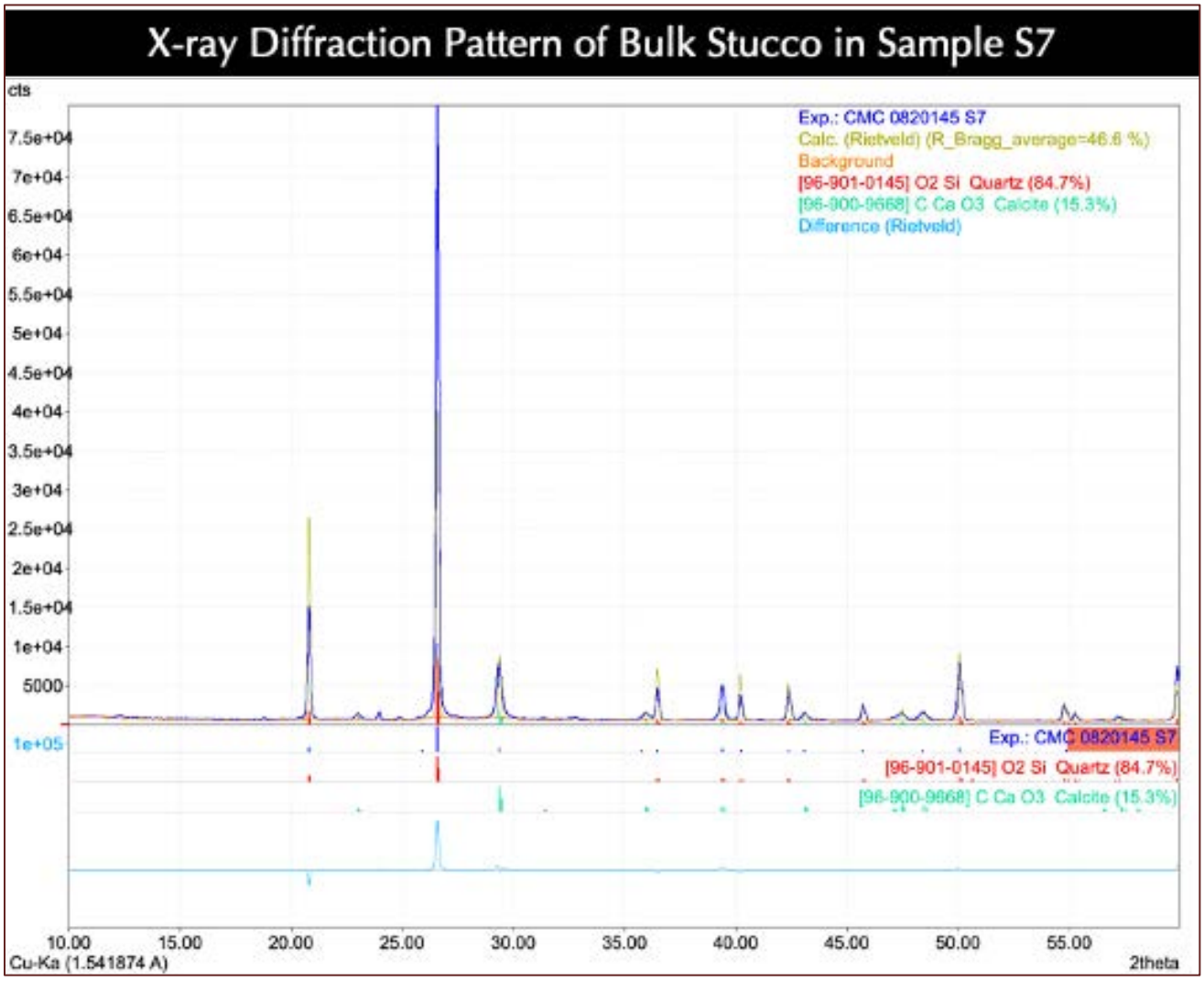

Figure 68: X-ray diffraction pattern of the entire stucco in S7 including both scratch and brown coats showing the dominance of crushed silica sand seen in optical micrographs of both coats as the dominant quartz peak followed by subordinate calcite from the overwhelming carbonated lime paste of lime binder.

XRD studies showed 84.7 percent quartz from quartz sand and 15.3 percent calcite from fine-grained carbonated lime paste.

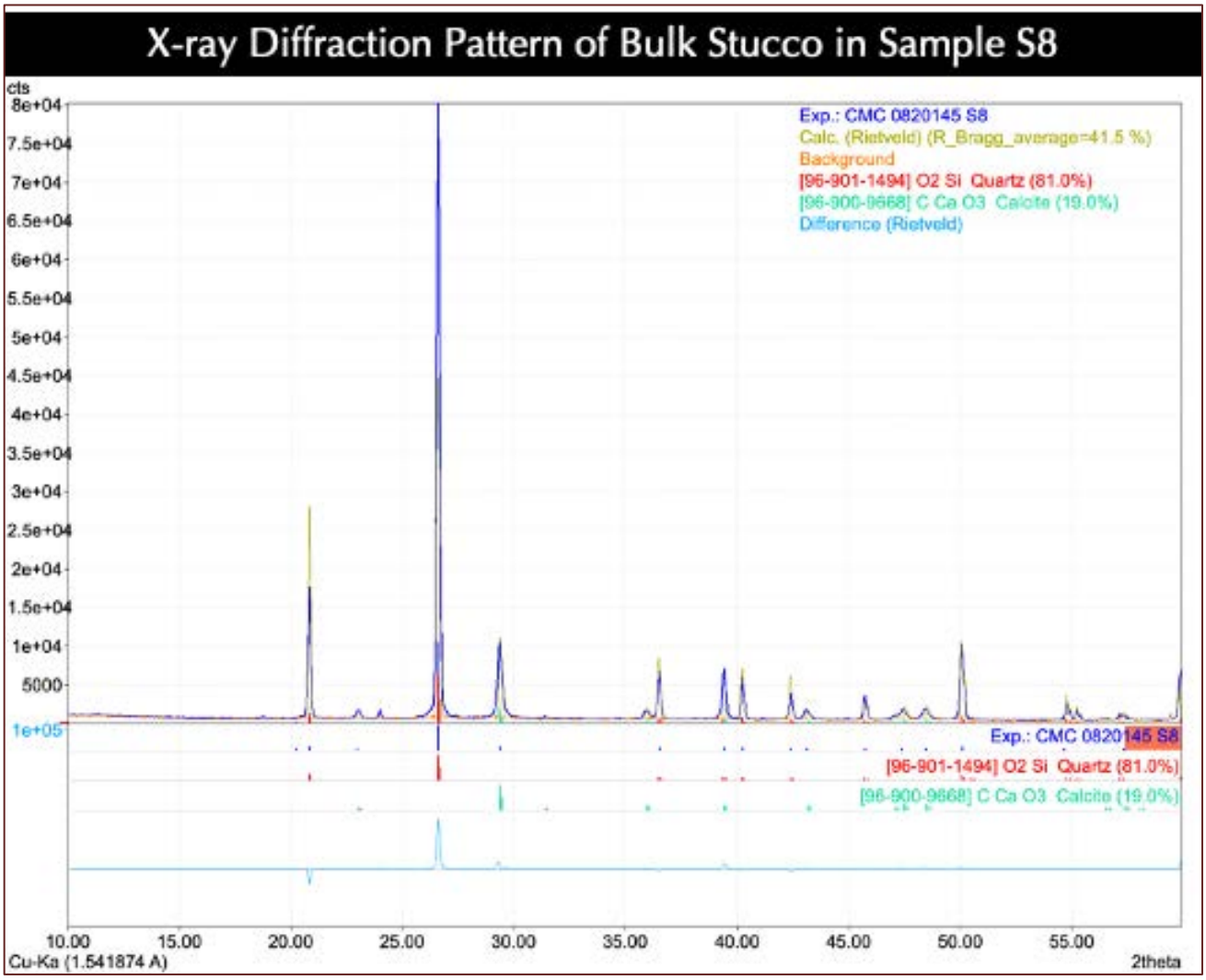

Figure 69: X-ray diffraction pattern of the entire stucco in S8 including both scratch and brown coats showing the dominance of crushed silica sand seen in optical micrographs of both coats as the dominant quartz peak followed by subordinate calcite from the overwhelming carbonated lime paste of lime binder.

XRD studies showed 81.0 percent quartz from quartz sand and 19.0 percent calcite from fine-grained carbonated lime paste.

X-RAY FLUORESCENCE

Bulk Chemical (Oxide Wt.%) Compositions of Stuccos From XRF												
Stucco	SiO_2	Al_2O_3	Fe_2O_3	CaO	MgO	Na_2O	K_2O	TiO_2	P_2O_3	SO_3	Balance (LOI)	Total
S4	72.8	0.826	0.773	9.83	2.49	ND	0.046	0.057	0.030	ND	13.2	100.0
S7	61.3	1.290	1.560	11.50	3.12	0.240	0.118	0.310	0.065	0.166	20.4	100.0
S8	63.5	0.867	1.380	10.80	3.07	ND	0.048	0.218	0.027	0.054	20.1	100.0

Figure 70: Major elemental oxide compositions of three stucco samples determined from X-ray fluorescence spectroscopy, which showed overall compositional similarities of all three stuccos having major amount of silica from quartz sand, followed by subordinate lime and magnesia from dolomitic lime binder.

SAND CONTENTS FROM ACID-INSOLUBLE RESIDUE CONTENTS AND IMAGE ANALYSES

Hydrochloric-acid insoluble residue contents of all three stucco samples show 69.34 percent residue in S4, 69.76 percent residue in S7 and 69.23 percent in S8. Considering the siliceous (dominant quartz) composition of the sand, which is insoluble in acid, the residue contents closely correspond to the sand contents of stucco, which also show a close correspondence to the bulk silica contents of stuccos determined from X-ray fluorescence spectroscopy.

Image analyses of micrographs of thin sections of all stucco samples showed the following percentages of sand in brown and scratch coats where sand contents are lower in brown coats than the scratch coats (corresponding to higher paste volumes in the brown coats, which are consistent with finer sand in brown coats) in S4 and S7 but higher sand volume in the brown coat of S8 than its scratch coat where sand size variations between the coats is less prominent than that seen in S4 and S7:

Stucco	Piece#	Sand content (vol %) in Brown Coat	Sand content (vol %) in Scratch Coat	Figure#	Average sand Content by volume from Image Analyses	Sand Content by mass from Acid Insoluble Residue	Sand Specific Gravity From Mass% and Vol% Calculations
S4	1	43.1	45.5	26	44.8	69.34	1.55
	2	45.3	45.6	30			
S7	1	43.7	48.7	32	46.2	69.76	1.51
	2	42.6	48.0	34			
	3	42.7	48.9	36			
	4	49.2	46.4	40			
S8	1	53.2	48.0	42	49.8	69.23	1.40
	2	51.2	46.8	44			

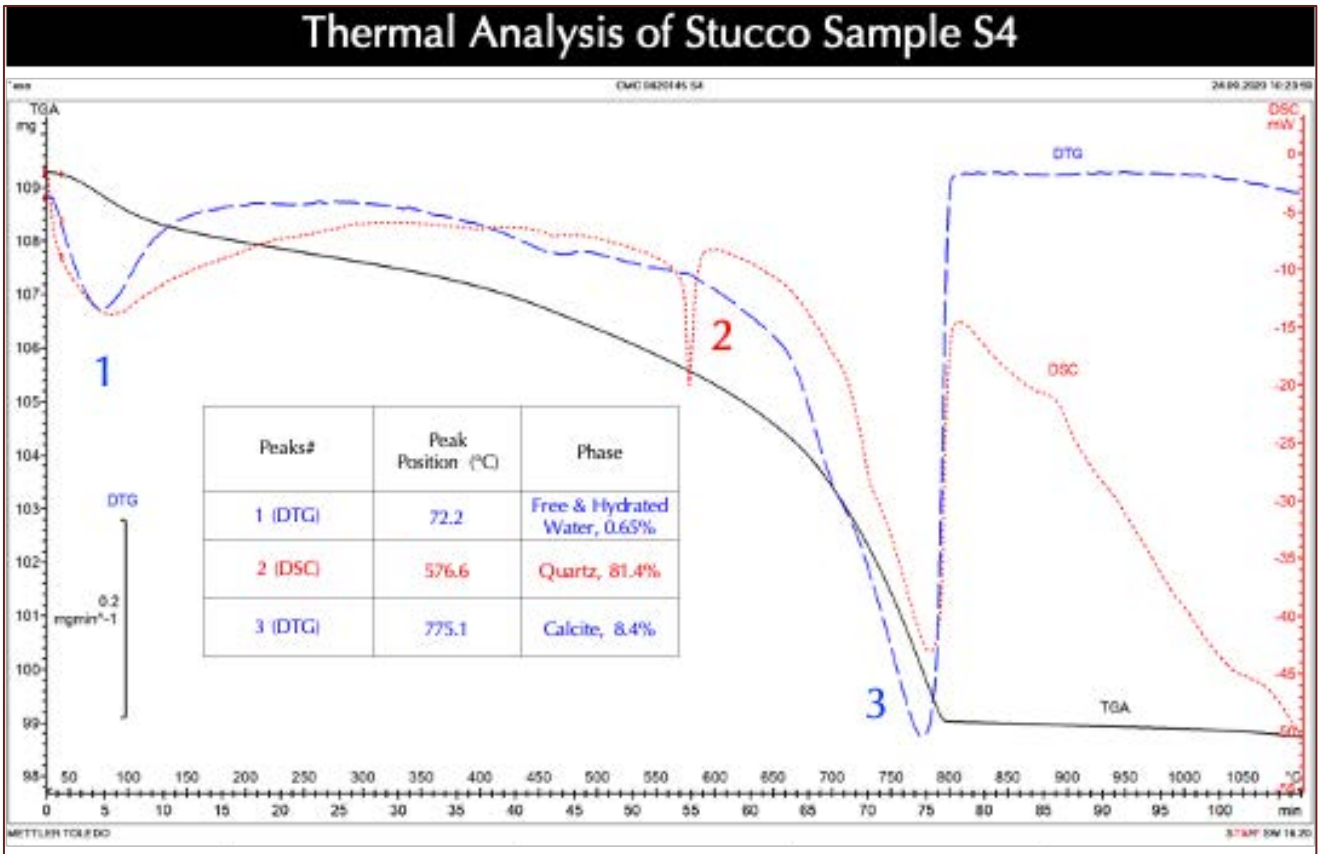

Peaks#	Peak Position (°C)	Phase
1 (DTG)	72.2	Free & Hydrated Water, 0.65%
2 (DSC)	576.6	Quartz, 81.4%
3 (DTG)	775.1	Calcite, 8.4%

T(°C)	Up to 120°C	120°C to 200°C	200°C to 600°C	> 600°C
Phases	Hygroscopic Water	Water from Hydrated Salts	Structural Water From Hydraulic Components	CO_2 from decomposition of carbonates
Mass Loss (%) from TGA	0.91	0.37	2.36	5.77

Figure 71: TGA (bold black), DSC (dotted red), and DTG (dashed blue) curves of stucco S4 showing losses in weight due to various decompositions (loss of water and carbon dioxide) during controlled heating in a Mettler-Toledo's simultaneous TGA/DSC 1 unit from 30ºC to 1000ºC in a ceramic crucible (alumina 70µl, no lid) at a heating rate of 10ºC/min in a nitrogen purge at a rate of 75 mL/min.

Milligrams of stucco sample S4 was subjected to controlled heating experiments in a Mettler-Toledo TGA/DSC simultaneous thermogravimetric and differential scanning calorimetry unit to detect the presence of various hydrous, sulfate, and carbonate phases and their relative abundances. Figure 71 shows TGA (in bold black), DSC (in dotted red), and DTG (in dashed blue) curves of stucco indicating losses in weight due to decompositions (loss of water and carbon dioxide) of various phases during controlled heating from 30ºC to 1000ºC in a ceramic crucible (alumina 70µl, no lid) at a heating rate of 10ºC/min in a nitrogen purge at a rate of 75 mL/min. Dehydration and decarbonation reactions are marked as endothermic peaks in the DTG curve, whereas alpha to beta-form polymorphic transition of quartz is marked at the characteristic temperature of 575 ºC in the DSC curve.

In the DTG curve, successive losses in weights were detected at (i) up to 120ºC from losses of free and combined water, (ii) from 120ºC to 200ºC for water from hydrated salts, (iii) from 200ºC to 600ºC for dihydroxylation of structural/hydrate water in various hydraulic components, and (iv) from 600ºC to 850ºC for decomposition of carbonate phases from limestone fines and fine-grained calcite in carbonated pastes. DSC curve shows polymorphic transition from alpha to beta form of quartz around 575ºC from silica (quartz) sand.

Result shows about 1 percent loss in mass from loss of free water and hydrate water at up to 120ºC followed by a lesser loss of 0.37 percent from 120ºC to 200ºC, then a loss of 2.36 percent from 200ºC to 600ºC due to loss of hydrate water from hydration products of hydraulic lime paste. Degree of carbonation is 5.77% due to decomposition of carbonate lime paste in stucco. Quartz content is around 80 percent determined from polymorphic transition of quartz around 575ºC.

FTIR SPECTRA OF PAINT COATS ON STUCCO

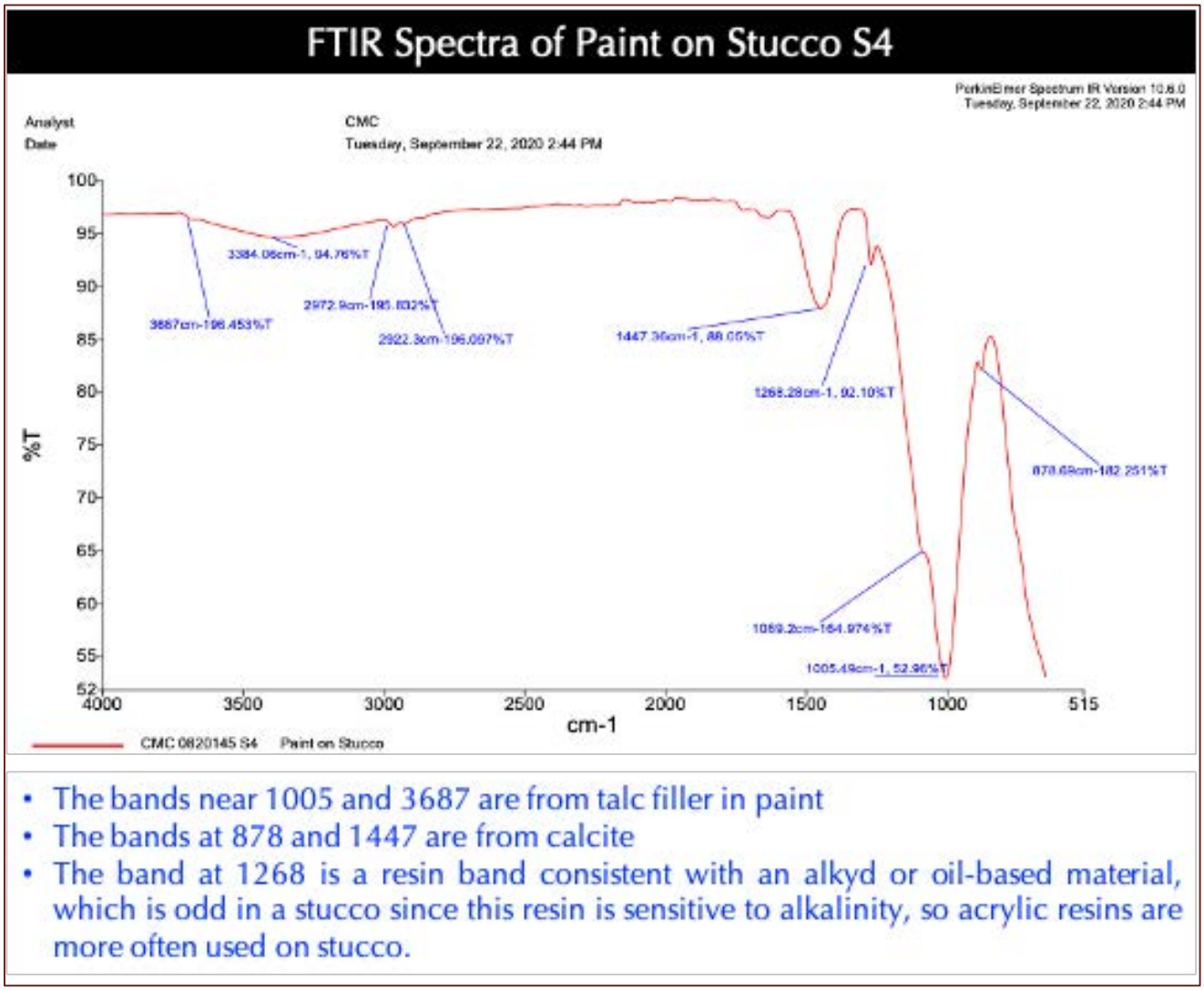

Figure 72: FTIR spectra of paint coat scrapped from the exterior face of Sample S4 showing: (a) bands near 1005 cm^{-1} and 3687 cm^{-1} corresponding to talc filler in paint; (b) bands at 878 cm^{-1} and 1147 cm^{-1} corresponding to

calcite partly from calcite filler in the bonding agent of paint and partly from contaminant carbonated lime binder of stucco; and (c) a band at 1268 cm^{-1} corresponding to an alkyd resin or oil-based binder, which is not resistant to the alkaline medium of stucco especially at the newly installed stage before the stucco surface that was painted has had a pH around 9 or lower from atmospheric carbonation to prevent alkali-induced deterioration of alkyd based paint. An acrylic paint would have produced a band near 1170 cm^{-1} sometimes with a smaller band near 1240 cm^{-1}.

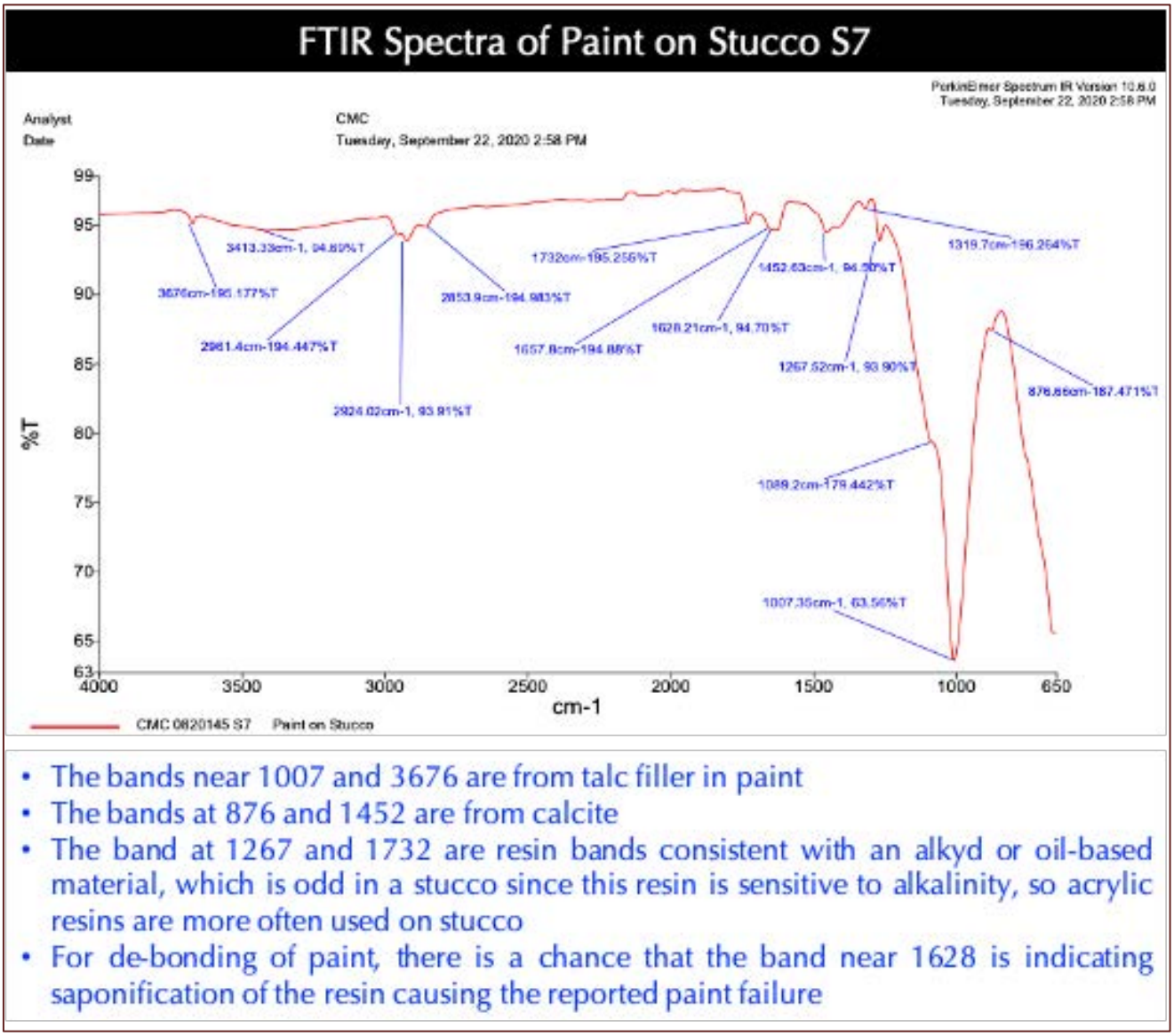

Figure 73: FTIR spectra of paint coat scrapped from the exterior face of Sample S7 showing: (a) bands near 1007 cm^{-1} and 3676 cm^{-1} corresponding to talc filler in paint; (b) bands at 876 cm^{-1} and 1452 cm^{-1} corresponding to calcite partly from calcite filler in the bonding agent of paint and partly from contaminant carbonated lime binder of stucco; and (c) bands at 1267 cm^{-1} and 1732 cm^{-1} corresponding to an alkyd resin or oil-based binder, which is not resistant to the alkaline medium of stucco especially at the newly installed stage before the stucco surface that was painted has had a pH around 9 or lower from atmospheric carbonation to prevent alkali-induced deterioration of alkyd based paint. For the reported peeling of paint, there is a possibility that the band near 1628 cm^{-1} is indicating saponification of the resin to cause the paint failure from alkaline degradation of alkyd-based paint. An acrylic paint would have produced a band near 1170 cm^{-1} sometimes with a smaller band near 1240 cm^{-1}.

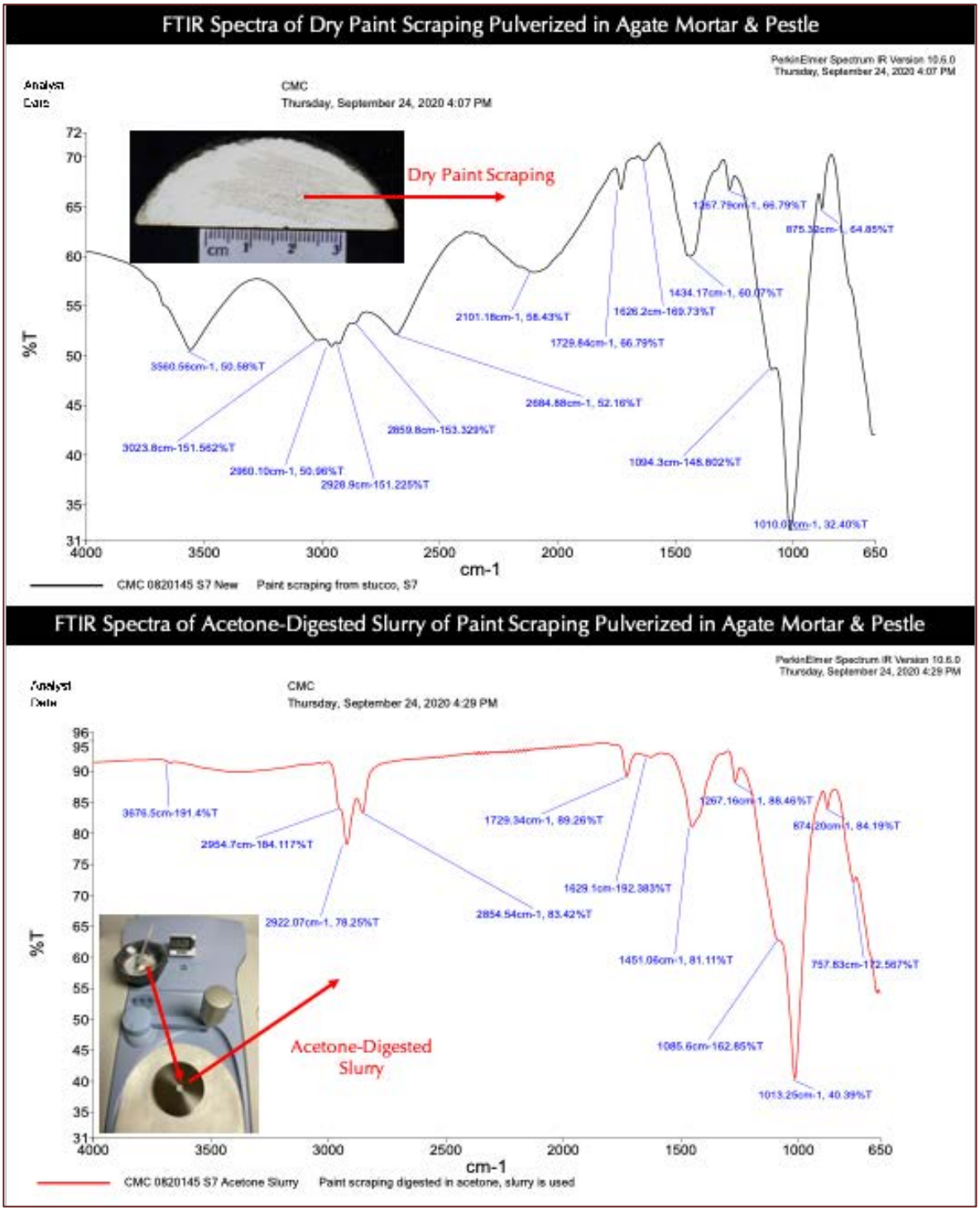

Figure 74: FTIR spectra of pulverized dry powder of paint coat scrapped from the exterior face of Sample S7 at the top, and the slurry after digesting the paint in acetone at the bottom showing: (a) bands near 1010 cm^{-1} and 3676 cm^{-1} corresponding to the talc filler in paint; (b) bands at 874 cm^{-1} and 1451 cm^{-1} corresponding to calcite partly from calcite filler in the bonding agent of paint and partly from contaminant carbonated lime binder of stucco; and (c) bands at 1267 cm^{-1} and 1729 cm^{-1} corresponding to an alkyd resin or oil-based binder, which is not resistant to the alkaline medium of stucco especially at the newly installed stage before the stucco surface that was painted has had a pH around 9 or lower from atmospheric carbonation to prevent alkali-induced deterioration of alkyd based paint. For the reported peeling of paint, there is a possibility that the band near 1628 cm^{-1} is indicating saponification

of the resin to cause the paint failure from alkaline degradation of alkyd-based paint. An acrylic paint would have produced a band near 1170 cm^{-1} sometimes with a smaller band near 1240 cm^{-1}..

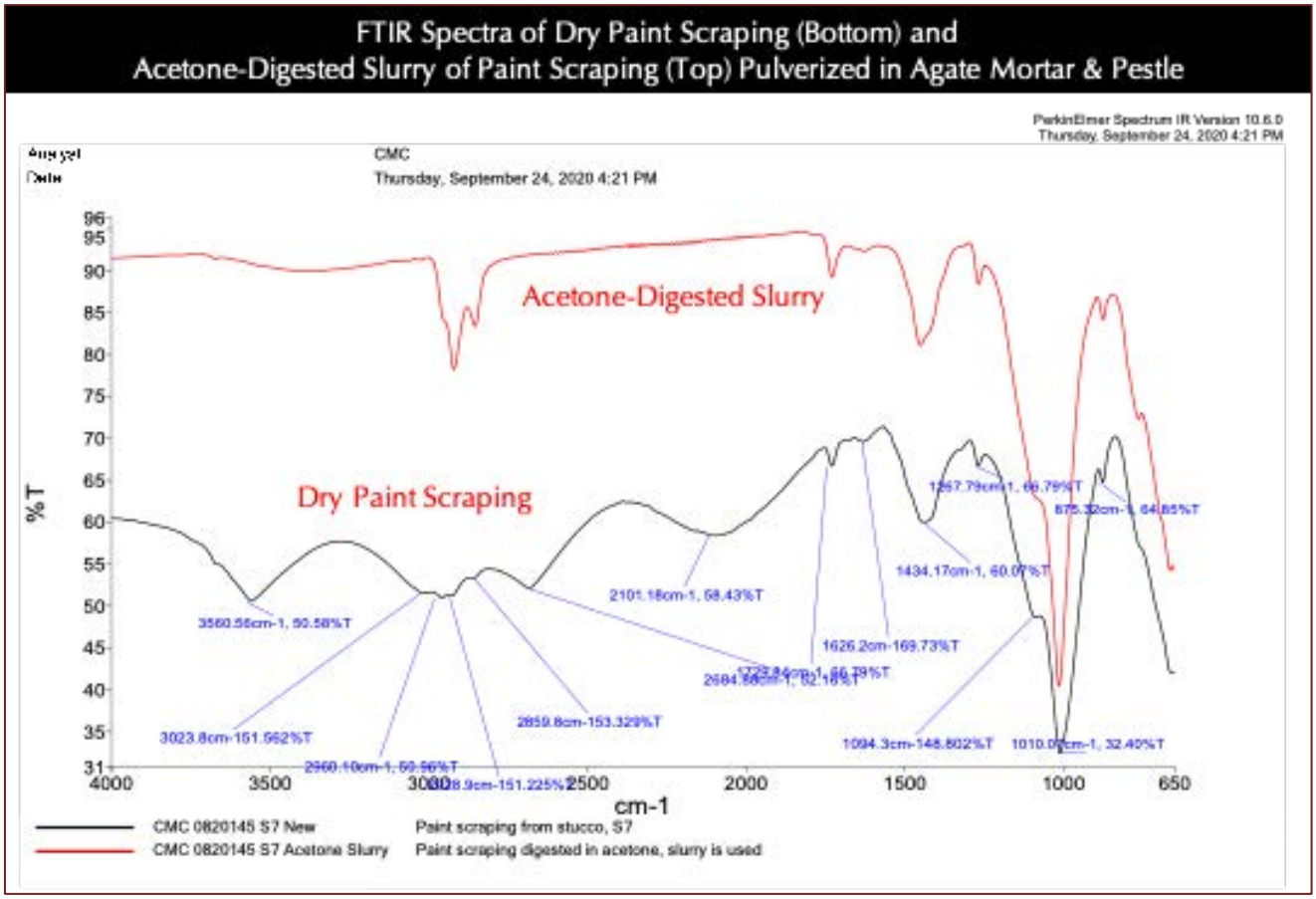

Figure 75: FTIR spectra of paint coat scrapped from the exterior face of Sample S8 showing: (a) bands near 1007 cm^{-1} and 3676 cm^{-1} corresponding to talc filler in paint; (b) bands at 872 cm^{-1} and 1406 cm^{-1} corresponding to calcite partly from calcite filler in the bonding agent of paint and partly from contaminant carbonated lime binder of stucco; and (c) bands at 1266 cm^{-1} and 1727 cm^{-1} corresponding to an alkyd resin or oil-based binder, which is not resistant to the alkaline medium of stucco especially at the newly installed stage before the stucco surface that was painted has had a pH around 9 or lower from atmospheric carbonation to prevent alkali-induced deterioration of alkyd based paint. For the reported peeling of paint, there is a possibility that the band near 1629 cm^{-1} is indicating saponification of the resin to cause the paint failure from alkaline degradation of alkyd-based paint. An acrylic paint would have produced a band near 1170 cm^{-1} sometimes with a smaller band near 1240 cm^{-1}.

There is no evidence of any other filler found in the optical microscopy, or SEM-EDS, or FTIR scans in Figures 72 through 76. For example, there is no nepheline syenite, diatom, dolomite, or silicon dioxide fillers found either in optical or electron microscopy, or in FTIR studies. Amorphous silica in diatom gives a large band near 1100 cm^{-1} with bands at 800 cm^{-1} and 500 cm^{-1}, which are not present. Crystalline silica has a characteristic doublet near 800/780 cm^{-1}, which is not present. Dolomite has large doublet at 1480/1410 cm^{-1} which are not present. Bands found at 1267 cm^{-1} and 1732 cm^{-1} correspond to an alkyd resin or oil-based binder, which is not resistant to the alkaline medium of stucco especially at the newly installed stage before the stucco surface that was painted has had a pH around 9 or lower from atmospheric carbonation to prevent alkali-induced deterioration of alkyd-based paint. For the reported peeling of paint, there is a possibility that the band near 1628 cm^{-1} is indicating saponification of

the resin to cause the paint failure from alkaline degradation of alkyd-based paint. An acrylic paint would have produced a band near 1170 cm^{-1} sometimes with a smaller band near 1240 cm^{-1}, which are not found. Siloxane would usually have a broader band between 1100 and 1000 cm^{-1}, which is not found.

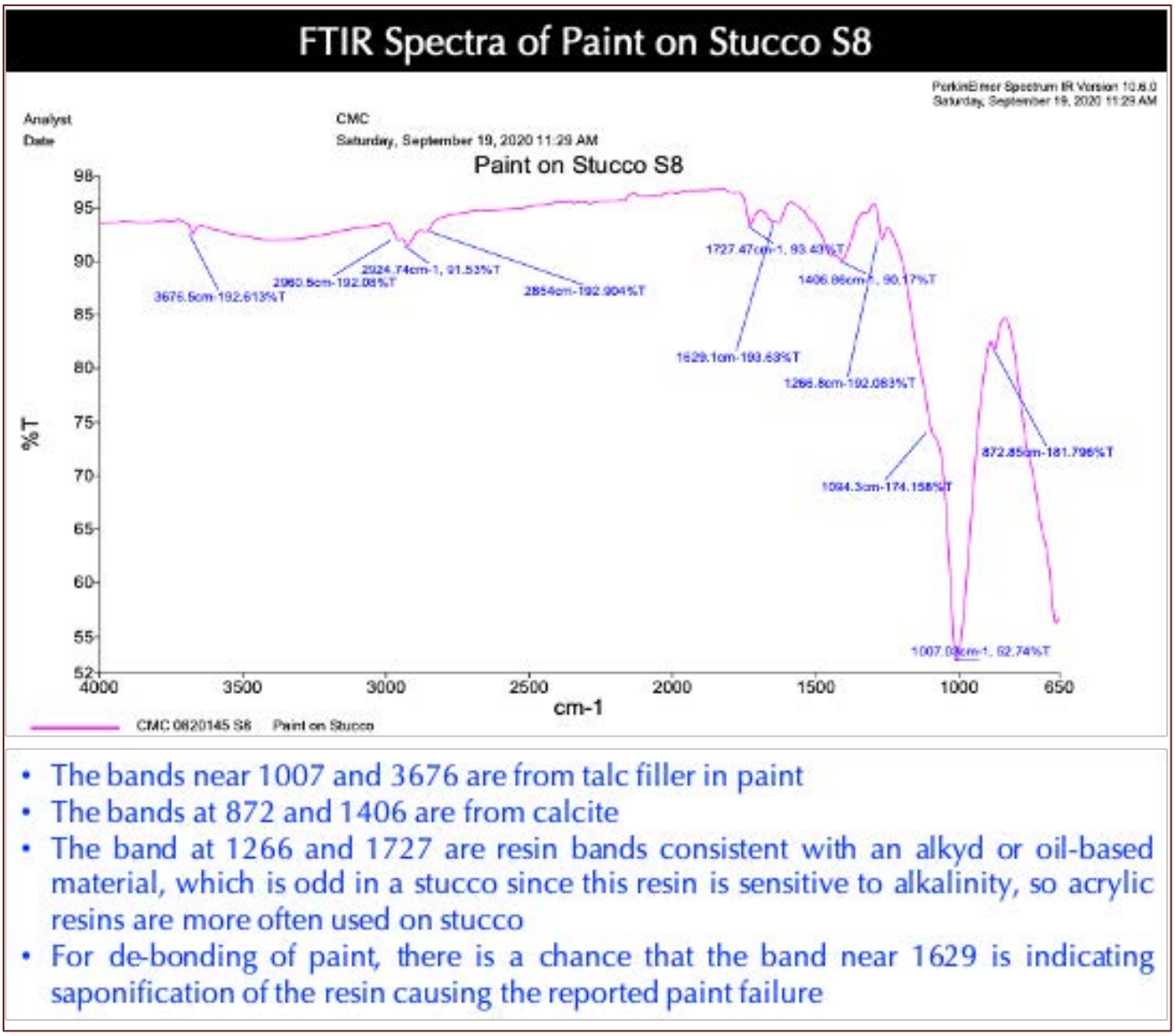

Figure 76: FTIR spectra of paint coat scrapped from the exterior face of Sample S8 showing: (a) bands near 1007 cm^{-1} and 3676 cm^{-1} corresponding to talc filler in paint; (b) bands at 872 cm^{-1} and 1406 cm^{-1} corresponding to calcite partly from calcite filler in the bonding agent of paint and partly from contaminant carbonated lime binder of stucco; and (c) bands at 1266 cm^{-1} and 1727 cm^{-1} corresponding to an alkyd resin or oil-based binder, which is not resistant to the alkaline medium of stucco especially at the newly installed stage before the stucco surface that was painted has had a pH around 9 or lower from atmospheric carbonation to prevent alkali-induced deterioration of alkyd based paint. For the reported peeling of paint, there is a possibility that the band near 1629 cm^{-1} is indicating saponification of the resin to cause the paint failure from alkaline degradation of alkyd-based paint. An acrylic paint would have produced a band near 1170 cm^{-1} sometimes with a smaller band near 1240 cm^{-1}.

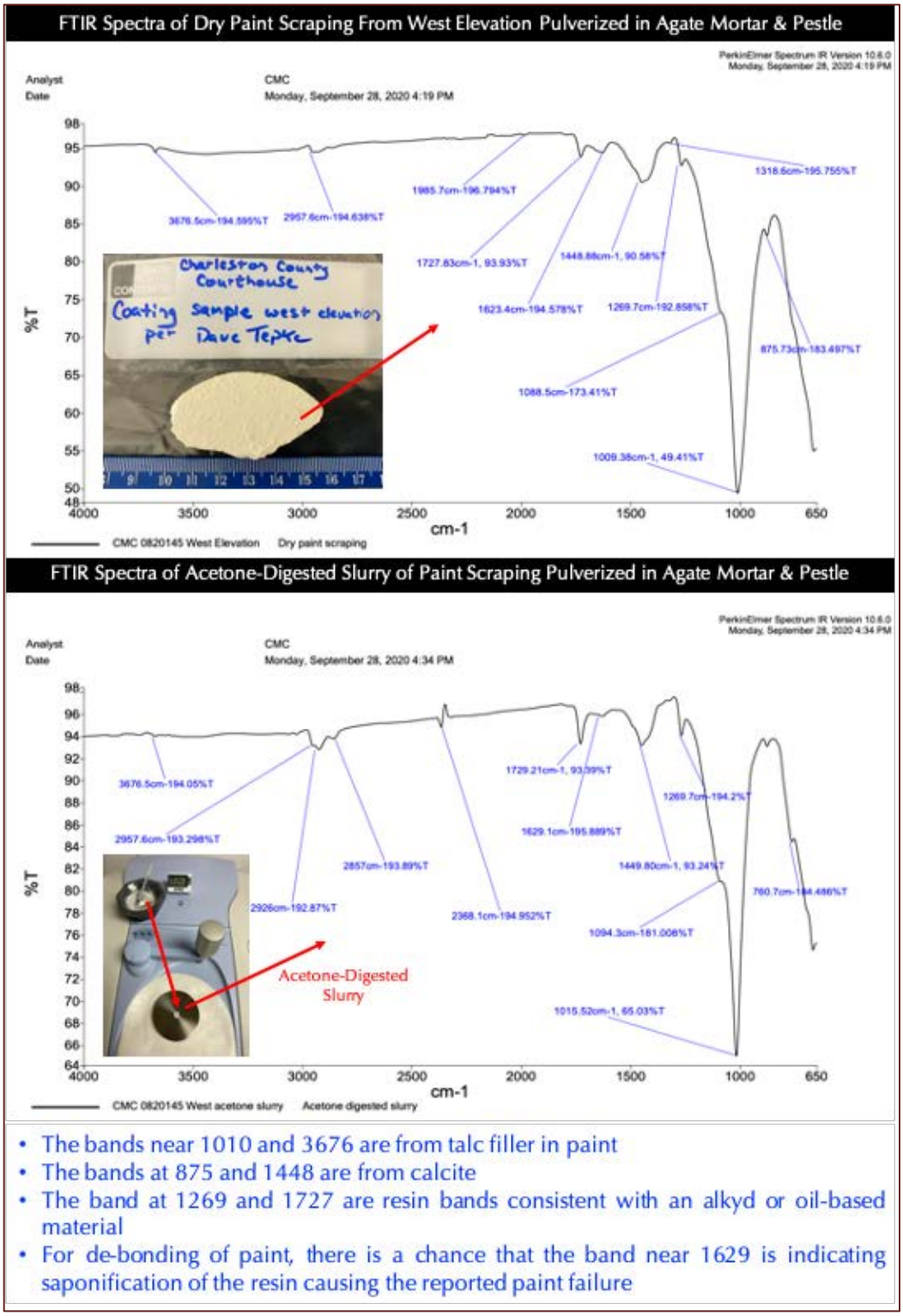

Figure 77: FTIR spectra of paint coat scrapped from the west elevation showing similar spectra as seen in other samples, e.g.,: (a) bands near 1010 cm^{-1} and 3676 cm^{-1} corresponding to talc filler in paint; (b) bands at 875 cm^{-1} and 1448 cm^{-1} corresponding to calcite partly from calcite filler in the bonding agent of paint and partly from contaminant carbonated lime binder of stucco; and (c) bands at 1269 cm^{-1} and 1727 cm^{-1} corresponding to an alkyd resin or oil-based binder. For the reported peeling of paint, there is a possibility that the band near 1629 cm^{-1} is indicating saponification of the resin to cause the paint failure from alkaline degradation of alkyd-based paint. An acrylic paint would have produced a band near 1170 cm^{-1} sometimes with a smaller band near 1240 cm^{-1}.

SUMMARY RESULTS

	S4 from North Elevation	S7 From South Elevation	S8 From East Elevation
Total Thickness, mm	18	16	22
Finish (Paint) coat, mm	< 0.25	< 0.25	< 0.25
Paint composition	Pigment – Titanium oxide; Filler – Talc, Calcite; Binder – Alkyd resin		
Bonding Agent to Paint	Diffused to stucco body, polymer based with a few residual cement particles	Diffused to stucco body, polymer based with a few residual cement particles	Distinct coat beneath paint polymer based with a few residual cement particles
Brown Coat Thickness, mm	8	7	8
Scratch Coat Thickness, mm	10	7	14
Bond of Paint to Brown Coat	Good	Good	Good
Bond of Brown and Scratch	Good	Good	Good
Sand in Brown Coat	Silica Sand, nominal 1 mm in size, well-graded, well-distributed, angular (crushed), sound		
Sand in Scratch Coat	Silica Sand, nominal 1.5 mm in size, well-graded, well-distributed, angular (crushed), sound; sand is coarser than sand in brown coat;		
Binder	Fine-grained, porous, carbonated dolomitic hydraulic lime paste determined from typical lime paste texture in optical microscopy, <1 paste-CI in SEM-EDS studies, high magnesium in paste from SEM-ESS studies from dolomitic lime		
Distinguishing features between brown and scratch coats	Finer sand and denser overall mass of brown coat compared to coarser sand and porous popcorn-type texture of scratch coat		
Air	Non air entrained stucco coats both brown and scratch coats 8 to 10 percent interstitial air by volume in brown coat and 16 to 20 percent by volume in scratch coat		
Cracking	Discontinuous, fine, hair-line shrinkage microcracks and carbonated lime paste mostly in the brown coat and also some in underlying scratch coat; no visible cracking in the coats		
Expanded Metal Lath Diamond Reinforcement in the scratch coat	No fiber mesh or metal lath reinforcement found in the scratch coat		
ASTM C 926 Recommended Nominal Thickness of 2-coat Plaster Thickness (mm) over cast-in-place or pre-cast concrete	Total thickness is less than the common industry (e.g., ASTM C 926)-recommended minimum 22-mm ($^{7}/_{8}$ in.) thickness of a stucco containing expanded metal lath diamond reinforcement.		

CONCLUSIONS

STUCCO COATS

All three stucco samples were examined by a comprehensive testing protocol including optical microscopy for overall compositions and microstructures of stuccos, SEM-EDS analysis for the compositions of paint coat and binder phases of stucco, X-ray fluorescence for overall bulk chemical compositions of stuccos, X-ray diffraction for overall mineralogical compositions of sand and binder components of stuccos, gravimetric (acid insoluble residue contents) analysis for sand contents of stuccos, thermal analysis for determining sand and calcite contents and possible presence of a hydraulic phase in the binder, which is confirmed from SEM-EDS analysis, and FTIR techniques for analysis of paint compositions, especially the binder phases of paints besides pigment and filler phases beyond determinations from SEM-EDS analysis.

All three stucco samples from north, south, and east elevations of courthouse are found to be compositionally similar three-coat stuccos consisting of: (a) a crushed silica sand and dolomitic hydraulic lime based scratch coat, (b) a similar crushed silica sand (though a bit finer in grain size) and dolomitic hydraulic lime based brown coat, and (c) an alkyd-resin based paint coat containing titanium oxide pigment and talc filler in alkyd resin binder. Total nominal thickness of stuccos are 18 mm in S4, 16 mm in S7, and 22 mm in S8. Paint coats are all less than 0.25 mm in thickness. Brown coats are 8 mm in S4, 7 mm in S7, and 8 mm in S8. Scratch coats are 10 mm in S4, 7 mm in S7, and 14 mm in S8. Bonds between paint and brown coat as well as between brown and scratch coats are good. Scratch and brown coats are differentiated on the basis of overall finer grain size of crushed sand particles in the brown coat in almost all three stuccos, and a variation in overall densities and color tones of coats where brown coats are overall denser than the scratch coats.

Major elemental oxide compositions of all three stuccos from X-ray fluorescence spectroscopy shows overall compositional similarities in having 60 to 70% silica, 0.8 to 1.2% alumina, 0.7 to 1.5% iron, 9.8 to 11.5% lime, 2.5 to 3.1% magnesia, and other oxides at lesser abundances all consistent with a silica sand and dolomitic hydraulic lime composition determined from optical and scanning electron microscopy and X-ray microanalysis. Acid insoluble residue contents are around 70 percent, which correspond to silica sand contents, and closely correspond to silica contents from XRF. Higher magnesia contents in paste from SEM-EDS studies as well as in bulk stucco samples from XRF studies compared to a non-hydraulic lime binder indicates use of a dolomitic lime. Additionally, higher silica contents in paste than a non-hydraulic lime binder and a higher loss of mass from decomposition of hydrate water in thermal analysis than a paste from a non-hydraulic lime binder indicates use of a hydraulic lime binder. No Portland cement or other cementitious or hydraulic phases are found in the porous, fine-grained severely carbonated lime paste showing characteristic fine discontinuous shrinkage microcracks as seen in many historic lime mortars.

PAINT ON STUCCO

The paint coat is found to be compositionally similar in all samples from all three elevations, including an additional one provided from the west elevation, all of which showed the presence of an alkyd resin-based paint as opposed to more common and alkali-resistant acrylic or latex or siloxane based paint. The talc filler and titanium oxide pigment in the paint are determined best from SEM-EDS studies from characteristic titanium, silica, and alumina enrichments in X-ray elemental maps of those elements in the paste, as well as from FTIR studies from characteristic absorption bands of talc in the FTIR spectra. Absorption bands near 1007 cm^{-1} and 3676 cm^{-1} correspond to talc filler in paint; bands at 876 cm^{-1} and 1452 cm^{-1} correspond to calcite partly from calcite filler in the bonding agent of paint and partly from contaminant carbonated lime binder of stucco. There is no evidence of any other filler found in the optical microscopy, or SEM-EDS, or FTIR scans. For example, there is no nepheline syenite, diatom, dolomite, or silicon dioxide fillers found either in optical or electron microscopy, or in FTIR studies. Amorphous silica in diatom gives a large band near 1100 cm^{-1} with bands at 800 cm^{-1} and 500 cm^{-1}, which are not present. Crystalline silica has a characteristic doublet near 800/780 cm^{-1}, which is not present. Dolomite has large doublet at 1480/1410 cm^{-1} which are not present. Bands found at 1267 cm^{-1} and 1732 cm^{-1} correspond to an alkyd resin or oil-based binder, which is not resistant to the alkaline medium of stucco especially at the newly installed stage before the stucco surface that was painted has had a pH around 9 or lower from atmospheric carbonation to prevent alkali-induced deterioration of alkyd-based paint. For the reported peeling of paint, there is a possibility that the band near 1628 cm^{-1} is indicating saponification of the resin to cause the paint failure from alkaline degradation of alkyd-based paint. An acrylic paint would have produced a band near 1170 cm^{-1} sometimes with a smaller band near 1240 cm^{-1}, which are not found. Siloxane would usually have a broader band between 1100 and 1000 cm^{-1}, which is not found.

STUCCO CONDITION

The soft, dusty nature of stucco is found to be due to use of a dolomitic hydraulic lime based binder in all three samples which has softened the overall conditions. The fragmented nature of S4 is judged to be at least partly due to its lime-based composition even though the other two samples have maintained their integrity during sample extraction and shipment to the laboratory.

Petrographic evidence showed overall good bond between paint, brown coat, and scratch coats of stucco with no evidence of paint peeling or debonding even though the samples reportedly came from locations that have shown paint peeling. Petrographic examinations indicated loss of moisture from stucco coats from many fine hair-line shrinkage microcracks which are also common in many lime pastes where shrinkage occurs not only from loss of mix water of stucco but also from loss of moisture from carbonation of lime binder.

COATING (PAINT) FAILURE

Based on detailed laboratory examinations, failure of paint coat at various locations and elevations of courthouse are judged to be due to a combination of following factors:

(a) Use of an alkyd resin-based paint as opposed to more common acrylic or latex-based paint, or, the reported alkyl alkoxy siloxane based paint of TiO_2 pigment, and diatom-quartz-dolomite-syenite fillers. Alkyd resin is vulnerable to degradation in an alkaline environment of stucco, especially at an early age when significant atmospheric carbonation of lime paste of stucco to reduce the pH to 9 or less has not occurred. FTIR studies found evidence of possible saponification of resin to cause peeling from the substrate. Due to pH dependance of paints, application of a paint on a newly placed stucco is usually not done until a pH (e.g., phenolphthalein) test on the stucco surface to be painted show a pH of 9 or less from atmospheric carbonation;

(b) Absence of a suitable bonding agent or primer prior to the application of the paint coat except a distinct agent found in S8, where lack of adequate bonding agent prevented development of a good mechanical bond to the stucco substrate; and,

(c) The soft porous, lime-based composition of the stucco substrate, which is more porous, dusty, and hence less receptive to a paint than a cement-lime or masonry cement based stucco substrate.

REFERENCES

ASTM C 856 "Standard Practice for Petrographic Examination of Hardened Concrete," Vol. 4.02, ASTM International, West Conshohocken, PA, 2017.

ASTM C 926, "Standard Specification for Application of Portland cement-Based Plaster," Vol. 4.01, ASTM International, West Conshohocken, PA, 2017.

ASTM C 1723, "Standard Guide for Examination of Hardened Concrete Using Scanning Electron Microscopy," In Annual Book of ASTM Standards, Section Four Construction, Vol. 04.02; ASTM Subcommittee C 9.65, 2017.

Jana, D., "Sample Preparation Techniques in Petrographic Examinations of Construction Materials: A State-of-the-Art Review," *Proceedings of the 28th Conference on Cement Microscopy (ICMA)*, 2006, pp. 23-70.

✪ ✪ ✪ END OF TEXT ✪ ✪ ✪

END OF REPORT[1]

[1] The CMC logo is made using a lapped polished section of a 1930's concrete from an underground tunnel in the U.S. Capitol.